T.R.
GEBZE TECHNICAL UNIVERSITY
GRADUATE SCHOOL OF NATURAL AND APPLIED SCIENCES

PREPARATION OF PZT AND PLZT THIN FILMS ON DIFFERENT SUBSTRATES BY SOL-GEL SPIN COATING METHODS AND INVESTIGATION OF THEIR PROPERTIES

MUSTAFA ÇAĞRI BAYIR
A THESIS SUBMITTED FOR THE DEGREE OF
MASTER OF SCIENCE
DEPARTMENT OF MATERIALS SCIENCE AND ENGINEERING

GEBZE
2019

T.R.

GEBZE TECHNICAL UNIVERSITY

GRADUATE SCHOOL OF NATURAL AND APPLIED SCIENCES

PREPARATION OF PZT AND PLZT THIN FILMS ON DIFFERENT SUBSTRATES BY SOL-GEL SPIN COATING METHODS AND INVESTIGATION OF THEIR PROPERTIES

MUSTAFA ÇAĞRI BAYIR

A THESIS SUBMITTED FOR THE DEGREE OF

MASTER OF SCIENCE

DEPARTMENT OF MATERIALS SCIENCE AND ENGINEERING

THESIS SUPERVISOR

PROF. DR. EBRU MENŞUR ALKOY

GEBZE

2019

T.C.
GEBZE TEKNİK ÜNİVERSİTESİ
FEN BİLİMLERİ ENSTİTÜSÜ

PZT VE PLZT İNCE FİLMLERİN FARKLI ALTLIKLAR ÜZERİNDE SOL-JEL SPİN KAPLAMA YÖNTEMİYLE HAZIRLANMASI VE ÖZELLİKLERİNİN İNCELENMESİ

MUSTAFA ÇAĞRI BAYIR
YÜKSEK LİSANS TEZİ
MALZEME BİLİMİ VE MÜHENDİSLİĞİ ANABİLİM DALI

DANIŞMANI
PROF. DR. EBRU MENŞUR ALKOY

GEBZE
2019

GEBZE TEKNİK ÜNİVERSİTESİ	**YÜKSEK LİSANS JÜRİ ONAY FORMU**

GTÜ Fen Bilimleri Enstitüsü Yönetim Kurulu'nun 30/05/2019 tarih ve 2019/25 sayılı kararıyla oluşturulan 11/06/2019 tarihinde tez savunma sınavı yapılan Mustafa Çağrı BAYIR'ın tez çalışması Malzeme Bilimi ve Mühendisliği Anabilim Dalında YÜKSEK LİSANS tezi olarak kabul edilmiştir.

JÜRİ

ÜYE (TEZ DANIŞMANI) : PROF. DR. EBRU MENŞUR-ALKOY

ÜYE : DOÇ. DR. KORAY ÖZTÜRK

ÜYE : DR. ÖĞR. ÜYESİ AYŞE BERKSOY-YAVUZ

ONAY

Gebze Teknik Üniversitesi Fen Bilimleri Enstitüsü Yönetim Kurulu'nun …/…/… tarih ve …/… sayılı kararı.

İMZA / MÜHÜR

SUMMARY

Piezoelectric and electrooptic materials have been used and researched for a long time. Thin film form of these materials possesses higher properties compared to its bulk form and especially lead-based systems are more preferred despite its toxicity. The aim of this study is to prepare the Lead Zirconate Titanate (PZT) and Lead Lanthanum Zirconate Titanate (PLZT) thin films with different compositions on different substrates by using sol-gel spin coating technique to determine the effect of these parameters on the material properties. In this study, PZT compositions were prepared with the specific amount of excess lead and, the films were annealed at various temperatures to obtain the pure perovskite phase. PLZT compositions were prepared with selected lanthanum content and again specific amount of excess lead. Annealing conditions were variable to obtain the phase for PLZT films. PZT and PLZT films were coated on platinum coated silicon substrates ($Pt_{(111)}/Ti/SiO_2/Si_{(100)}$) and gallium-doped zinc oxide (GZO) coated glass substrates as a transparent conductive oxide (TCO). Thin films were prepared as the five-layered structure and between the coating steps, pyrolysis steps were carried out to the films for crystallization at various temperature and time. Effect of pyrolysis, annealing temperature and time on crystallinity were characterized by X-ray diffraction patterns (XRD) and scanning electron microscope (SEM) analyses. UV-Vis measurements were also done for the films coated on GZO coated glass substrates to characterize the optical properties of the films such as transparency, absorption. Platinum were sputtered to the films as an electrode by using RF magnetron sputtering method and electrodes with different diameters were coated on the films synthesized on platinum coated silicon substrates. Current-voltage (I-V) measurements, temperature dependent dielectric measurements and piezo response force microscope (PRFM) analyses were carried out to characterize the electrical properties of the films.

Keywords: Lead Zirconate Titanate, Lead Lanthanum Zirconate Titanate, Sol-Gel, Spin Coating, Gallium doped Zinc Oxide, Transparent Conductive Oxide.

ÖZET

Piezoelektrik ve elektro-optik malzemeler uzun süredir araştırılmakta ve kullanılmaktadır. Bu malzemelerin ince film formları kütlesel forma göre daha yüksek özellikler sergilemektedir. Özellikle kurşun esaslı sistemler toksik olma sorunlarına rağmen tercih edilmektedir. Bu çalışmada Kurşun Zirkonat Titanat (PZT) ve Kurşun Lantan Zirkonat Titanat (PLZT) ince filmlerin farklı kompozisyonlarda çeşitli altlıklar üzerine sol-jel spin kaplama yöntemiyle kaplanması ve bu parametrelerin malzeme özelliklerine etkisinin incelenmesi amaçlanmıştır. PZT kompozisyonları belirlenen miktarda kurşun fazlası ile hazırlanmış, saf perovskit fazının eldesi için farklı sıcaklıklarda tavlanmıştır. Ayrıca PLZT kompozisyonları seçilen lantan içeriği ve belirlenen miktarda kurşun fazlası ile hazırlanmıştır. Farklı sıcaklık koşullarında tavlama işlemi PLZT filmler için de uygulanmıştır. Filmler platin kaplı silisyum ($Pt_{(111)}/Ti/SiO_2/Si_{(100)}$) ve bir saydam iletken oksit olan galyum doplanmış çinko oksit (GZO) kaplı cam altlıklar üzerine kaplanmıştır. Filmler 5 katman olarak hazırlanmış ve kaplama aşamalarının arasında farklı sıcaklık ve zaman koşullarında ısıl işlem uygulanarak kristalizasyonun sağlanması amaçlanmıştır. Isıl işlem ve tavlama koşullarının kristalinite üzerine olan etkisi X-ışını kırınım desenleri (XRD) ve taramalı elektron mikroskobu (SEM) analizleri ile incelenmiştir. UV-Vis ölçümleri GZO kaplı cam altlıklara kaplanan filmlerin geçirgenlik, absorbsiyon gibi optik özelliklerinin karakterizasyonu için gerçekleştirilmiştir. Filmlerin üzerine elektrot oluşturulması için RF manyetik sıçratma yöntemiyle platin sıçratılmış ve platin kaplı silisyum altlıklar üzerinde üretilen filmlere üç farklı çapta kaplanmıştır. Akım-voltaj (I-V) ölçümleri, sıcaklığa bağlı dielektrik ölçümler ve piezo kuvvet mikroskobu analizleri filmlerin elektriksel özelliklerinin karakterizasyonu için tamamlanmıştır.

Anahtar Kelimeler: Kurşun Zirkonat Titanat, Kurşun Lantan Zirkonat Titanat, Sol-Jel, Spin Kaplama, Galyum doplanmış Çinko Oksit, Saydam İletken Oksit.

ACKNOWLEDGEMENT

First of all, my biggest gratefulness is to my advisor, mentor and pathfinder Prof. Ebru MENŞUR-ALKOY for giving her full support to me in writing this thesis and doing all our scientific researches. This support and trust encouraged me to going further and being better every time. I would like to thank to Prof. Sedat ALKOY for answering my endless questions, giving his advises and support for this study.

I would like to thank Dr. Seniz Türküz and Alperen Sezgin from Şişecam for their help to provide supplies for this thesis. Also, I would like to thank Assoc. Prof. Burç MISIRLIOĞLU and Omid MORADI from Sabancı University for opening their laboratories and helping to me for my measurements. Also, I would like to thank Prof. Ayşe Gül GÜREK from Gebze Technical University, Chemistry department for helping me about my measurements. I would like to thank NanoMagnetics Company from Middle East Technical University for their help to carry out characterizations.

I would like to thank Adem ŞEN and Ahmet NAZIM for their help on this study. I also would like to thank all "PiezoResearch Group" members for their support and fruitful discussions.

I would like to express my thankfulness to my fellows Ayşe KAVRUK, Fatma ERKOLLU and Uğur BİLEN. The days we got sleepless because of studying brought us to the place we are. I thank to life for bringing us together.

Lastly and the most important gratitude is to my family, my mother Leyla BAYIR, my father Ali BAYIR and my beloved sister Beyza BAYIR. Despite to the miles among us, you've always been there for me. I will always try to be a son and brother that you all can proud. Thank you very much!

This thesis study was supported by Gebze Technical University Scientific Research Projects #2018-A101-08.

TABLE OF CONTENTS

	Page
SUMMARY	v
ÖZET	vi
ACKNOWLEDGEMENT	vii
TABLE OF CONTENTS	viii
LIST OF ABBREVIATIONS AND ACRONYMS	x
LIST OF FIGURES	xiii
LIST OF TABLES	xviii
1. INTRODUCTION	1
1.1. Aim of the Study	2
2. LITERATURE REVIEW	3
2.1. Polarity of Crystal Classes	3
2.2. Ferroelectricity	4
2.2.1. Phase Transitions	6
2.3. Domains	8
2.4. Relaxor Ferroelectrics	9
2.5. Piezoelectricity	9
2.6. Ferroelectric Materials	12
2.6.1. Lead Zirconate Titanate	12
2.6.2. Lead Lanthanum Zirconate Titanate	15
2.7. Optical Approach to Ferroelectrics	16
2.7.1. Photovoltaic Effect and Technology	17
2.7.2. Ferroelectric Photovoltaics	17
2.7.3. Electro-Optic Effect of PLZT	18
2.8. Thin Film Technology	19
2.8.1. Substrates	20
2.8.2. Deposition Techniques	22
2.8.2.1. Physical Techniques	22
2.8.2.2. Chemical Processes	24
2.8.3. Strain in the Films	26
2.9. Transparent Conductive Oxides	27
2.9.1. Indium Tin Oxide	28

2.9.2. Gallium Zinc Oxide 29
3. EXPERIMENTAL STUDY 30
3.1. Preparation of Precursor Solutions 30
3.2. Preparation of the Surface of the Substrates for Coating 33
3.3. Spin Coating Process of the Films 33
3.4. Obtaining of the Top Electrode of the Films by RF Sputtering 36
3.5. Synthesis and Processing of Powders from the Solutions 36
3.6. Characterization of the Films and Bulk Samples 38
4. RESULTS AND DISCUSSION 40
4.1. PZT and PLZT Films Obtained on the Platinum Coated Silicon Substrates 40
4.1.1. Phase Analyses of the Films 40
4.1.2. SEM Analyses of the PZT and PLZT Thin Films 45
4.1.3. Electrical Characterization of the PZT and PLZT Thin Films 51
4.2. PZT and PLZT Films Obtained on the Gallium doped Zinc Oxide (GZO) Coated Glass Substrates 56
4.2.1. Phase Analyses of the Thin Films 56
4.2.2. SEM Analyses of the PZT and PLZT Thin Films 58
4.2.3. Optical Measurements of the PZT and PLZT Thin Films 65
4.2.4. Piezo Response Force Microscope and Atomic Force Microscope Analyses of the Films 69
4.3. Bulk PZT and Cobalt doped PZT Studies 72
4.3.1. Phase Analyses of the Calcined PZT and Cobalt doped PZT Powders 73
4.3.2. Phase Analyses of the Sintered PZT and Cobalt doped PZT Samples 75
4.3.3. Polarization and Strain Behavior of PZT and Cobalt doped PZT Samples 77
5. CONCLUSION 80

REFERENCES 81
BIOGRAPHY 87

LIST OF ABBREVIATIONS AND ACRONYMS

Abbreviations and Acronyms		Explanations
Å	:	Angstrom
E_g	:	Band Gap
C	:	Capacitance
cm	:	Centimeter
CSD	:	Chemical Solution Deposition
CVD	:	Chemical Vapor Deposition
E_C	:	Coercive Field
C	:	Coulomb
T_C	:	Curie Temperature
I-V	:	Current - Voltage
ºC	:	Degree Celsius
K	:	Dielectric Constant
tanδ	:	Dielectric Dissipation Factor
D	:	Dielectric Loss
DRAM	:	Dielectric Random Accessible Memory
DTA	:	Differential Thermal Analyses
DC	:	Direct Current
ε	:	Electrical Permittivity
E	:	Electric Field
k	:	Electromechanical Coupling Factor
eV	:	Electrovolt
FRAM	:	Ferroelectric Random Accessible Memory
Hz	:	Hertz
h	:	Hour
kHz	:	Kilohertz
kV	:	Kilovolt
kV/cm	:	Kilovolt per centimeter
MHz	:	Megahertz
MPa	:	Megapascal
m	:	Meter

m^2	:	Meter square
μm	:	Micrometer
$\mu C/cm^2$	:	Microcoulomb per centimeter square
MEMS	:	Microelectromechanical Systems
MBE	:	Molecular Beam Epitaxy
nm	:	Nanometer
min	:	Minute
MPB	:	Morphotropic Phase Boundary
%	:	Percentage
pC/N	:	Picocoulomb per Newton
PRFM	:	Piezo Response Force Microscope
τ	:	Pockels Coefficient
PVDF	:	Polyvinylidene Fluoride
PLD	:	Pulsed Laser Deposition
RF	:	Radio Frequency
n	:	Refractive Index
P_r	:	Remnant Polarization
RTA	:	Rapid Thermal Annealing
rpm	:	Revolutions per Minute
P_s	:	Spontaneous Polarization
S	:	Strain
SEM	:	Scanning Electron Microscope
TG	:	Thermogravimetric
~	:	Tilde
TCO	:	Transparent Conductive Oxide
UV-Vis	:	Ultra Violet – Visible Spectroscopy
V	:	Voltage
wt	:	Weight
XRD	:	X-ray Diffraction
$BaTiO_3$	:	Barium Titanate
GZO	:	Gallium doped Zinc Oxide
ITO	:	Indium doped Tin Oxide
PLZT	:	Lead Lanthanum Zirconate Titanate
PMN	:	Lead Magnesium Niobate

PT	:	Lead Titanate
PZ	:	Lead Zirconate
PZT	:	Lead Zirconate Titanate

LIST OF FIGURES

Figure No:		Page
2.1:	Crystal classes scheme for ferroelectric, pyroelectric and piezoelectric properties.	3
2.2:	Ferroelectric hysteresis loop.	5
2.3:	Distorted structure of PZT along tetragonal direction.	5
2.4:	Dielectric constant of $PbZrO_3$ (PZ) with temperature dependence.	7
2.5:	Typical double hysteresis loop.	7
2.6:	Domain formation scheme for cooling step.	8
2.7:	Direct and converse type of piezoelectricity.	10
2.8:	Perovskite structure of PZT; a) cubic non-polarized and b) tetragonal polarized.	11
2.9:	Phase structures of PZT; a) Ferroelectric, b) Paraelectric.	13
2.10:	Phase diagram of the PZT.	14
2.11:	Phase diagram of PLZT.	16
2.12:	Photovoltaic mechanism; a) Semiconductor p-n junction and b) ferroelectric thin film.	18
2.13:	Thermal evaporation systems.	22
2.14:	Pulsed laser deposition system.	23
2.15:	Physical sputtering system.	23
2.16:	Sol-gel thin film coating process.	25
2.17:	Thin film deposition by spin-coating method.	26
2.18:	Indium crystal structure.	28
3.1:	PZT precursor solution preparing route.	31
3.2:	Cobalt doped PZT precursor solution preparing route.	32
3.3:	PLZT solution preparing route.	32
3.4:	Substrate cleaning procedure.	33
3.5:	Electrode diameters of the mask measured by SEM.	36
4.1:	DTA-TG analyses of the PZT with 2%-mole Pb excess.	41
4.2:	DTA-TG analyses of the PLZT with 5%-mole Pb excess.	42
4.3:	XRD patterns of the a) $Pt_{(111)}/Ti/SiO_2/Si_{(100)}$ substrate, b) PZT thin films with 2%-mole Pb excess coated on $Pt_{(111)}/Ti/SiO_2/Si_{(100)}$ substrates.	43

4.4: XRD patterns of the PLZT thin films with 5%-mole Pb excess coated on $Pt_{(111)}/Ti/SiO_2/Si_{(100)}$ substrates. 44

4.5: SEM micrograph of the PZT thin film (TF10) with stoichiometric composition annealed at 600ºC for 1 hour. 45

4.6: SEM micrographs of the PZT thin film (TF9) with 2%-mole Pb excess annealed at 600ºC for 1 hour; a) 1000x and b) 5000x. 46

4.7: SEM micrographs of the PZT thin film (TF14) with 2%-mole Pb excess annealed at 700ºC for 1 hour; a) 1000x, b) 2000x, c) 5000x and d) 10000x. 46

4.8: SEM micrographs of cross-section of the PZT thin film (TF13) with 2%-mole Pb excess annealed at 700ºC for 1 hour; a) 10000x, b) 50000x. 47

4.9: SEM micrographs of the PLZT thin films with the 5%-mole Pb excess annealed at 650ºC for 1 hour; a) 2000x (TF25) and b) 5000x (TF24). 48

4.10: SEM micrographs of the PLZT thin film (TF26) with the 5%-mole Pb excess annealed at 725ºC for 1 hour; a) 1000x, b) 5000x and c) 10000x. 48

4.11: SEM micrographs of the PLZT thin film (TF29) with the 5%-mole Pb excess annealed at 725ºC for 1 hour; a) 500x, b) 1000x, c) 2000x and d) 5000x. 49

4.12: SEM micrographs of the PLZT thin film (TF30) with the 5%-mole Pb excess annealed at 725ºC for 1 hour; a) 1000x, b) 2000x, c) 5000x and d) 10000x. 50

4.13: SEM micrographs of the PLZT thin film (TF27) with the 20%-mole Pb excess annealed at 725ºC for 1 hour; a) 500x, b) 1000x, c) 5000x, d) 5000x, e) 10000x and f) 20000x. 51

4.14: Thin film probe station. 52

4.15: Dielectric constant versus temperature of the PZT thin film (TF7) with 2%-mole Pb excess composition, annealed at 600ºC for 1 hour. 53

4.16: Dielectric constant versus temperature of the PZT thin film (TF16) with 2%-mole Pb excess composition, annealed at 700ºC for 1 hour. 53

4.17: Dielectric constant versus temperature of the PLZT thin film (TF20) with 5%-mole Pb excess composition, annealed at 650ºC for 1 hour. 54

4.18: Dielectric constant versus temperature of the PLZT thin film (TF27) with 5%-mole Pb excess composition, annealed at 725ºC for 1 hour. 54
4.19: J-E characteristics of the PZT thin film with the 2%-mole Pb excess composition annealed at 600ºC for 1 hour (TF9). 55
4.20: J-E characteristics of the PZT thin film with 2%-mole Pb excess composition annealed at 700ºC for 1 hour (TF16). 56
4.21: XRD pattern of the GZO coated glass substrate. 57
4.22: XRD patterns of the PZT thin films with 2%-mole Pb excess coated on GZO coated glass substrates. 57
4.23: XRD patterns of the PLZT thin films with 5%-mole Pb excess coated on GZO coated glass substrates. 58
4.24: SEM micrographs of the PZT thin film (TCO3) with the 2%-mole Pb excess annealed at 600ºC for 1 hour; a) 1000x, b) 5000x. 59
4.25: SEM micrographs of the PZT thin film (TCO7) with the 2%-mole Pb excess annealed at 700ºC for 1 hour; a) 1000x, b) 1000x, c) 5000x and d) 5000x. 59
4.26: Selected spots of the TCO7 thin film for EDX analyses. 60
4.27: EDX analyses of the inside of the rosette (Area 1) for TCO7. 61
4.28: EDX analyses of the matrix phase (Area 2) for TCO7. 61
4.29: SEM micrographs of the PZT thin film (TCO27) with the 2%-mole Pb excess annealed at 725ºC for 1 hour; a) 1000x, b) 5000x. 62
4.30: SEM micrographs of cross-section of the PLZT thin film (TCO16) with 5%-mole Pb excess annealed at 650ºC for 1 hour; a) 20000x, b) 20000x. 62
4.31: SEM micrographs of the PLZT thin film (TCO23) with the 5%-mole Pb excess annealed at 700ºC for 1 hour; a) 1000x, b) 5000x, c) 20000x. 63
4.32: SEM micrographs of the PLZT thin film (TCO29) with the 5%-mole Pb excess annealed at 725ºC for 1 hour; a) 125x, b) 1000x, c) 2000x. 64
4.33: SEM micrographs of the PLZT thin film (TCO30) with the 5%-mole Pb excess annealed at 725ºC for 1 hour; a) 125x, b) 250x, c) 1000x. 64

4.34: SEM micrographs of the PLZT thin film (TCO31) with the 5%-mole Pb excess annealed at 725ºC for 1 hour; a) 125x, b) 250x, c) 1000x. 65
4.35: Optical transmittance values of the PZT thin films with the 2%-mole Pb excess composition and annealed at 600ºC and 725ºC. 66
4.36: Optical band gap values of the PZT thin films with the 2%-mole Pb excess composition and annealed at 600ºC and 725ºC for 1 hour. 67
4.37: Optical transmittance values of the PLZT thin films with the 5%-mole Pb excess composition and annealed at 700ºC and 725ºC. 68
4.38: Optical band gap values of the PLZT thin films with the 5%-mole Pb excess composition and annealed at 650ºC, 700ºC and 725ºC. 68
4.39: PRFM analyses of PZT thin film (TCO6) annealed at 700ºC for 1 hour; a) Topography, b) PRFM Phase and c) PRFM Amplitude. 69
4.40: PRFM analyses of PLZT thin film (TCO32) annealed at 700ºC for 1 hour; a) Topography, b) PRFM Phase and c) PRFM Amplitude. 70
4.41: AFM surface image of PLZT film annealed at 725ºC and pyrolysis steps as 200ºC 2 min + 430ºC for 5 min. 71
4.42: AFM surface image of PLZT film annealed at 725ºC and pyrolysis steps as 200ºC 5 min + 430ºC for 10 min. 71
4.43: AFM surface image of PZT film annealed at 600ºC and pyrolysis steps as 250ºC 5 min + 400ºC for 5 min. 72
4.44: AFM surface image of PZT film annealed at 700ºC and pyrolysis steps as 250ºC 5 min + 400ºC for 5 min. 72
4.45: XRD pattern of PZT powders with 2%-mole Pb excess calcinated at 800ºC for 2 hours. 73
4.46: XRD pattern of 0.05-Co PZT powders calcinated under different conditions. 74
4.47: XRD pattern of 0.20-Co PZT powders calcinated under different conditions. 74
4.48: XRD pattern of 0.20-Co PZT powders prepared with isopropanol and calcinated under different conditions. 75
4.49: XRD patterns of PZT pellets with 1%-mole and 2%-mole Pb excess sintered at 1260ºC for 4 hours. 75
4.50: XRD patterns of 0.05-Co PZT pellets sintered at 1260ºC for 2 hours. 76

4.51: XRD patterns of 0.20-Co PZT pellets sintered at 1260ºC for 2 hours and 4 hours. 76
4.52: Polarization-electric field hysteresis loops of the PZT with 1%-mole Pb excess. 77
4.53: Strain-electric field hysteresis loops of the PZT with 1%-mole Pb excess. 78
4.54: Polarization-electric field hysteresis loops of the 0.05-Co PZT. 78
4.55: Strain-electric field hysteresis loops of the 0.05-Co PZT. 79

LIST OF TABLES

Table No:		Page
2.1:	Substrate materials for PZT and their prominent features.	21
3.1:	Chemicals used for solution preparing.	30
3.2:	Spin coating parameters for solution types.	34
3.3:	Pyrolysis and annealing conditions of the films.	35
3.4:	Calcination parameters of the powders	37
3.5:	Sintering parameters of the pellets.	38
4.1:	Dielectric values of the measured films.	55
4.2:	EDX analyses of the inside of the rosette (Area 1) for TCO7.	60
4.3:	EDX analyses of the outside of the rosette (Area 2) for TCO7.	60
4.4:	Band gap values of the films.	69

1. INTRODUCTION

In recent years, there is a big demand for electronic devices due to the development of technology and its place in human life. This demand led to a lot of scientific research on wide areas [1]. The devices which we are using in our daily life are getting smaller, and also they are expected to be really fast [2]. Some materials such as $BaTiO_3$ (BTO), $PbTiO_3$ (PT), $Pb(Zr, Ti)O_3$ (PZT), $Pb(La, Zr, Ti)O_3$ (PLZT) have especially drawn attention from the researchers working on electronic materials. These materials are ceramics and they exhibit ferroelectric behavior [3]. Ferroelectric materials have spontaneous polarization under a critical temperature called the Curie temperature (T_c). It is possible to reorient their polarization states under electric field [2]. One of the most significant application areas of the materials which possess ferroelectric behavior is non-volatile memories. Ferroelectric materials also exhibit many important characteristic features like piezoelectricity, pyroelectricity and electro-optic properties [3]. These features led to many application areas like sensors, flexible microelectronics, energy harvesting systems, transducers, actuators and capacitors [4, 5].

Some ferroelectric materials such as PZT mentioned above are solid solution and PZT has good dielectric properties and electromechanical coupling coefficients at the specific composition called as morphotropic phase boundary (MPB). PZT is one of the most studied solid solutions to achieve superior electrical properties. Its compositions close to the MPB have large spontaneous polarization, electromechanical coupling factor and, low dielectric loss [3, 5]. Besides the electronic properties, optical properties have also been studied. The combination of electronic and optical properties "the ferroelectric photovoltaic" devices have also been studied [6]. Studies in this area has opened a way to produce devices like optic shutters, displays, modulators, color filters, the optical waveguide for photonic systems [7-9]. PLZT is another popular ferroelectric photovoltaic material for these studies due to its transparency and electrical properties. Lanthanum adding to PZT as a A-site dopant enhances domain mobility, as a result of this improvement occurs on dielectric properties and optical transparency [10, 11].

This study has focused on the preparation of PZT and PLZT thin films by sol-gel spin-coating method on different substrates. Beside this study, bulk PZT was also studied using powders synthesized with sol-gel process. Conventionally, PZT has been produced by the solid-state reaction method. This procedure requires high processing

temperatures (~>1250ºC). Solid-state reaction method may have large particle size distribution, impurities from ball milling. The sol-gel method is an alternative low-temperature process to obtain powders with homogeneous size and composition [12].

1.1. Aim of the Study

The aim of the study was the investigation of the electrical and optical properties of PZT and PLZT thin films deposited on $Pt_{(111)}/Ti/SiO_2/Si_{(100)}$ and gallium-doped zinc oxide (GZO) coated glass substrates with different precursor solutions and processing conditions. Current-voltage (I-V), UV-Vis measurements, scanning electron microscope (SEM), X-ray diffraction (XRD), piezo response force microscope (PRFM) and electrical characterizations were done on the way of this aim.

2. LITERATURE REVIEW

2.1. Polarity of Crystal Classes

Crystalline materials exist with 7 basic crystal systems. These crystal systems are cubic, orthorhombic, monoclinic, triclinic, hexagonal, tetragonal and trigonal. These systems create different atomic orders. Each crystal system also has symmetry with respect to a point. All symmetry elements are being grouped as “crystal classes”. These crystal classes can be also called “point groups” because of they are qualifying the crystal systems by to their symmetry for a point. For the 7 crystal classes, there are 32-point groups, they can be seen in Figure 2.1 [2]. Symmetry relations can be explained by 4 basic symmetry operators. These operators are the translation, mirror, rotation, and inversion. Depending on these operators some of these point groups possess centrosymmetric or non-centrosymmetric behavior. 11-point groups are centrosymmetric and 21 of them are non-centrosymmetric. This difference brings many different properties to materials. 20-point group of the non-centrosymmetric group has a relation between stress and polarization. These materials which one of these 20-point group can have polarization when they are applied stress. This behavior called as “piezoelectricity” occurs due to atomic displacements. These atomic displacements create a non-compensated charge balance. Due to that material possess polarization [2, 13].

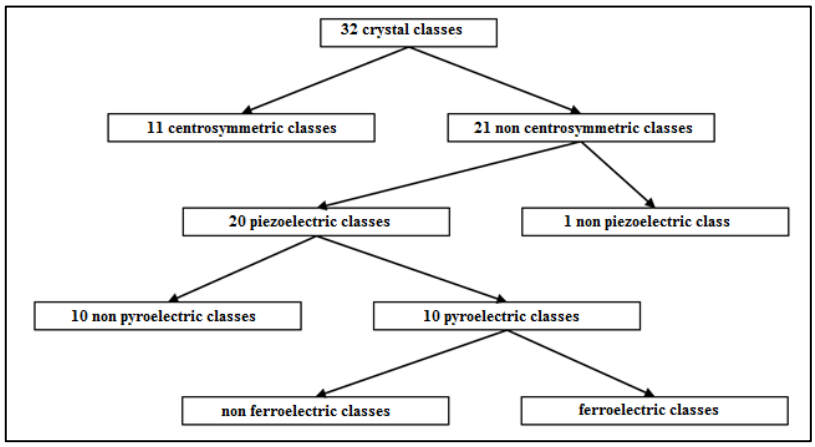


Figure 2.1: Crystal classes scheme for ferroelectric, pyroelectric and piezoelectric properties.

These 20 non-centrosymmetric point groups are divided into another two groups due to their “pyroelectric” properties. 10-point groups possess this pyroelectric property due to their polar axis. These point groups have spontaneous polarization, so they have a polar axis. Spontaneous polarization is temperature dependent in these point groups. With temperature dependence, a charge flow can be observed because of the existence of spontaneous polarization. With reversible spontaneous polarization, it is possible to reorient the positive and negative charges. This property called “ferroelectricity” and the materials that possess it named “ferroelectric materials” [2].

2.2. Ferroelectricity

Ferroelectricity indicates the polar materials with spontaneous polarization. The spontaneous polarization is generated from the non-centrosymmetric arrangement in the unit cell. This polarization can be reoriented between two equilibrium states. Switching process is done by applying of sufficient electric field to the dipoles i.e. to the material. This switching mechanism brings a hysteresis loop on polarization level (P) versus electric field (E) which can be seen in Figure 2.2 [14, 15].

By applying a low-level electric field to the material, polarization increases linearly. This part of the electric field applied can be seen as A-B in Figure 2.2. With the increment at the electric field, the domains discordant to electric field direction starts to be being orientated (B-C). After a certain electric field level, all domains are aligned in the same direction. This point referred to as C in the figure. At the following application of the electric field, polarization increases linearly a small amount. Domains lose their orientation when the electric field starts to being applied in a different direction. At the point that the electric field is zero, these materials still have polarization. This polarization named as “remnant polarization”, point E in Figure 2.2. The amount of electric field needed to decrease polarization to zero is referred to as “coercive field” (E_C). This electric field level can be seen at the F point in the figure. At the G point, all domains are aligned in the opposite direction of C point. This process creates a hysteresis loop [14].

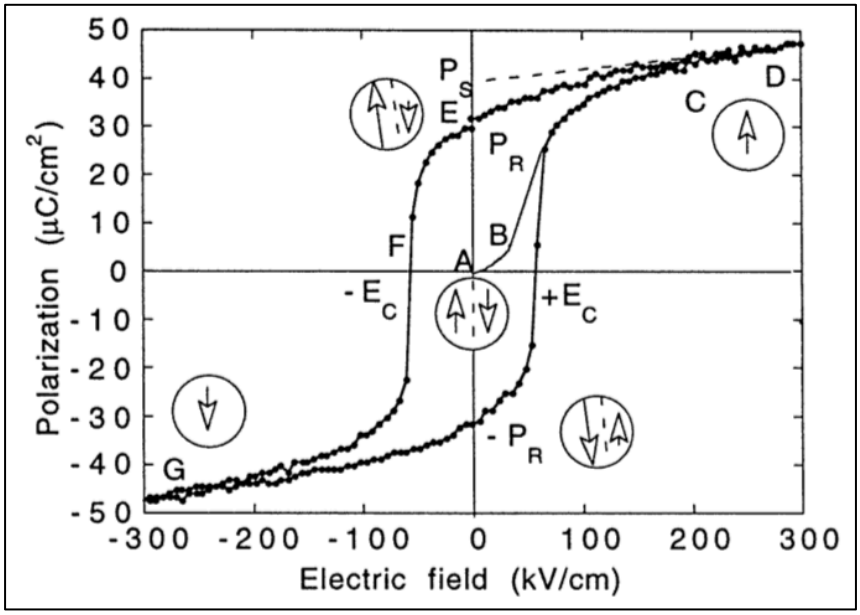


Figure 2.2: Ferroelectric hysteresis loop.

In order to their piezoelectric properties, ferroelectric materials create a strain (S) versus electric field (E) loop too. Due to the converse piezoelectric effect, domain walls move during the electric field applied. This loop can be symbolized with butterfly shape [14]. Ferroelectric crystals have regions with a uniform alignment of dipoles but also spontaneous polarization in some regions may be different. These regions with spontaneous polarization are domains [16].

For a typical ferroelectric material, generally, its unit cell type is ABO_3 perovskite structure. Also, the structures of tungsten-bronze, pyrochlore phase etc. possess ferroelectric properties without crystallizing in perovskite structure. Perovskite structure can be seen in Figure 2.3.

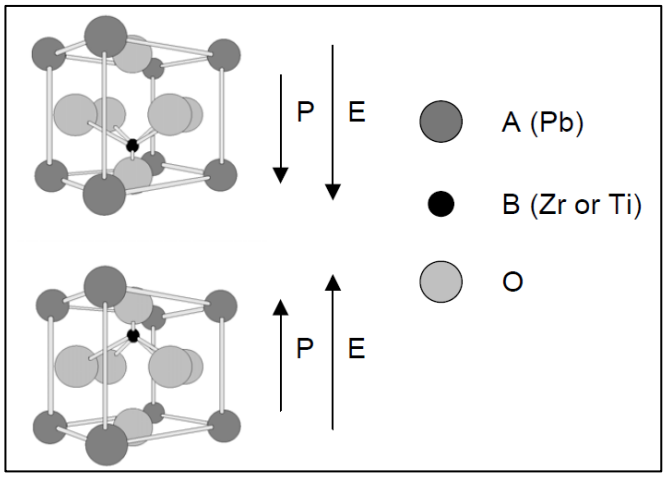


Figure 2.3: Distorted structure of PZT along tetragonal direction.

At the corners, A atom locates. Center of faces located by oxygen atoms and finally in the body center B atom locates [2, 16]. Perovskite structure consists of oxygen octahedra links. In ferroelectric materials, "A" atom is generally large atoms such as K^{+}, Ba^{2+}, and "B" atom is small atoms such as Ti^{4+}, Zr^{4+}. Some structural distortions exist in these systems due to sizes of cations. This situation affects the stability of the perovskite structure [16]. There is a tolerance factor described as "t" for perovskite structure. If t value is between 0.88 and 1.09, perovskite structure can be defined as stable [17].

2.2.1. Phase Transitions

Ferroelectric materials possess a critical structural phase transition at a certain temperature. This phase transition temperature called as Curie temperature (T_c). This phase transition takes place between the high-temperature paraelectric phase and low-temperature ferroelectric phase. This phase transition creates dimensional changes in the unit cell of the crystal structure. Dimensional changes in the crystal cause important for the electrical properties. For a cubic structure, all dimensions of the cube are the same and the angles between them are 90 degrees. When the temperature decreases some elongations occurs. The elongation directions changes with the current stable phase. While rhombohedral structure's elongation occurs along the [111] direction, for the tetragonal structure, it occurs along the [001] direction and finally, for the orthorhombic structure it is [110] direction [18].

Above the certain temperature, ferroelectric material possesses paraelectric phase and this phase has no spontaneous polarization [18]. Thermodynamic properties of material changes dramatically and also crystal structure changes at the close temperatures to the Curie temperature, Dielectric constant is one of these thermodynamic properties and it changes with respect to Curie-Weiss Law given in Equation 2.1. Dielectric constant reaches to the maximum level near the Curie temperature. It can be seen in Figure 2.4 [19].

$$\boldsymbol{\varepsilon = \varepsilon_0 + \frac{C}{T - T_O} \approx \frac{C}{T - T_O}} \tag{2.1}$$

According to this law, it can be seen that when the temperature increases above to the Curie temperature, dielectric property falls abruptly. In Equation 2.1, T_0 can be different from Curie temperature with respect to the phase transition order. For first-order phase transition $T_0 < T_c$, second-order transition $T_0 = T_c$ [19].

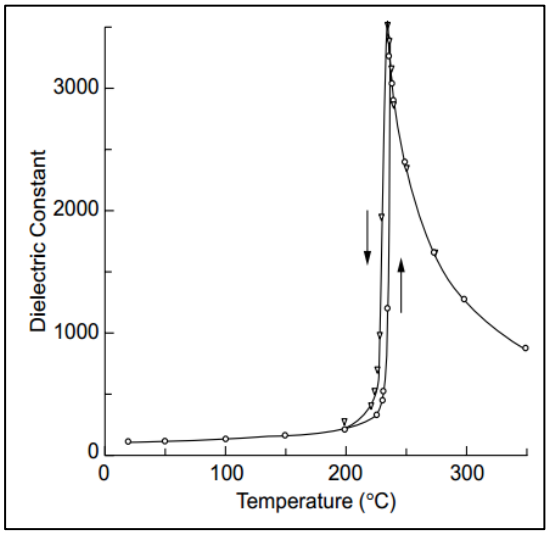


Figure 2.4: Dielectric constant of $PbZrO_3$ (PZ) with temperature dependence.

Antiferroelectricity is another phenomena for the materials. These materials consist of adjacent rows of dipoles. The dipoles are aligned antiparallel to each other, so this leads to no net total polarization. With the applying an external electric field, these dipoles can be aligned to a parallel state. The phase turns to ferroelectric by the induced electric field. As a result of this, antiferroelectric materials possess double hysteresis loop on the P-E diagrams which is given in Figure 2.5 [19, 20].

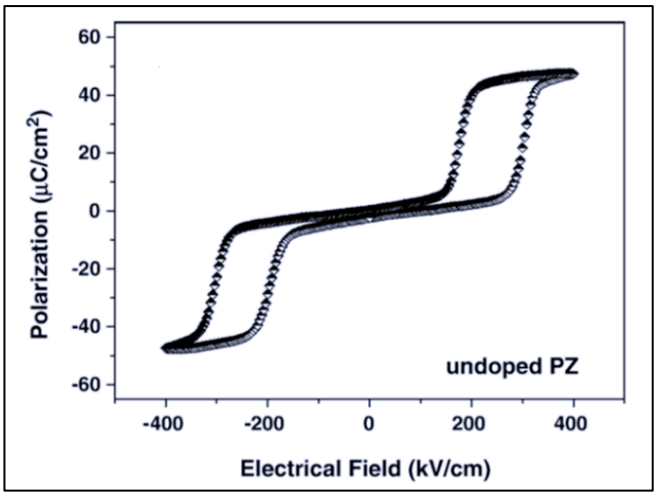


Figure 2.5: Typical double hysteresis loop.

2.3. Domains

Ferroelectric materials cannot be polarized uniformly without any external field. If all of the dipoles aligned with one direction, the energy of the system would be high, and this brings the instability. Spontaneous polarization can have more than equivalent directions. This situation leads to the material to create regions with same polarization direction called as “domain”. The reason for the formation of these walls is minimizing the electrical and mechanical constraints of the material i.e. system tends to decrease energy level. Any group of unit cells with same polarization route forms a domain. It means a domain has homogenous polarization direction. The domain created by unit cells with any other polarization direction separated with the other domains by “domain walls”. Domain walls with 180 degrees separate the domains with the opposite spontaneous polarization direction. If the domain walls are separated with 90 degrees, it means the angle of the spontaneous polarization direction of the domains is 90 degrees. Domain wall angle is effective on strain tensor for ferroelectric materials. If the domain wall has 90 degrees angle, the material is also ferroelectric and ferroelastic. The direction of spontaneous polarization, so the direction of each region called as a domain can be transformed into the same direction. This process called “poling” and needs a strong electric field. A schematic view of domain structure is given in Figure 2.6 [2, 14, 19, 21].

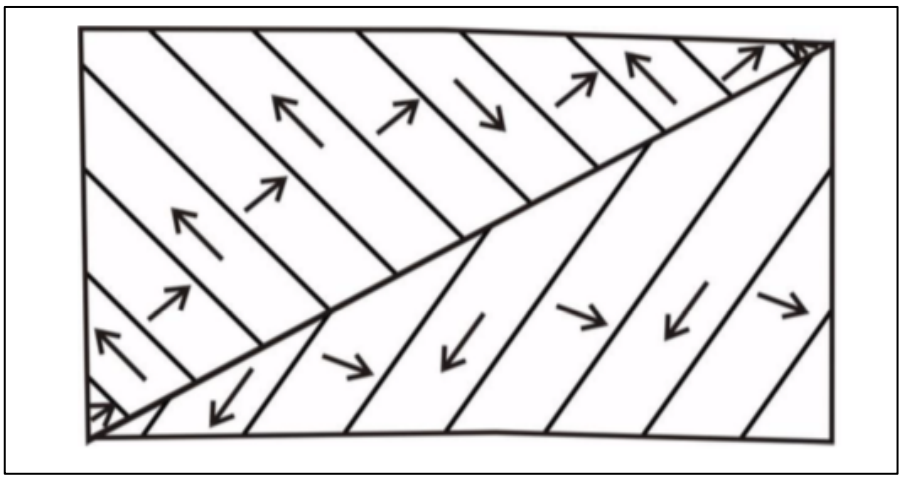


Figure 2.6: Domain formation scheme for cooling step.

2.4. Relaxor Ferroelectrics

Relaxor ferroelectrics are one of the classes of ferroelectric materials with a specific behavior. Ferroelectrics can be grouped into three classes. The classification is done with the basis of material's electrical properties and phase transition behavior. The main difference between normal ferroelectrics and relaxor ferroelectrics can be seen at phase transitions. Phase transition of a normal ferroelectric material occurs with a sharp transition without any inter-phases [16, 22].

Relaxor state occurs with the appearing of polar regions with distributed orientations while the material is being cooled under the certain temperature called "Burns temperature". The most-known example to relaxor material is $Pb(Mg_{1/3}Nb_{2/3})O_3$ (PMN) in the perovskite structure with disordered non-isovalent ions [23].

Under the Curie temperature, normal ferroelectric materials possess polarization-electric field hysteresis loop. Mostly these materials have large remnant polarization values. Relaxor ferroelectric materials shows slim hysteresis loop. With the application of a sufficient high electric field level, the polar regions of the relaxor material at the nanoscale can be induced. Most of the time, the polar regions stay at their random orientation positions resulting with small remnant polarization. Also, normal ferroelectrics losses their polarization at the Curie temperature. Above this temperature, the material doesn't have polar domains and net spontaneous polarization. Contrary to this, the induced polarization of the relaxor ferroelectric material decreases slowly. Dielectric permittivity of the normal ferroelectrics shows a sharp and narrow peak at the Curie temperature. This relation being explained with Curie-Weiss Law. Dielectric response of the material and Curie temperature is independent of the frequency for normal ferroelectrics. For the relaxor ferroelectrics, these materials have broad peaks with frequency dependence [24, 25].

2.5. Piezoelectricity

Piezoelectrics are the materials produce mechanical output with an electrical input or the inversion of that. This property was discovered in 1880 by Curie brothers. First application area of piezoelectricity were ultrasonic transducers with natural piezoelectric material quartz. During the Second World War, $BaTiO_3$ and $Pb(Zr,Ti)O_3$ started being used due to their higher piezoelectric properties [2]. With the following

years that, piezoelectricity gained a more important role in the commercial area like transducers, medical instruments, actuators. Due to the development of technology, these materials started being produced in thin film forms for microelectromechanical systems [26].

Piezoelectricity defines the linear relationship between mechanic and electrical forces. The materials which exhibit this property can create polarization as a result of the mechanical pressure. This piezoelectric behavior called as “direct effect”. Tensile and compressive stresses create opposite directions of polarity and the value of generated voltage is proportional with the applied stress. These materials also possess strain when they exposed to the electric field. This behavior called as “converse effect”. Direct and converse effect of piezoelectricity is given in Figure 2.7. The piezoelectric material creates space charges on its surface when the material applied a certain amount of stress. Mechanism of this space charge creation explained with the deformation of the crystal structure. This deformation creates dipole moments in the crystal. As mentioned above, the inverse effect is valid too. Displacement of ions in crystal structure results with a strain in the material [2, 14].

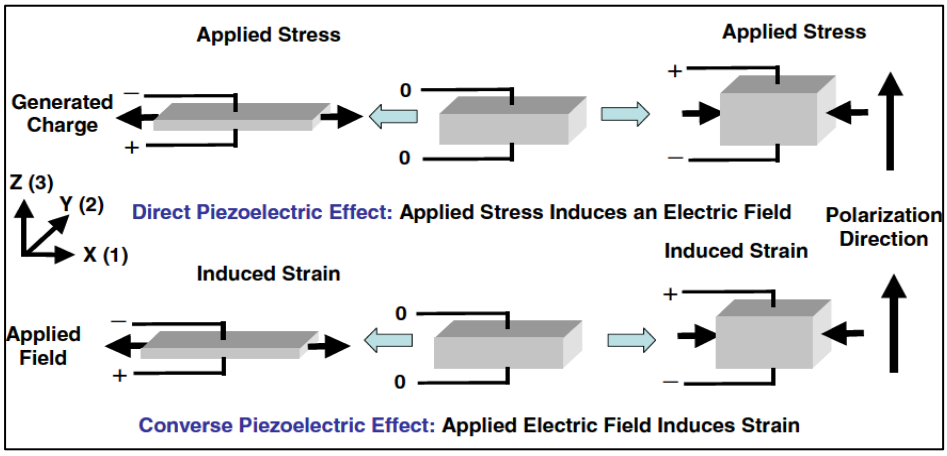


Figure 2.7: Direct and converse type of piezoelectricity.

To describe the piezoelectric effect, there are two different equations being used for direct and converse effect.

$$\boldsymbol{D_i = d_{im} X_m} \tag{2.2}$$

$$\boldsymbol{x_{ij} = d_{mi} E_i} \tag{2.3}$$

X sign represents the applied stress, E is the electric field applied, x is the strain, ε is the dielectric constant and s is the compliance of material. d_{ijk} and d_{mij} are the piezoelectric coefficients with third-rand tensors. Unit of these coefficients are C/N and m/V, respectively. Value of "i" can be 1, 2 or 3 and "m" can be 1 to 6. Strain and stress tensors are symmetrical. Also, the piezoelectric coefficient tensor is symmetric too for the same indices. So, d_{im} is equal to d_{mi}. Direct and converse effect equations given at above defines the piezoelectric property with respect to direction, i.e., these properties are directional. D_{33} defines the polarization at the direction 3, and this polarization occurs due to stress applied from direction 3. This notation is valid for converse effect too. For obtaining all of the directions, the matrix of the materials can be prepared with respect to direct and converse effect equations [14, 16]. In Figure 2.8, polarized structure of PZT is given [2].

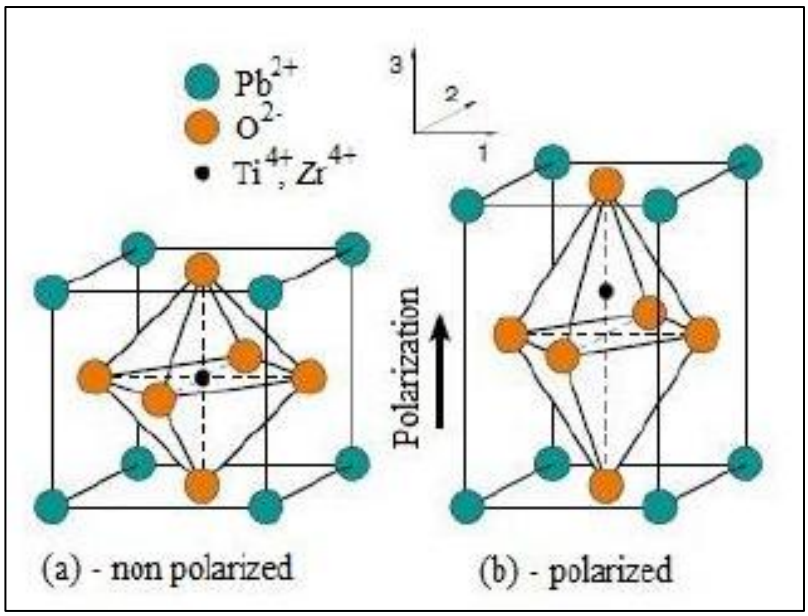


Figure 2.8: Perovskite structure of PZT; a) cubic non-polarized and b) tetragonal polarized.

Electromechanical coupling factor characterizes the total electromechanical strength of the system. This factor is showed as "k_{33}" generally. "k" is the root of the ratio of stored mechanical energy to given electrical energy or stored electrical energy to given mechanical energy. The value of "k" can never be equal to 1 because of the energy losses and impossible energy conversion with 100% efficiency [14, 16].

2.6. Ferroelectric Materials

Ferroelectric materials are being used widely in commercial scale due to their spontaneous polarization property and the other properties like piezoelectricity and pyroelectricity. Barium titanate, potassium niobate, barium strontium titanate can be shown as typical examples of ferroelectric properties [14, 27]. They have been studied in the bulk form for a long time. Besides these bulk materials, thin film forms of these compositions showed important properties [28]. For the thin film form of ferroelectrics, polycrystalline thin films are mainly being deposited on substrates like fused quartz, silicon, platinum, gold and more. From the 1960s, ferroelectric and piezoelectric thin films were fabricated to produce acoustic wave devices, memory applications, electro-optic devices. With the development in the ferroelectric industry in the 1980s and 1990s, PZT became the most important ferroelectric material and started being used for waveguide devices, pyroelectric sensors, FRAM applications and also PLZT have taken interest for mainly electro-optic applications [5, 28]. Thin film technology led to the development of numerous applications. For recent years, the main study area of the thin films is microelectromechanical systems (MEMS). These systems realize the miniature devices with important properties [29].

For the PZT side, this material became the most studied one. By Chengtao, PZT thin films were deposited on Pt/Ti/SiO_2/Si substrates with pulsed laser deposition (PLD) method to reveal remnant polarization and coercive field levels to lead a route to DRAM and FRAM targets [30]. Also, Lee Sung developed PZT multilayer systems with the films had different Ti/Zr ratio for transducers. PLZT is also studied widely [31]. Khodorov studied with Lanthanum doping effect on electrical properties of PZT with 65/35 ratio of Zr to Ti [9].

2.6.1. Lead Zirconate Titanate

MEMS need devices like microsensors, microactuators. These materials have to be the ability to convert energy types one to another. This requirement takes interest to the piezoelectric materials. In recent years, PZT is the most commercialized and widely studied piezoelectric materials with its high dielectric properties and piezoelectric coefficients. Beside of PZT, polyvinylidene fluoride (PVDF) and zinc oxide (ZnO) are the other important piezoelectric materials for MEMS applications. PVDF as a polymer material, being used widely in biomedical applications because of

its bio-compatible property. ZnO is bio-compatible like PVDF. This material is being produced in shapes like nanowires, nanobelts easily but its low dielectric properties is a problem beside the production costs [14, 32, 33].

Compared to the others, PZT possess unique electrical behaviors. With the larger bandwidth, sensitivity, strength of the energy density, actuating performance, PZT is the most important lead-based ferroelectric system for nowadays. These materials can be used in FRAMs, transducers, actuators, sensors, energy harvesting systems and more [5, 28].

PZT is a solid solution ceramic and its open formula is $Pb(Zr_xTi_{1-x})O_3$. This solid solution has perovskite type ABO_3 with its piezoelectric and pyroelectric properties connected with ferroelectricity [2].

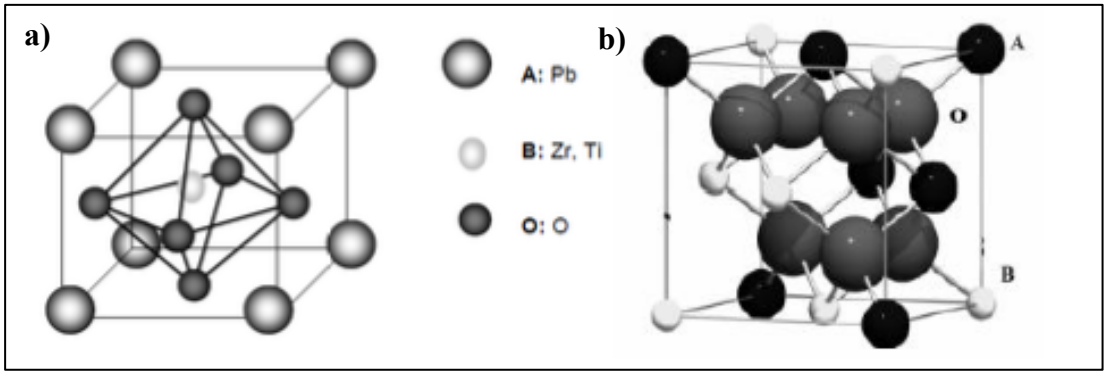


Figure 2.9: Phase structures of PZT; a) Ferroelectric, b) Pyrochlore.

ABO_3 perovskite structure can be seen in Figure 2.9, this is the main structure for PZT but, most of the time lead-deficient pyrochlore phase accompanies to perovskite structure because of crystallization kinetics. Pyrochlore phase exists with $A_2B_2O_7$ stoichiometric ratio. This phase occurs with deficiency of lead. In the atmosphere with partial oxygen pressure, non-equilibrated oxygen transport mechanism causes the pyrochlore phase. While PZT material being crystallized oxygen and lead reacts to form PbO. Deficiency of Pb keeps the PbO more stable. Adding the excess amount of Pb is a widely used solution to avoid this paraelectric pyrochlore phase. Excess lead compensates the volatile characteristic of PbO. Oxygen loss and gain is the main factor between perovskite and pyrochlore phases. With the deficiency of lead, oxygen gain is greater than the loss. So, the pyrochlore phase becomes stable. The excess amount of lead can cause greater oxygen loss to gain. This mechanism also causes the stabilization of pyrochlore with a fine matrix. Due to the adding excess amount of lead, the second mechanism is more common. Oxygen loss

and gain balance lead to the material to the complete perovskite phase from pyrochlore phase. Pyrochlore phase is strongly effective on the both of microstructure and electrical properties of the material. Presence of the pyrochlore phases reduces the electrical and piezoelectric properties of the material. Because of this, the processing step of the PZT is important to eliminate or limit the amount of pyrochlore phase [2, 34].

Phase diagram of the PZT solid solution can be seen in Figure 2.10. PZT can possess ferroelectric, anti-ferroelectric and, paraelectric phases with respect to composition and temperature. These electrical phases occur with different symmetry orders like tetragonal, orthorhombic, cubic and rhombohedral structures. With the dependency of the zirconium to titanium ratio, PZT transforms to tetragonal or rhombohedral phase as it can be seen in the figure. Higher titanium content leads the material to the tetragonal phase. Distortion of the structure can occur in several directions as mentioned before. These directions create different domain formations. Different domain formations separated by boundaries named as “domain walls” with 90 or 180 degrees [2, 34].

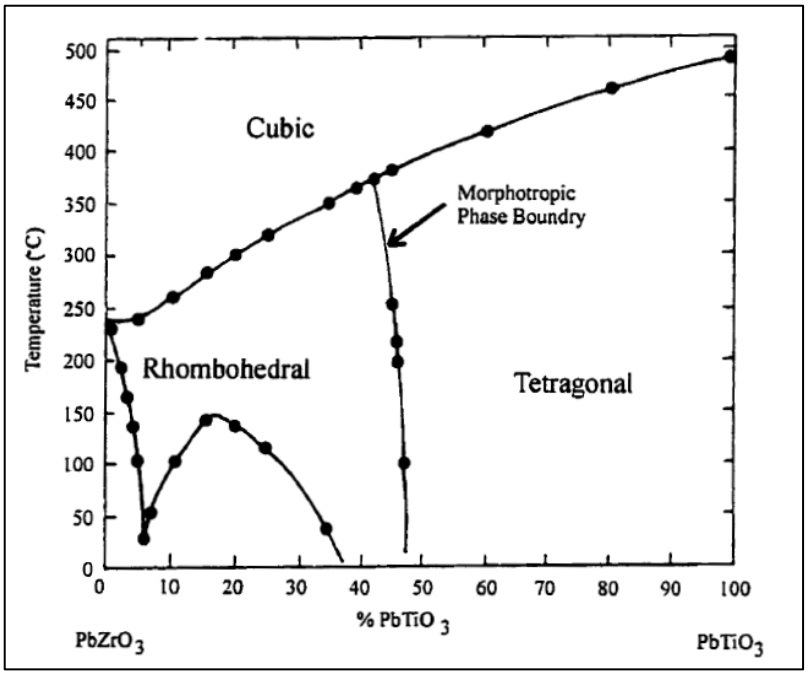


Figure 2.10: Phase diagram of the PZT.

The most studied composition of the PZT contains 52%-mole $PbZrO_3$ and 48%-mole $PbTiO_3$. This composition has been widely studied because of its position in the phase diagram. This ratio of zirconium to titanium occurs in the boundary of

tetragonal and rhombohedral phases called as “morphotropic phase boundary” (MPB). Dielectric and piezoelectric properties of the PZT reaches its highest level in this composition. The reason for this situation can be explained with the free energy level of the phases. At this composition, free energy levels are approximately equal for both phases and the electric field can induce all the domains in both phases. Total 14 directions for orientating the polarization is available at this boundary [2, 35].

For the perovskite phase, PZT has three main directions to crystallization. These directions are <100>, <110>, <111>. Obtaining the PZT with a preferred orientation leads material to higher dielectric and piezoelectric properties. If PZT doesn’t have a trigger mechanism for crystallization in a preferred orientation, different amount of the planes with different orientations occurs. Fabricating the PZT with adding template particles or growing it on epitaxial substrates induces the crystallization in one direction with nucleation. Crystallization of the planes depends on the thermodynamics. (100) is the most stable plane and this makes it promoted phase. With different techniques as mentioned above, crystallization proceeds with a preferred orientation due to lower free energy with the epitaxial condition [2].

Thin film form of PZT comes with problems named as defects. There are so many techniques for fabricating these films. Every fabricating technique brings challenges like residual stresses, interface adhesion problems, thermal mismatches between substrate and film etc. These challenges can be resulted with delamination of the films, peeling off to the substrate, surface cracks. Also, sol-gel spin-coated thin film annealing creates another problem like shrinkage and this creates a void on the surface due to evaporation of the solvent [36, 37].

2.6.2. Lead Lanthanum Zirconate Titanate

Lead lanthanum zirconate titanate is another solid solution with formula $Pb_{1-x}La_x(Zr_yTi_{1-y})_{1-x/4}O_3$ (PLZT). Considering the PLZT materials for dielectric applications started with the Heartling since he discovered PLZT at 1971. These materials are taking interest in high power capacitors, FRAMs, actuators due to their dielectric properties. PLZT is the most significant example to A-site substituted PZT based relaxor materials. Lanthanum addition to the PZT induces the relaxor behavior of the material. It leads material to have a wide range of lattice and domain structure. Obviously, these wide range parameters create gradually changing in electrical properties of the material. The addition amount of lanthanum is generally until 0.1%-

mol. To achieve the best dielectric properties, lanthanum addition is generally selecting as 0.09%-mol for studying close to MPB of the PLZT. Phase diagram of PLZT is given in Figure 2.11 [26, 38-40].

Selection of the composition is variable and important because of the target application. Increasing amount of lanthanum addition results with the changing in hysteresis loop of material. An increasing lanthanum makes hysteresis loop slimmer. This is an important feature for energy storage applications. This slim hysteresis loop indicates more efficient energy storage performances [40, 41]. It can be said that La^{+3} ions change the behavior of material to relaxor ferroelectric from normal ferroelectric and this degree of relaxor behavior increases with the added La amount [39, 41].

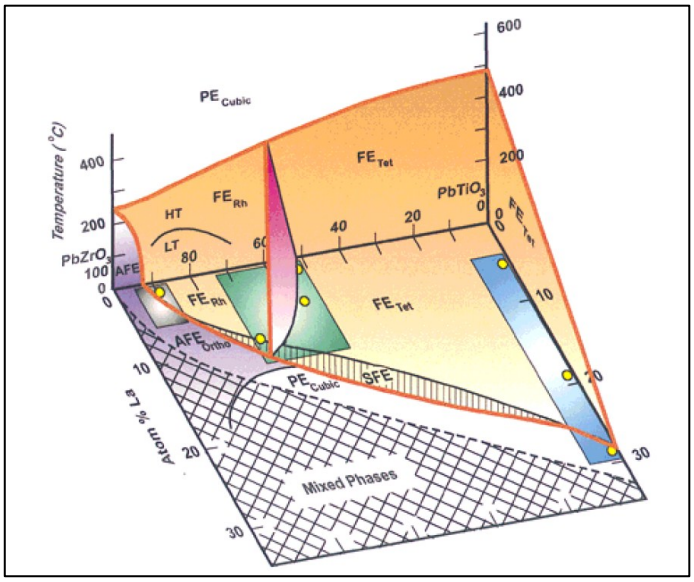


Figure 2.11: Phase diagram of PLZT.

Lanthanum addition to PZT also stabilizes antiferroelectric phase. This behavior is important especially for titanium-rich compositions as easer to sintering, with lanthanum addition, the electric field for switching decreases. Titanium-rich compositions also have lowered transition temperature [40, 41].

2.7. Optical Approach to Ferroelectrics

In this section of the thesis optical behavior of the ferroelectric materials will be discussed.

2.7.1. Photovoltaic Effect and Technology

Photovoltaic technology can be defined as the generating of electricity from a light source. Photovoltaic cells are called as “solar cells” widely because of sunlight is the main light source for our world. This technology has an important role on the way of converting energy to electricity because of its path to do that. Photovoltaics generates electricity with a clean and reliable route. Nowadays, the photovoltaic industry is based on semiconductor solar cells. For a typical solar cell, with the illuminating, electron and hole pairs are being generated at the depletion region. These pairs act as charge carriers and they create photocurrent and voltage. Harvested amount of the voltage changes with the energy band gap of the material. Photovoltaic cells require to have a good conversion efficiency. For that, silicon and group III-V semiconductor compounds are being studied widely. Single and multi-junction types of photovoltaic cells are useful for space and terrestrial applications. In recent 30 years, at the point researches achieved approximately 43.5% efficiency about these solar cells. Costs to produce solar cells, increasing efficiency are still the main problems in this industry [29, 42].

2.7.2. Ferroelectric Photovoltaics

As mentioned in the previous sections, ferroelectric materials have a non-centrosymmetric arrangement, and this leads materials to have spontaneous polarization. PZT can be shown as the main example for these materials. It was discussed lanthanum adding to PZT can cause photovoltaic responses. PZT has its highest dielectric and piezoelectric properties at the Ti to Zr ratio at 48/52 composition. Niobium doping to this composition increasing the “transverse piezoelectric coefficient” of the material and also pyroelectric response. With the same approach, a doping element, lanthanum with a certain amount enhances the optical properties of the PZT [29, 42].

The ferroelectric photovoltaic mechanism can be explained with the wavelength and energy band relationship. A schematic view of the mechanism is given in Figure 2.12. An illuminated ferroelectric photovoltaic creates electron and hole pairs corresponding to the wavelength of the light. With the “internal electric field” created by the polarization of the material drives the charge carriers to the electrodes. As a result of this, the photovoltaic output voltage achieved. Junction systems separate the

electron and hole pairs to the p and n junctions. The system separates these pairs by the electric field at the depletion layer. So, junction systems have a different route about the photovoltaic effect with comparing to bulk and film types [29, 43].

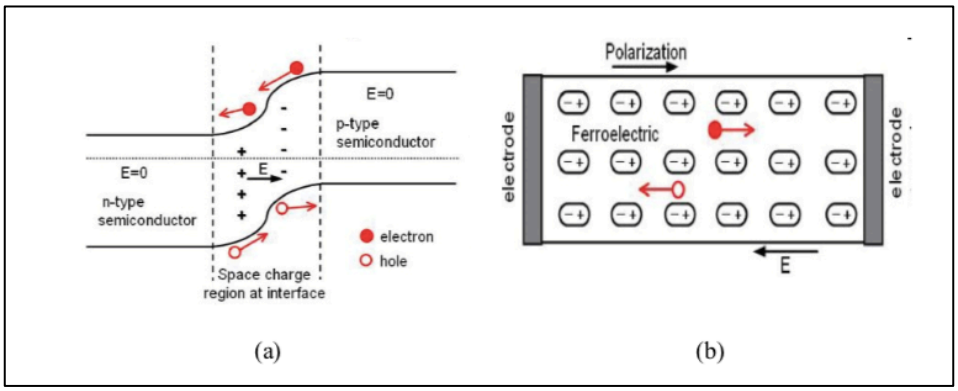


Figure 2.12: Photovoltaic mechanism; a) Semiconductor p-n junction and b) ferroelectric thin film.

In $BiFeO_3$ thin films, it was found that the photovoltage values are higher than the band gap of the material. This material gave approximately 20V with its 2.67 eV band gap (E_g) value. This showed that the photovoltage level of a material can be increased by polarization values of material. Poling of the material was the first approximation to achieve higher photovoltaic output levels. Poling process is giving voltage higher than the coercive field to the ferroelectric material. It causes the orientation of the domains in the same direction and achieving the maximum level of polarization [42].

2.7.3. Electro-Optic Effect of PLZT

Electro-optic effect defines the materials possess a change in refractive index when an external electric field applied to itself. Taylor expansion, which is given in Equation 2.4, can explain this modifying in refractive index due to the electric field.

$$\boldsymbol{n(E) = n_0 + a_1 E + \frac{1}{2} a_2 E^2 + \cdots} \tag{2.4}$$

In this equation, n_0 represents the unperturbed refractive index. a_i is the expansion coefficient. Terms higher than second order are at the weak levels and most

of the time negligible for PLZT. With the neglected part of the formula electro-optic effect of PLZT can be written as:

$$\boldsymbol{n(E) \approx n - \frac{1}{2}\tau\, n^3 E} \tag{2.5}$$

τ sign means the Pockels coefficient. PLZT is an anisotropic material which possesses different level properties at different directions and its electro-optic effect represented as an ellipsoid. Einstein's notation defines the coordinates for this anisotropy with the using of tensors [43].

$$\boldsymbol{\eta_{ij} = \eta_{ij}(0) + \tau_{ijk} E_k} \tag{2.6}$$

2.8. Thin Film Technology

Thin film materials are being fabricated by deposition of the atoms on a substrate. Thin films are low-dimensional materials with the thickness less than 2μm. These materials have been used for many years. First application area of the thin films were optical coatings, hard coatings and then some thin films transistor studies were made. Thin film technology gives the chance to fabricate two-dimensional nanomaterials. Nanomaterials are materials with one or more nanometer level dimension. They can be classified into three groups: zero-dimensional (quantum dots), one-dimensional (quantum wires), two-dimensional (thin films) [44].

For the best properties of the material, the general approach is to achieve single crystal structure or to have the closest structure to that. Besides that, synthesis of the films on different substrates showed important dielectric properties. These properties are higher than its levels in the bulk. Strain in the thin film can make the change in ferroelectricity, transition temperature and more. Films try to form domains and reducing the strain. Substrate and film tend to match because of having an epitaxial structure [18].

2.8.1. Substrates

Selecting of the substrate for thin film deposition has an important role to achieve target morphological and electrical properties. Substrate selection has a strong effect on the density, cracks and all other features of the film. The substrate has a critical effect on the crystallization of the films with respect to its orientation. The crystalline structure of the film mainly grows with a preferred orientation which matches with the substrate. Preferred orientation strongly increases the dielectric, piezoelectric properties of the films. Films are generally in an amorphous state when they are fabricated. Annealing process starts with the crystallization of the films. Crystallization starts from the substrate and nucleation of the crystalline grains leads the route. It can be said that; nucleation mechanism needs higher energy than growth. Substrate's texture, composition, and other properties affects the orientation of the crystalline structure [2, 45].

Grain growth kinetics and the thermodynamic selects the crystallization direction of the material. A substrate with preferred orientation, promotes its direction for the crystallization. Thermodynamic promotes the most stable condition. One of these two kinetics decides the crystallization direction of the film. If the substrate has preferred orientation, the film tends to have crystallization in the same direction with the substrate because of minimizing the interface energy amidst substrate and deposited film. Nucleation sites are another parameter to decide which direction will be promoted. A great number of nucleation site leads to film have an orientation which matches with the substrate, but if nucleation occurs in a small area thermodynamic decides to the orientation of the crystallization process. If crystallization occurs with the pairing direction of the substrate, grain dimensions smaller than comparing to the crystallization process done by thermodynamics. This situation explains which crystallization kinetic is more rapid. More nucleation sites and rapid crystallization results with small grains. Another parameter is annealing temperature, obviously. Pyrochlore phase was defined in the previous sections. Stability of this phase has an important role for grain growth mechanism. Rapid thermal annealing method speed up the crystallization process and the grain growth mechanism go further with tend to match with substrate orientation [2, 46, 47].

For many years, selection of the substrate for PZT films were studied. The most used substrates can be seen in Table 2.1 with their prominent features [2].

Thermal expansion difference between substrate and film is an important parameter for selecting the substrate material. This difference must low as much as possible. Also, substrate material has to exist after a process with oxygen atmosphere without degradation or creating interface layers. Metal substrates such as cobalt, titanium, nickel will quickly be oxidized under an oxygen atmosphere. Aluminum creates an interface film with a non-piezoelectric property. For eliminating this, processing temperature should be selected under 480°C. Platinum electrodes with titanium layer have been used widely. Also, transparent conductive oxides like indium tin oxide (ITO) acts as successful substrates for films. ITO comes with a disadvantage. Its n-type conductivity related with the oxygen vacancies results in reducing of the films when they are annealed under an oxygen atmosphere. The most used substrate is platinum coated SiO_2/Si wafers. With its inert behavior and avoiding from diffusion makes it a good choice. Besides that, platinum coated silicon oxide wafers also promote the structure to form perovskite phase. For platinum, the crystallization direction is (111) usually and this promotes (100) and (111) planes for PZT, with the dependency of temperature. To enhance adhesion of platinum to silicon oxide, titanium is used. To avoid the diffusion of titanium to film, a layer of TiO_2 being used [2, 45].

Table 2.1: Substrate materials for PZT and their prominent features.

Substrate Materials	
Stannic oxide	Medium resistance
Indium tin oxide	Medium resistance
Ti – Platinum	Good and reproducible
Aluminum	Temperature limited
Silver	High adhesion
Stainless steel	Good at low temperature
Nickel, Cobalt, Titanium, Wolfram	Oxidized
Nickel based alloy	High conductivity
Ruthenium oxide	High conductivity
Yttrium copper barium oxide	Lattice match

As mentioned above, some certain conditions lead the nucleation and growth with (111) preferred orientation although most stable orientation is (100). To obtain

(111) crystallized grains, titanium diffusion to the substrate surface, some intermetallic phases like Pt-Ti, the residual stress of Pt are so effective. A seed layer like TiO_2 promotes the (111) orientation. Also, residual tension promotes the growth of (111) orientation and residual compression promotes (100) orientation. Annealing of the platinum layer results with these residual stresses. The conventional type of annealing creates higher residual stresses with compared to rapid thermal annealing. This tension decreases the mismatch and interfaces energy. So, platinum and PZT grows with a matched structure easily [2].

2.8.2. Deposition Techniques

There are various deposition methods to growth films on substrates. These methods can be count as sol-gel, metalorganic deposition, sputtering, pulsed laser deposition and more [44]. In this section, most used deposition techniques to grow thin films will be introduced.

2.8.2.1. Physical Techniques

Physical processes can be divided into two groups as thermal process and sputtering. The vacuum evaporation method is one of the thermal processes. This method evaporates the source materials in a vacuum chamber. Evaporated atoms being condensed on the substrate. To evaporate the source material, resistive heating is the main method. A filament made of metals like W, Ta, Mo. In the electron beam deposition, refractory metals are being evaporated which is not possible with the resistive heating method. In Figure 2.13, thermal evaporation system can be seen [44, 48].

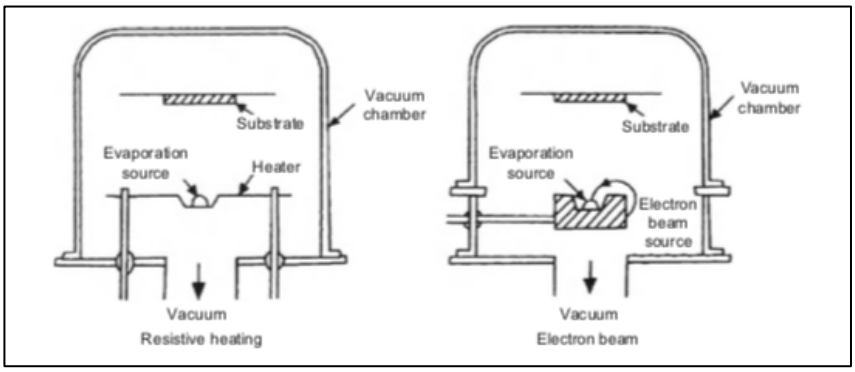


Figure 2.13: Thermal evaporation systems.

Pulsed laser deposition (PLD) is another thermal process to deposit films. Schematic view of this method is given in Figure 2.14. The main advantage of this method is the ability to control the composition of the compound or alloy. With the using of a high-power UV pulsed laser and quartz window to increase its energy, this energy is being focused on the target. Evaporated or ablated atoms of the target being deposited to substrates in the system. In this system, a point on the target is being melted locally and vaporized under vacuum circumstances. Besides all the advantages like composition control and high purity, target options are another advantage. PLD system can use powder, pellets and many types of material as the target source [44, 49].

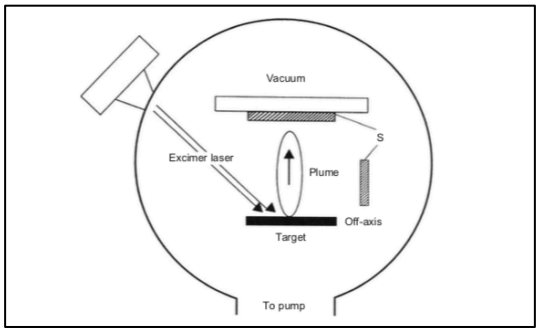


Figure 2.14: Pulsed laser deposition system.

Molecular beam epitaxy (MBE) is one of the most decisive deposition techniques for thermal processes. MBE process gives the control chance to the evaporation rate of targets and resulting with a controlled composition of the film. The process chamber has 3 parts as growth, analysis and sample chambers [44].

Sputtering is the method to gain atoms of the target by ion bombarding. With the collisions between ions and atoms at the surfaces, these surface atoms are scattered. This process called “sputtering” and can be seen in Figure 2.15. In a sputtering process, some scattered atoms can transmit through the source [44].

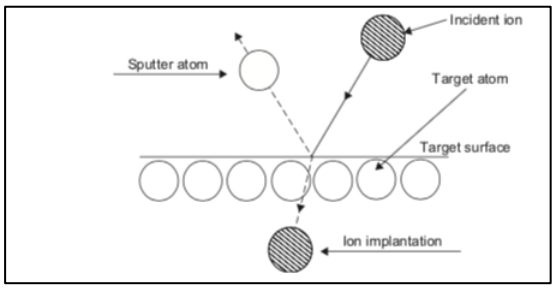


Figure 2.15: Physical sputtering system.

There are several types of the sputtering process as RF, DC and Magnetron sputtering. DC sputtering system uses planar electrodes as anode and cathode. The cathode electrode is covered by the target material which will be deposited, and the substrate is being located at the anode. Sputtering systems contains an atmosphere like argon. With the discharge, argon ions in the glow discharge are being accelerated to the cathode and finally, sputtering takes place. DC sputtering requires metallic electrodes due to the glow discharge. For sputtering an insulator material, RF (radio frequency) sputtering is being applied to the target. In this method, thin films created by directly from insulator target without a glow discharge [44, 50].

2.8.2.2. Chemical Processes

Chemical vapor deposition is another thin film depositing method. In this process, the compound of the material which will be deposited is vaporized and this vapor reacts with other gases at the substrate. At the result, nonvolatile products of the reactions deposited on the substrate. This process called “Chemical Vapor Deposition (CVD)”. CVD technique needs high temperatures like 1000ºC and a few Torr above the pressure of atmosphere [44].

Chemical solution deposition (CSD) techniques contain mainly metalorganic and sol-gel processes. These two processes are separated by the chemistry of prepared solution. CSD technique requires to prepare the homogeneous solution with using the precursors of the target composition and dissolving these precursors in the appropriate solvent. Then, coating this solution mainly by spin or dip coating methods. Homogenous solution is a key parameter to avoid from the nanoscale island on the film. Dip or spin coating of the solutions on to substrate followed with pyrolysis steps at certain temperatures, after completing the coating procedure film are being annealed at high temperatures for crystallization. CSD can be classified as two steps: solution preparing and film deposition. Specific coating techniques are being used to deposit the film. Spin coating, spray coating, and dip coating methods are the most used methods. The sol-gel method is a method for CSD and sol-gel route is given in Figure 2.16. CSD doesn’t require a vacuum chamber and can be done under atmosphere condition, so, the sol-gel method can be done under these conditions [21, 51, 52].

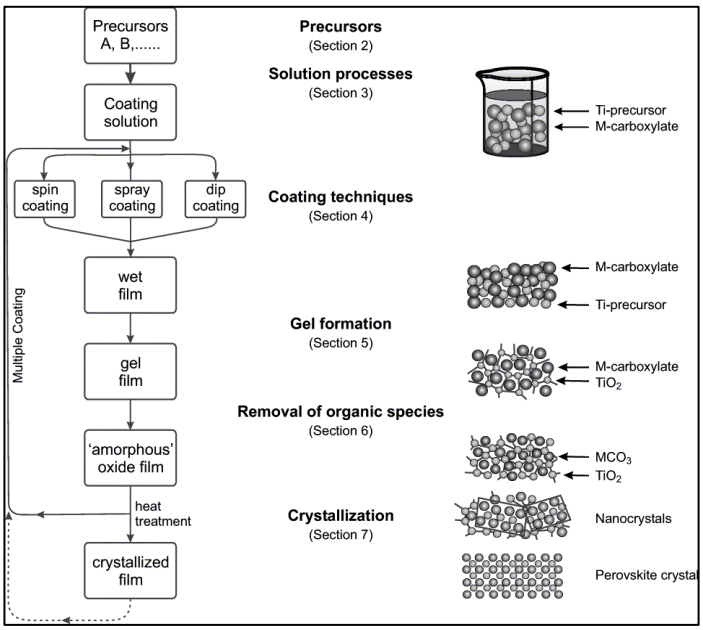


Figure 2.16: Sol-gel thin film coating process.

The sol-gel procedure starts with the preparing of the "sol" by the precursors and solvents. Precursor material contains metal alkoxides, metal salts. Hydrolysis and polymerization steps occur with the further parts of the sol-gel method. Hydrolysis process is done with the replacing the alkoxide with hydroxyl. Condensation step contains the reaction of two partially hydrolyzed or one alkoxide and partially hydrolyzed molecules. With these reactions, water or alcohol molecules are being produced [53].

$$M(OR)_n + H_2O \leftrightarrow OH - M(OR)_{n-1} + ROH \quad \text{(Hydrolysis)}$$

$$M(OR)_{n-1}\text{-}OH + OR\text{-}M(OR)_{n-1} \leftrightarrow M(OR)_{n-1}\text{–}O\text{–}M(OR)_{n-1} + ROH \quad \text{(Condensation)}$$

$$M(OR)_{n-1}\text{-}OH + HO\text{-}M(OR)_{n-1} \leftrightarrow M(OR)_{n-1}\text{–}O\text{–}M(OR)_{n-1} + H_2O \quad \text{(Condensation)}$$

These steps lead to creating cross-linked chains in the sol. Hydrolysis and condensation reactions with a non-equilibrium state, they create macromolecules and these molecules can result with precipitations. Eventually, the polymeric network increases the viscosity of solution and gelation starts. Precipitation occurs with different speed depending on the parameters like temperature, pH of the solution. Due to the reaction characteristics of hydrolysis and condensation, these steps can be reversed. The speed of the reactions defines the route of reactions. At the equilibrium state, the speed of these reactions would be the same, and the solution will not have reactions for gelation. Amount of the solvent can change the direction reaction.

Evaporation of the solvent results with reactions on the way gelation. This procedure is a way to fabricate thin films. When stable sol obtained, the spin coating method can be done. Spin coating process can be seen in Figure 2.17. This method is applied by dropping a certain amount of sol onto the substrate and spinning of this substrate with a certain rpm. After this spin coating step, pyrolysis needs to be done for each layer. Pyrolysis step burns the organic compounds and sometimes it called as “firing”. Spinning movement evaporates most of the solvent. Heating of the coated layer for a selected time and temperature conditions lead the film decomposes gel to amorphous phase and with the further step, crystallization occurs. Pyrolysis steps gives the activation energy for nucleation and growth of the crystal structure. Processing temperature levels are lower than the sintering of bulk materials. Final step can be done with the rapid thermal annealing (RTA) cause of avoid from cracks or can be done with the conventional way [2, 51, 53, 54].

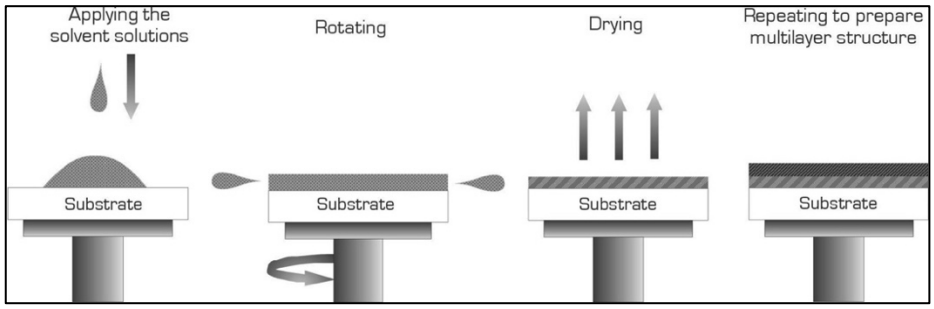


Figure 2.17: Thin film deposition by spin-coating method.

Eventually, the sol-gel technique is a common method to deposit films with compare to other physical and chemical methods. Thin films with high dielectric properties have been achieved with this method. One of the advantages of this method its cheap processing costs. Also, this method is so applicable for complex compositions [47, 55].

2.8.3. Strain in the Films

Lattice mismatch creates strain in the films. Many parameters are effective on this undesired result. The deposition method of the thin film, pyrolysis steps were made during coating of multilayers, thermal property differences of the film and substrate. This strain has an important effect on the domain structure of the films and

obviously electrical and optical properties. There are several strain types can be seen in films [18, 56].

Epitaxial strain resulting from the lattice mismatch between film and substrate. This mismatch can be defined with the formula:

$$\boldsymbol{\varepsilon_s = \frac{(a_s - a_f)}{a_s}} \tag{2.7}$$

a_s is the lattice parameter for substrate and a_f is for the film. If the substrate is thicker than the film, there will be tensile stress, and as opposite of this compressive stress occurs. Lattice mismatch formations occur mainly phase transition points as a result of changing the structure cubic to tetragonal [18].

$$\boldsymbol{\varepsilon_{xx} = \varepsilon_{yy} = \frac{[a(T) - a(C)]}{a(C)}} \tag{2.8}$$

$$\boldsymbol{\varepsilon_{zz} = \frac{[c(T) - a(C)]}{a(C)}} \tag{2.9}$$

a(T) and c(T) defines the lattice parameters for tetragonal and a(C) is the lattice parameter for cubic phase [18].

The thermal strain caused by the mismatch between film and substrate. For the cubic phase, depending on the process temperature and phase transition temperature. $a_f(C)$ defines the thermal expansion coefficient of the film in cubic phase, strain can be written as:

$$\boldsymbol{\varepsilon_T = [\alpha_f(C) - \alpha_s]\Delta T} \tag{2.10}$$

Residual strain is the total strain in the film resulting from all the processes for preparation of film. Thin films tend to reduce strain by formation of domains [18].

2.9. Transparent Conductive Oxides

Transparent conductive oxides (TCO) possess high transparency in the visible range of light at combines that with the electrical conductivity due to wide band gap

higher than 3 eV. These properties made TCO materials are useful for a wide application type. First main application area of TCOs was for military industries at the World War II. During the war, TCOs were used as anti-freezing windshields which can be heated with electric. With the 1960s and beginning of 1970, these materials became potential materials for energy efficiency applications. Today, indium and zinc are the most researched elements for TCO materials for a long time [42, 57].

2.9.1. Indium Tin Oxide

Transparent and conductive behavior can be achieved by a material which has wide band-gap and with doped non-stoichiometric composition. ITO is a well-known TCO material which achieved by doping of tin atom to indium oxide structure. This doping causes the create a wide n-type band-gap. ITO films are being used in liquid crystal screens, solar cells, anti-static coating and more cause of their high light transparency in the visible range and high conductivity [57-59].

For atmospheric pressure and room temperature In_2O_3 has cubic bixbyite structure with 1.0118 nm lattice parameter. Crystal structure of In is given in Figure 2.18. In this structure one anion of four is missing, due to that, indium cations locate in two non-equilibrium positions. Amount of the charge carriers can be increased by doping like Sn doping to In_2O_3. Sn^{+4} cations substitutes with In^{+3} cations [57, 58].

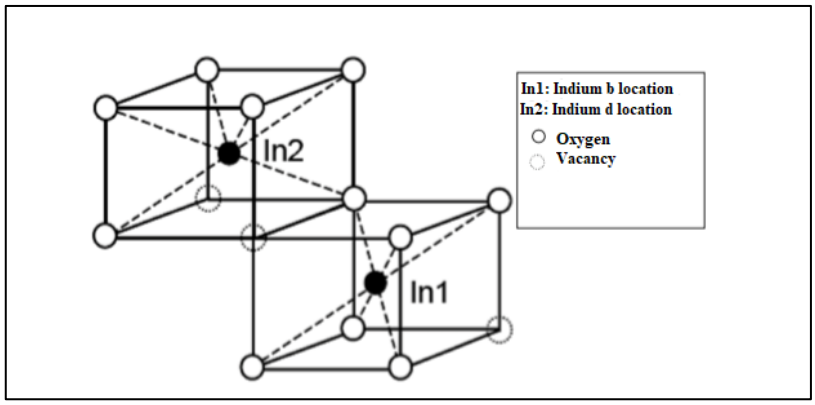


Figure 2.18: Indium crystal structure.

Electrical properties of ITO films can be characterized by free charge carrier density, carrier mobility, conductivity, and resistance. With the increasing amount of charge carrier density and mobility, electrical conductivity also increases. Carriers in the ITO films occur mainly with In^{+4} cations. Sn acts cationic in the structure of In_2O_3

and substitutes with In, as a result of In^{+3} this Sn doping causes an electron transfer to the conduction band. For ITO films there is a balance requirement for electrical conductivity and transparency. Any decreasing in resistance causes from the increment in either carrier amount or carrier mobility. Increasement in the amount of carrier also increases the absorption level of light, for this reason, to obtain best transparency and conductivity properties it is important to increase the mobility of carriers [57-59].

There are several electron scattering reasons like grain boundaries, phonon, lattice defects. With the good crystallization and grain growth, grain boundary amount decreases, as a result of this scattering also decreases [57-59].

2.9.2. Gallium Zinc Oxide

ZnO is one of the important materials for semiconductor applications with band-gap about 3.4 eV for room temperature. The binding energy of ZnO is approximately 60 meV. This high level of binding energy makes this material useful for optical applications. Another important property of ZnO is its piezoelectric property. High piezoelectric coefficient values open a way for actuating and sensing applications [60, 61]. ZnO is also a nontoxic material. Undoped form of the ZnO films has hexagonal wurtzite structure. n-type conduction occurs in these materials due to the nonstoichiometric structure and this material also possess high electrical resistivity because of its low carrier concentration. This behavior makes Al, In or Ga to dope to the ZnO and improve the electrical properties [62].

p-type doping has been studied intensely for ZnO researches. Besides p-type doping, n-type materials were promising because of the features like high crystallinity, ability to control electron carrier concentration. These features promoted n-type doping for an electrooptic application. Doping of group III elements to ZnO made this material promising and alternate to expensive ITO. Gallium has taken interest among these elements. Its reactivity lower and oxidation resistance higher than Al. Also, ionic radius of the Ga^{3+} ions are smaller than Zn^{2+}, but at the same time, it is higher than Al^{3+}. This radius led to material fit into the ZnO lattice. Formation of gallium zinc oxide (GZO) possesses compatible covalent bond length with compare to indium. Gallium-oxygen forms covalent bond with 1.92 Å and gallium-zinc form covalent bond with 1.97 Å. Indium-oxygen forms covalent bond with 2.1 Å. Bond length of the Ga and O is smaller than Zn and O. This is important for the deformation of ZnO lattice [62-64].

3. EXPERIMENTAL STUDY

3.1. Preparation of Precursor Solutions

In this study, the sol-gel method was selected to fabricate both thin films and bulk samples and several precursors with different compositions were prepared. PZT, cobalt (Co) doped PZT and PLZT precursor solutions were used in this study.

$Pb(Zr_xTi_{1-x})O_3$ (PZT) precursor solutions were prepared with x=0.52 stoichiometric ratio. $PbTi_{0.5}Zr_{0.5-x}(Co_x)O_3$ (Co-doped PZT) precursor solution was prepared with x=0.05 and x=0.2 stoichiometric ratio and $Pb_{1-x}La_x(Zr_yTi_{1-y})_{1-x/4}O_3$ (PLZT) precursor solution was prepared with x=0.09 and y=0.65 stoichiometric ratio.

To prepare solutions; lead acetate trihydrate, titanium n-butoxide, zirconium n-propoxide, lanthanum acetate, cobalt acetate was used as metal precursors and acetylacetone, 2-methoxyethanol, acetic acid, isopropanol chemicals were used as solvent and stabilizer for the solution. Detailed information is given in Table 3.1. Different solution preparing routes were followed for composition [1, 9, 45].

Table 3.1: Chemicals used for solution preparing.

Chemical	**Chemical Formula**	**Brand**
Lead (II) acetate trihydrate	$C_4H_6O_4Pb.3H_2O$	Merck
Zirconium (IV) n-propoxide, 70% w/w in n-propanol	$Zr(OCH_2CH_2CH_3)_4$	Alfa-Aesar
Cobalt (II) acetate tetrahydrate	$(CH_3COO)_2Co.4H_2O$	Sigma-Aldrich
Lanthanum (III) acetate hydrate	$La(CH_3CO_2)_3.xH_2O$	Sigma-Aldrich
Titanium (IV) n-butoxide	$Ti(OCH_2CH_2CH_2CH_3)_4$	Alfa-Aesar
2-Methoxyethanol	$CH_3OCH_2CH_2OH$	Sigma-Aldrich
Acetylacetone	$CH_3COCH_2COCH_3$	Merck
Acetic acid	CH_3CO_2H	Sigma-Aldrich
Isopropanol	$CH_3CH(OH)CH_3$	Merck

PZT, PLZT, and cobalt doped PZT solutions prepared with the selected amount of excess lead content to avoid lead deficiency during annealing process.

First of all, the titanium and zirconium precursor solutions were prepared separately in 2-methoxyethanol at room temperature and stirred for 30 minutes. Lead

acetate trihydrate also was dissolved in 2-methoxyethanol at 80°C for 30 minutes on hot plate. Then, these solutions were dehydrated at 120°C for 90 minutes. After the dehydration step, solutions were mixed and stirred at 80°C for 30 minutes and route completed with further dehydrating step at 120°C for 90 minutes. The route to prepare PZT solution was given in Figure 3.1.

Cobalt doped PZT precursor solution were also prepared with another preparation route. In the first step, titanium precursor solution dissolved at room temperature in isopropanol. Acetylacetone was added to stabilize the solution and then, zirconium precursor solution added to that. Lead and cobalt precursors were dissolved in the mixture of acetic acid and water at 80°C for 2 hours. Lead and cobalt solution added into titanium-zirconium solution, 5 ml water also added to obtain a clear solution. This solution was stirred at 80°C for 2 hours and dried at 120°C. Besides the preparing the cobalt added PZT solution with using isopropanol as solvent, it was prepared also with 2-methoxyethanol as solvent. The route to prepare Co added PZT solution can be seen in Figure 3.2.

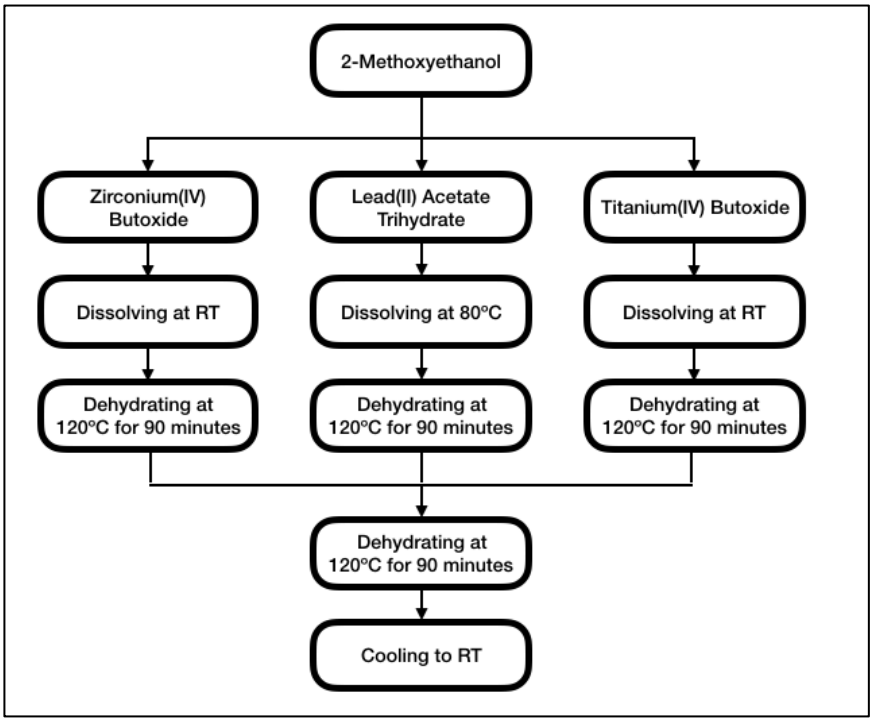


Figure 3.1: PZT solution preparing route.

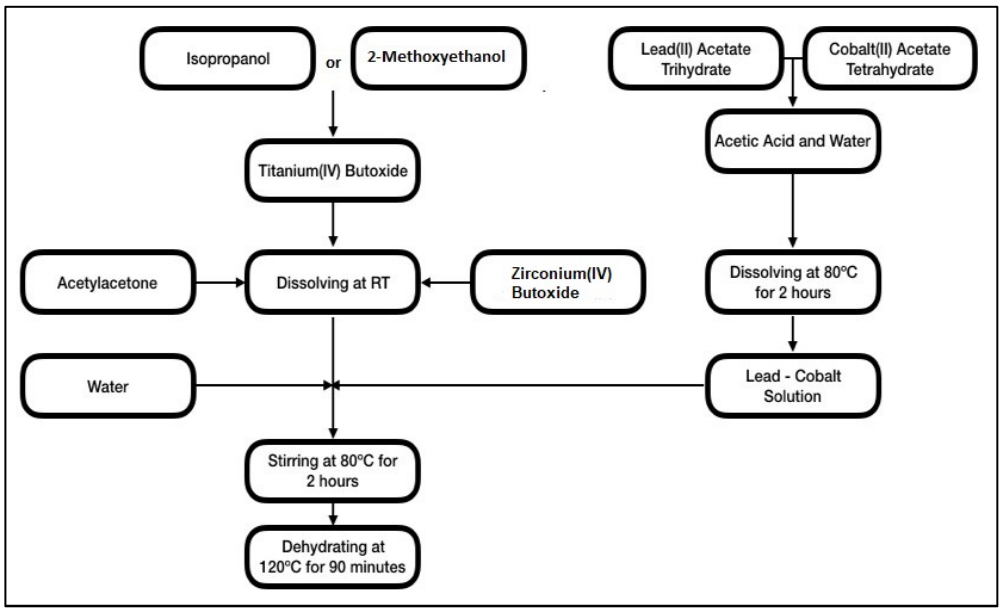


Figure 3.2: Cobalt doped PZT solution preparing route.

PLZT precursor solution preparation started with dissolving the Pb and La precursors in 2-methoxyethanol at 80°C for 30 minutes and dehydrated at 120°C for 90 minutes. Ti and Zr precursor solutions were added, and this solution dissolved at 80°C for 30 minutes again, dehydrated at 120°C for 90 minutes. The route to prepare PLZT solution is given in Figure 3.3.

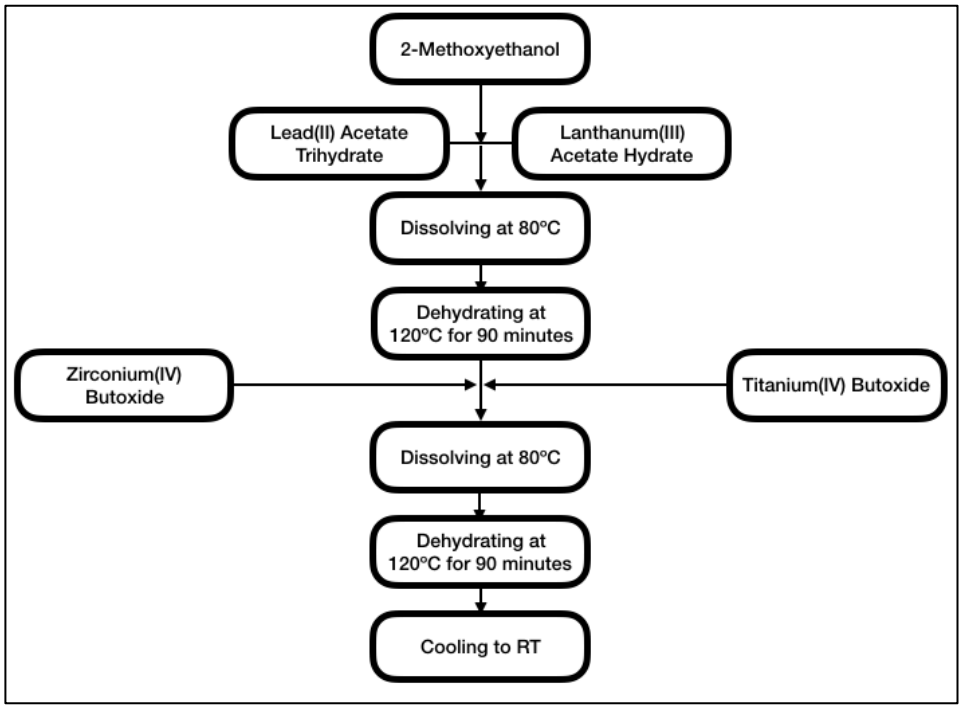


Figure 3.3: PLZT solution preparing route.

3.2. Preparation of the Surface of the Substrates for Coating

In this study, two types of substrates were used: Platinum coated silicon oxide ($Pt_{(111)}/Ti/SiO_2/Si_{(100)}$) and gallium-doped zinc oxide (GZO) coated glass substrates. To avoid any dirtiness, substrate cleaning was one of the key steps for fabricating of the films.

To clean the substrates, a cleaning procedure with three steps were followed. Schematic figure of this cleaning procedure is given in Figure 3.4. These steps were:

- Keeping the substrate in ethanol for 5 minutes, then spin coating with ethanol.
- Keeping the substrate in acetone for 5 minutes, then spin coating with acetone.
- Keeping the substrate in isopropanol for 5 minutes, then spin coating with isopropanol.

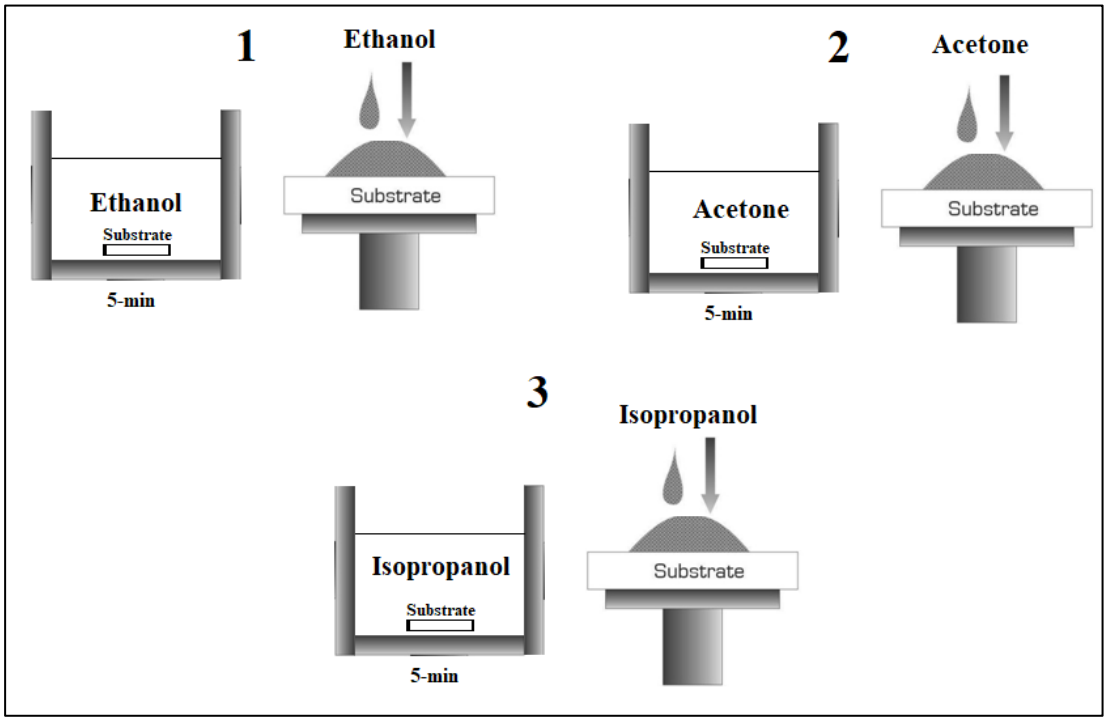


Figure 3.4: Substrate cleaning procedure.

3.3. Spin Coating Process of the Films

Spin coating of the solutions onto the substrates was done by using Brewer Science – CEE Spin Coater, USA. The system has a vacuum pump, solution delivery part, and a lid. Before starting the coating process, stock solutions were filtered with

Sartorius 0.25 μm filters to avoid any contamination and particles in the films. Filtered solutions were withdrawn to the syringe. As another prevention to contamination and particles, another extra filter attached to the syringe. This additional syringe filter has been changed with a new filter after coating of every three layers.

Spin coating parameters were selected from the literature and our previous works to achieve homogeneous films. The detailed parameters of spin coating are given in Table 3.2. All films were produced as five layered structure, and two drops of solution was used for each layer. After coating every layer, pyrolysis step was carried out.

Table 3.2: Spin coating parameters for solution types.

Solution	**First Step (rpm)**	**Time (s)**	**Second Step (rpm)**	**Time (s)**
PZT	600	6	3000	30
PLZT	2500	30	-	-

After coating five layer, the films were annealed at different temperatures to understand annealing temperature effect on the crystallization of the films. Annealing process was done by the method named as “rapid thermal annealing” (RTA). The films were put to the furnace at the target temperature in this RTA process and then kept for a selected time.

Table 3.3. shows the pyrolysis and annealing conditions of films with different compositions. PZT compositions were prepared with 52/48 ratio of Zr/Ti. Solutions were prepared with 2%-mole excess. PLZT compositions were prepared with x=0.09 lanthanum content and 65/35 ratio of Zr/Ti. These solutions were prepared with 5%-mole and 20%-mole lead excess. The detailed compositions of PZT and PLZT were given as $Pb(Zr_xTi_{1-x})O_3$ and $Pb_{1-x}La_x(Zr_yTi_{1-y})_{1-x/4}O_3$, respectively.

Pyrolysis step and annealing temperature parameters were variable to achieve a fully crystallized microstructure. After every parameter change, SEM analyses were done characterize the microstructure and variables were reviewed again. The main approach was to eliminate the secondary rosette phases detected by SEM.

Table 3.3: Pyrolysis and annealing conditions of the films.

Substrate	Composition	First Step (°C) of Pyrolysis	Time (min)	Second Step (°C) of Pyrolysis	Time (min)	Annealing Temperature (°C) – (1 hour)
Pt coated Si	Stoichiometric PZT	250	5	400	5	600
	PZT w/ 2%-mole Pb excess	250	5	400	5	600
						700
	PLZT w/ 5%-mole Pb excess	200	2	430	5	650
						725
	PLZT w/ 20%-mole Pb excess	150	5	430	10	725
GZO coated glass	PZT w/ 2%-mole Pb excess	250	5	400	5	600
						700
						725
	PLZT w/ 5%-mole Pb excess	200	2	430	5	650
						700
						725
		200	5	430	5	725
		200	5	430	10	725
		200	2	430	10	725
	PLZT w/ 20%-mole Pb excess	150	5	430	10	725

3.4. Obtaining of the Top Electrode of the Films by RF Sputtering

The Pt coated top layer of the substrates was used as the bottom electrode for the films obtained on the Pt coated Si substrates. Covering of the small area of the substrate with tape sheets provided a clean bottom electrode. For top electrode of the films sputtering method was used. Platinum was sputtered using a platinum target and electrodes was obtained with 100 nm thickness. A thin mask with different diameters was used to prepare electrodes. The three different electrode sizes can be seen in Figure 3.5. After sputtering of Pt top electrodes, the films were annealed at 600°C for 30 minutes, in the furnace. For top electrode of the films coated on GZO coated glass substrates, air dry silver contacted to the surface area with using a thin mask.

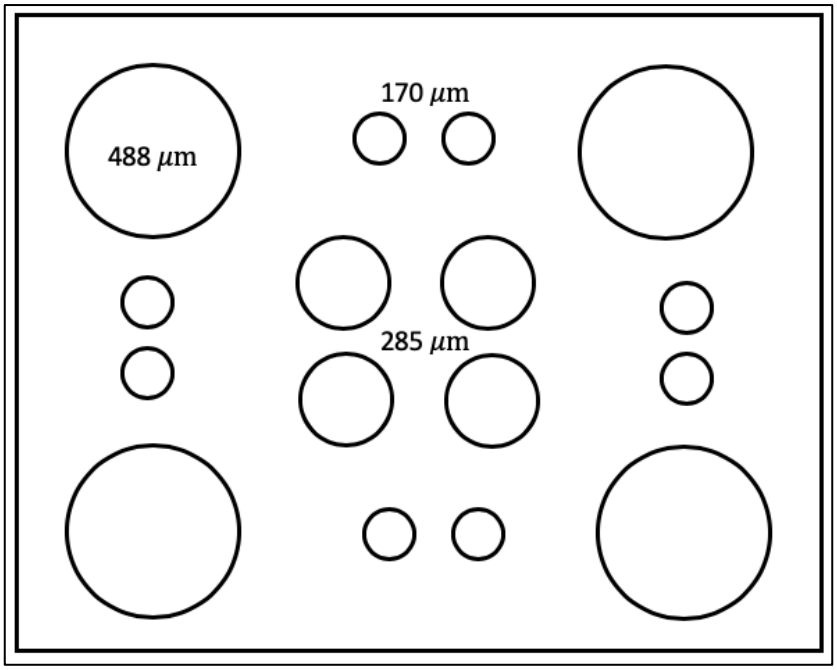


Figure 3.5: Electrode diameters of the mask measured by SEM.

3.5. Synthesis and Processing of Powders from the Solutions

Synthesis of the powders from sol-gel stock solutions and processing of the bulk samples were another aim of the study. First of all, the sol-gel precursor solutions were dried at 120°C to obtain powders. Drying process of solutions was not completed in a specific time.

After drying process, powders were crushed. Then, different calcination processes were done for each specific composition. XRD analyses were carried out to investigate and confirm crystallization of the phases. The detailed compositions of derived powders and calcinating parameters are given at Table 3.4.

Table 3.4: Calcination parameters of the powders.

Composition	**Temperature (°C)**	**Time (h)**
PZT w/ stoichiometric ratio (52:48)	800	2
PZT w/ 1%-mole Pb excess (52:48)	800	2
PZT w/ 2%-mole Pb excess (52:48)	800	2
Co-PZT with Co mole 0.20 – Prepared with Isopropanol	800	2
	850	4
Co-PZT with Co mole 0.20 – Prepared with 2-Methoxyethanol	800	2
	850	4
Co-PZT with Co mole 0.05 – Prepared with 2-Methoxyethanol	800	2
	850	4

After calcination step, 5%-weight binder was added to the powder. With binder, an appropriate amount of methyl ethyl ketone was also added to this mixture. In this step, there was not applied any ball-milling process, only crushing was done. After the evaporation of the methyl ethyl ketone at the room temperature powders was dried. Powders were dry-pressed under 100 MPa for 2 minutes. Pellets with different powder compositions were sintered at different sintering conditions which is given at Table 3.5. The sintering temperature was 1260ºC for all composition. Sintering time was 2 hours and 4 hours for the Co added compositions.

Table 3.5: Sintering parameters of the pellets.

Composition	Temperature (°C)	Time (h)
PZT w/ stoichiometric ratio (52:48)	1260	4
PZT w/ 1%-mole Pb excess (52:48)	1260	4
PZT w/ 2%-mole Pb excess (52:48)	1260	4
Co-PZT with Co mole 0.20 – Prepared with Isopropanol	1260	4
Co-PZT with Co mole 0.20 – Prepared with 2-Methoxyethanol	1260	2
	1260	4
Co-PZT with Co mole 0.05 – Prepared with Isopropanol	1260	2

3.6. Characterization of the Films and Bulk Samples

Thin films were characterized by several measurement methods. First characterizations made for structure. X-ray diffraction (Rigaku DMax 2200, Tokyo, Japan) with using Cu-Ka radiation were done to reveal crystallization of the films. Also, differential thermal analyses (DTA) and thermogravimetric analyses (TG) (Netzsch STA 449 F3, Jupiter, Deutschland) showed the temperature levels for phase transitions and evaporation. These DTA-TG analyses were done with the powder gained from the solution. Results gave an approach for pyrolysis steps and annealing temperature. SEM analyses (Philips XL30, FEI Co., USA) were done to get information about the microstructure of the films and comparing it with XRD results. These analyses helped to see the changing in rosette phases with different pyrolysis steps.

For electrical characterization, I-V measurements were done by an established system with an optical microscope, source meter, and software. Current and voltage values of the films coated on platinum substrate measured for 40kV/cm at 4 steps. Measurements were done for three sizes of electrodes. Also, as another electrical characterization, dielectric properties of films were measured with temperature dependency by a system with heating elements. Measurements were done in the range

of 1 kHz to 1 MHz and capacitance, dielectric loss, dielectric constant values of the films characterized. Finally, the piezo response force microscope analyses (PRFM) were done.

Optical measurements were applied to films coated on GZO coated glass substrates because of the combining transparent conductive oxide property of the substrate with the transparent behavior of the PZT and PLZT in the film form. UV-Vis measurements were done in the range of 200-1000 nm and transparency, reflectance and absorbance values are characterized. Also, these data were used to calculate energy band-gap values of the films.

XRD and DTA-TG analyses were done for the structural characterization of the bulk studies. Dielectric measurements completed with LCR meter (Hioki 3552-50, Japan) in the range of 1 kHz to 5 MHz. Capacitance, dielectric loss, dielectric constant values were calculated. Piezoelectric characterization of the samples was done with the piezometer. Measurements were done in the range of 10-40 kV with 1000 ms frequency. Polarization versus electric field and strain versus electric field measurements were carried out.

4. RESULTS AND DISCUSSION

In this section, the parameters such as lanthanum addition and its amount, coating parameters, type of substrate, pyrolysis steps and its temperature, annealing temperature on the structural, electrical and, optical properties of the films were investigated with various characterization method. Results were the discussed in detail in the light of literature.

4.1. PZT and PLZT Films Obtained on the Platinum Coated Silicon Substrates

In this part of this study, phase and microstructural analyses and, electrical properties of the films coated on $Pt_{(111)}/Ti/SiO_2/Si_{(100)}$ substrates will be discussed.

4.1.1. Phase Analyses of the Films

Differential thermal analyses (DTA) and thermogravimetric analyses (TG) were done in the temperature range between room temperature to 1000ºC and these analyses were used to select pyrolysis steps and annealing temperatures.

In the Figure 4.1, DTA-TG analyses of the PZT with 2%-mole Pb excess composition is given. DTA analyses was revealed there is a stable temperature range about phase transitions between 150ºC and 300ºC. Pyrolysis steps which were given in Table 3.3 were selected depending on this data. In this temperature range, crystallization of the films was intended. Also, the annealing temperature was selected in the light of this data. As it can be seen from the figure, there is a transition at the ~720ºC. Annealing temperature of the films were selected as 600ºC as first temperature value and then it was increased. Increasing of the annealing temperature was promoted the further crystallization of the films and these results will be discussed in next sections detailly. TG analyze was resulted with 30.47% mass change. It is believed that, this relatively big amount of mass change reasoned from the organic content from the preparing of the precursor solution with metal alkoxides.

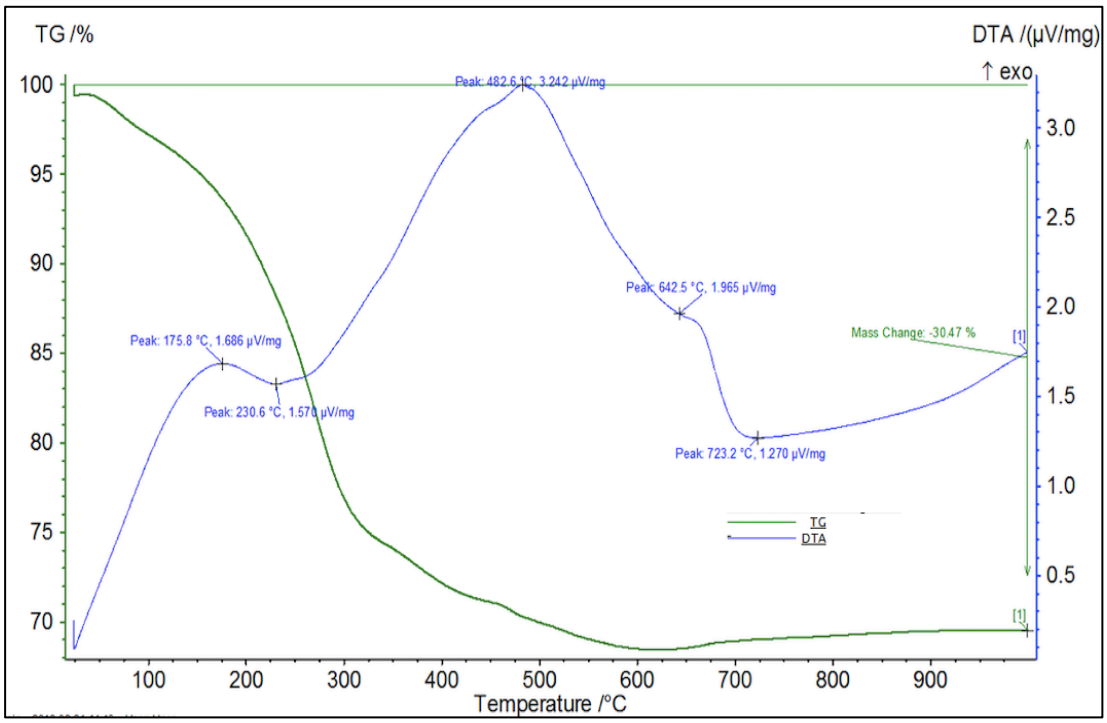


Figure 4.1: DTA-TG analyses of the PZT with 2%-mole Pb excess.

In the Figure 4.2, DTA-TG analyses of the PLZT with 5%-mole Pb excess composition is given. Pyrolysis steps were selected from DTA analyze results. These steps were close to the temperatures selected for PZT. The annealing temperature was selected from this data too. As it can be seen from the figure, there is a transition at the ~790ºC. Annealing temperature of the films were selected as 650ºC for the first temperature value because of the peak at ~640ºC. Then, this temperature was increased. TG analyze was resulted with 36.34% mass change. This amount of mass change was higher than PZT. It is believed that, this change reasoned from using one more metal alkoxide while preparing the precursor solution.

These analyses were helped to understand which temperature levels will be sufficient for nucleation and crystallization. Different pyrolysis step temperatures were resulted with important microstructural changes in the films which will be discussed in next sections.

The effect of the changing of these parameters were discussed in a study with $PbZrO_2$ (PZ) composition and with the optimum parameters by formation of an intermetallic phase, films were crystallized in a preferred orientation without any secondary phases [65].

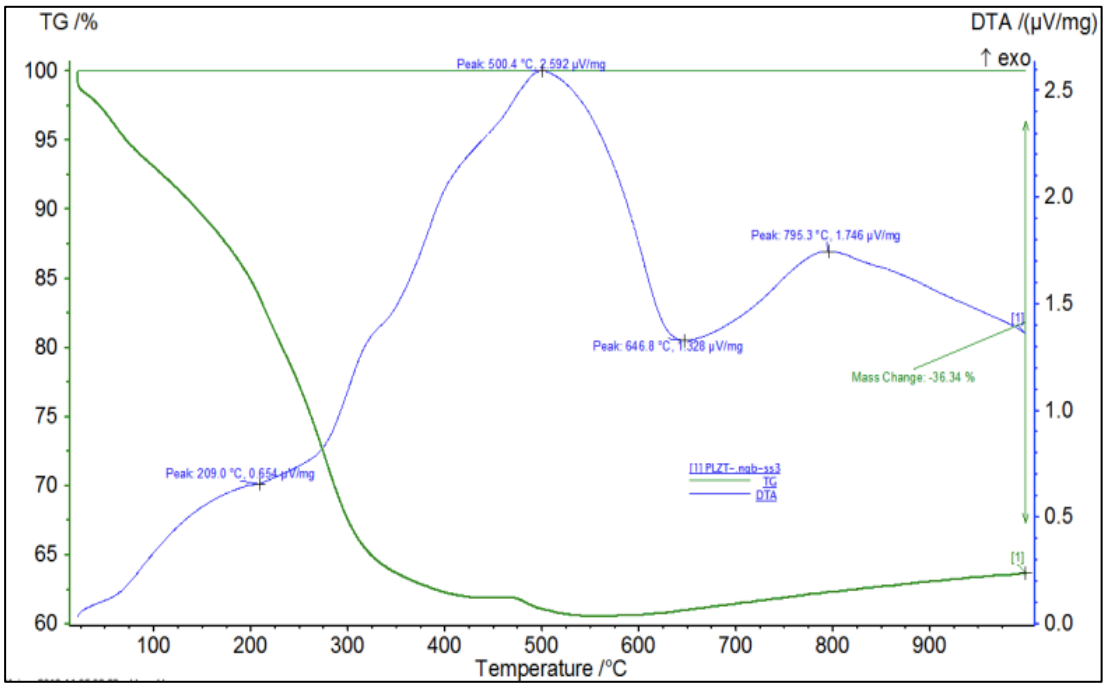


Figure 4.2: DTA-TG analyses of the PLZT with 5%-mole Pb excess.

The phase analyses of the all films were done by XRD method. Results of the XRD analyses for PZT thin films revealed the importance of the annealing temperature on crystallization. XRD patterns of the films were taken in the range of 2θ=20º-60º.

XRD patterns of the substrate and PZT (PDF# 01-074-9194) films are given in Figure 4.3. For the 2θ=22º and 2θ=45º, it can be seen that with the increased annealing temperature crystallization of the (100) and (200) planes are promoted. Also, for the 2θ=38º, further crystallization of the (111) plane is promoted. As another parameter, the excess amount of lead content showed an important effect on the crystallization of the films. Both of the films annealed at 600ºC with different amount of excess lead content have possessed different XRD patterns. Film with 2%-mole Pb excess showed further crystallization with (100), (111) and (200) planes. It can be seen that there is a little peak of (111) plane for the film with the stoichiometric composition of PZT annealed at 600ºC, but with increasing of lead content (111) crystallization was promoted. Annealing temperatures cause the lead loss and with the lead deficiency oxygen gain stabilize the pyrochlore phase. The excess amount of lead can compensate for the volatility of the lead. Both of the XRD patterns of the films TF15 and TF9 showed no pyrochlore phase and crystallized in perovskite structure. The reason of the selecting annealing temperature as 700ºC is to achieve covered surface by merged rosettes and eliminating them.

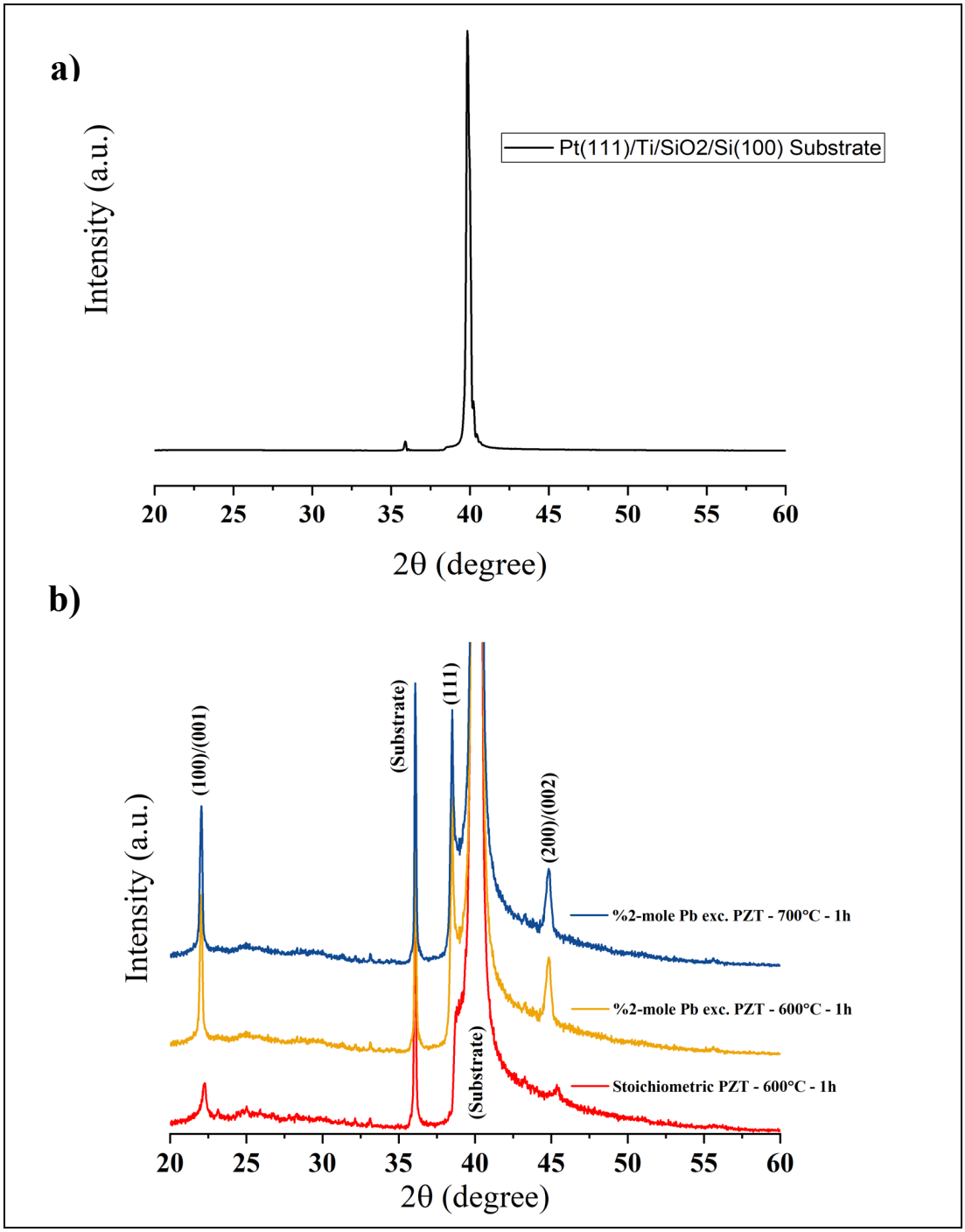


Figure 4.3: XRD patterns of the a) $Pt_{(111)}/Ti/SiO_2/Si_{(100)}$ substrate, b) PZT thin films with 2%-mole Pb excess coated on $Pt_{(111)}/Ti/SiO_2/Si_{(100)}$ substrates.

For the conventional processing of PZT without any substrate to promote preferred orientation of crystallization, it results with highest diffraction from (110) plane. This crystallization type can be defined as polygonal crystallization in contrary to cubic structure. Processing of the PZT on the substrate with (100) orientation promotes the crystallization with cubic structure and (100) plane. This processing type promotes (100) plane because of lowering the lattice mismatch between film and

substrate. From the XRD patterns from Figure 4.3 (b), it can be seen that (100) and (200) planes were crystallized and they match with substrate. Even though this preferred crystallization, it can be seen that (111) peak were observed too. This means the films were crystallized partially epitaxial and it can be defined as pseudo-cubic structure [66].

XRD patterns of the PLZT (PDF# 00-046-0336) thin films are given in Figure 4.4. Increased annealing temperature resulted with likely peaks at 2θ=21º which is (100) plane and 2θ=45º which is (200) plane. As mentioned above, DTA analyze of the PLZT showed a transition at ~790ºC. This could be reason of the not observing any evident changes. Also, peaks observed at the around of 2θ=33º were identified as PbO (PDF# 00-027-1201). This PbO content can be referring require to the increment of annealing temperature. In this study, the aim was the discussing comparing the structure-property relations of the PZT and PLZT films on different substrates and 790ºC annealing temperatures were not possible for GZO coated glass substrates. This annealing parameter left for another study. Besides that, comparing with the XRD patterns of PZT, it can be said that PLZT films were crystallized more epitaxially.

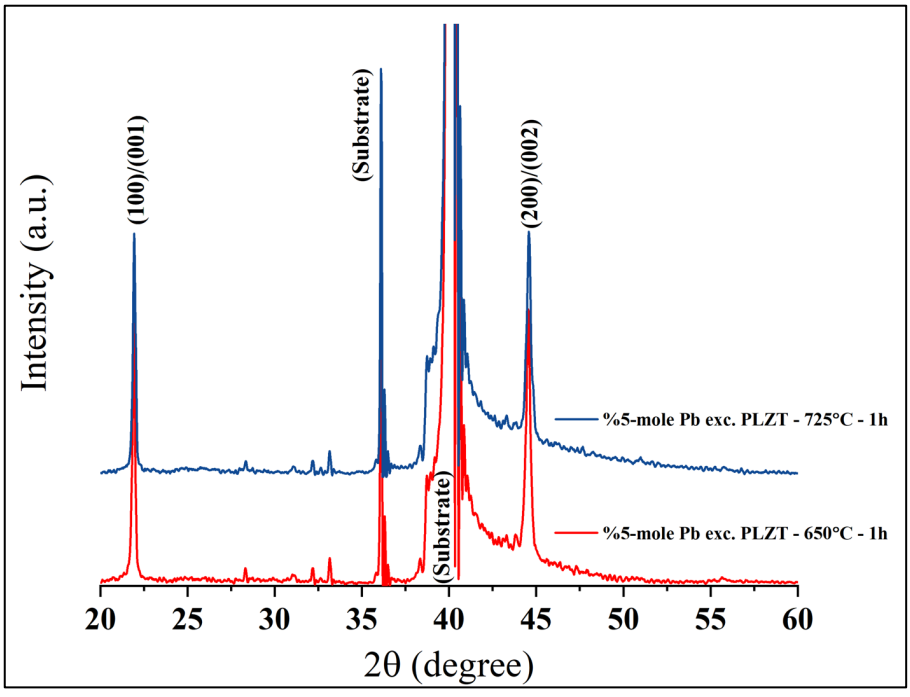


Figure 4.4: XRD patterns of the PLZT thin films with 5%-mole Pb excess coated on $Pt_{(111)}/Ti/SiO_2/Si_{(100)}$ substrates.

4.1.2. SEM Analyses of the PZT and PLZT Thin Films

SEM analyses were done to characterize the microstructure of the films. In SEM micrographs, it is clearly seen that the annealing temperature and pyrolysis steps have an important effect on the microstructure. SEM micrograph of PZT film with stoichiometric composition is given in Figure 4.5, it can be seen from this figure that there are linked rosette phases and matrix phases in these rosette phases. Rosette phases is a crystalline phase and pyrochlore phase between the rosettes with dark contrast is mainly lead deficient phases. Rosette is a polycrystalline phase consisting of submicron grains. From Figure 4.5, it is also understood that 600ºC as an annealing temperature is not enough for these films. This conclusion was also supported by XRD pattern in Figure 4.3. Crystallinity of this films was very low according to this figure [65].

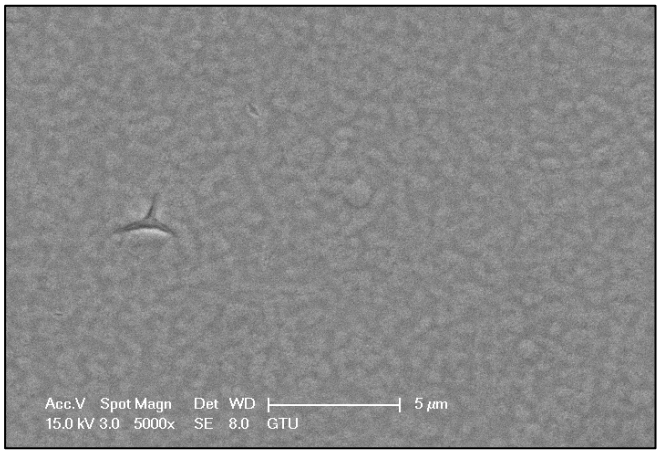


Figure 4.5: SEM micrograph of the PZT thin film (TF10) with stoichiometric composition annealed at 600ºC for 1 hour.

In Figure 4.6, SEM micrographs of the PZT thin film with 2%-mole Pb excess film is given. This film was also annealed at 600ºC for 1 hour. From the micrograph, it can be said that the microstructure is very similar to the films prepared with stoichiometric composition. Again, rosette phases were obtained for that film. But from Figure 4.1, XRD pattern of this PZT film with 2%-mole Pb excess shows that crystallinity is very high, and this phase is a pure perovskite. These results show that rosette phase is a microstructural feature that is related to the lead content of the film.

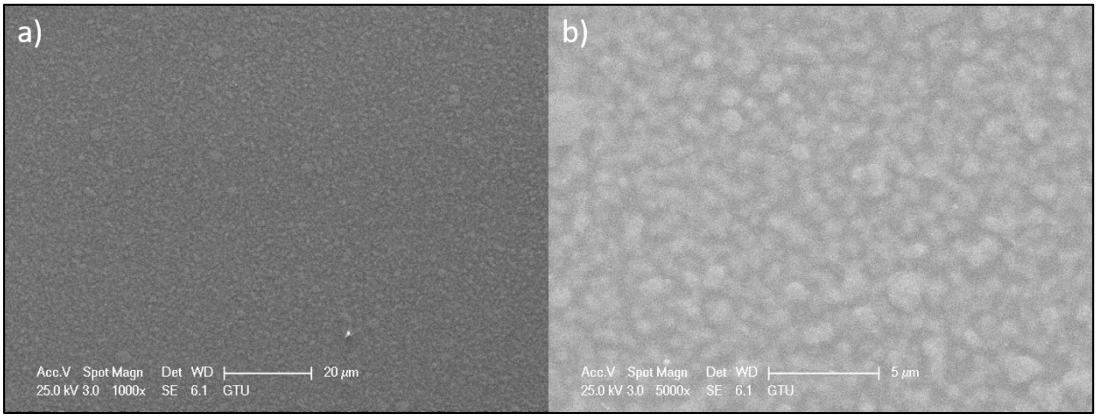


Figure 4.6: SEM micrographs of the PZT thin film (TF9) with 2%-mole Pb excess annealed at 600ºC for 1 hour; a) 1000x and b) 5000x.

Figure 4.7 shows the SEM micrographs of the PZT thin films with 2%-mole Pb excess and annealed at 700ºC for 1 hour. These micrographs show the annealing temperature has an important effect on the crystallization of the films. Rosette sizes are ~1μm and the amount of rosette phases of this film are higher than TF9.

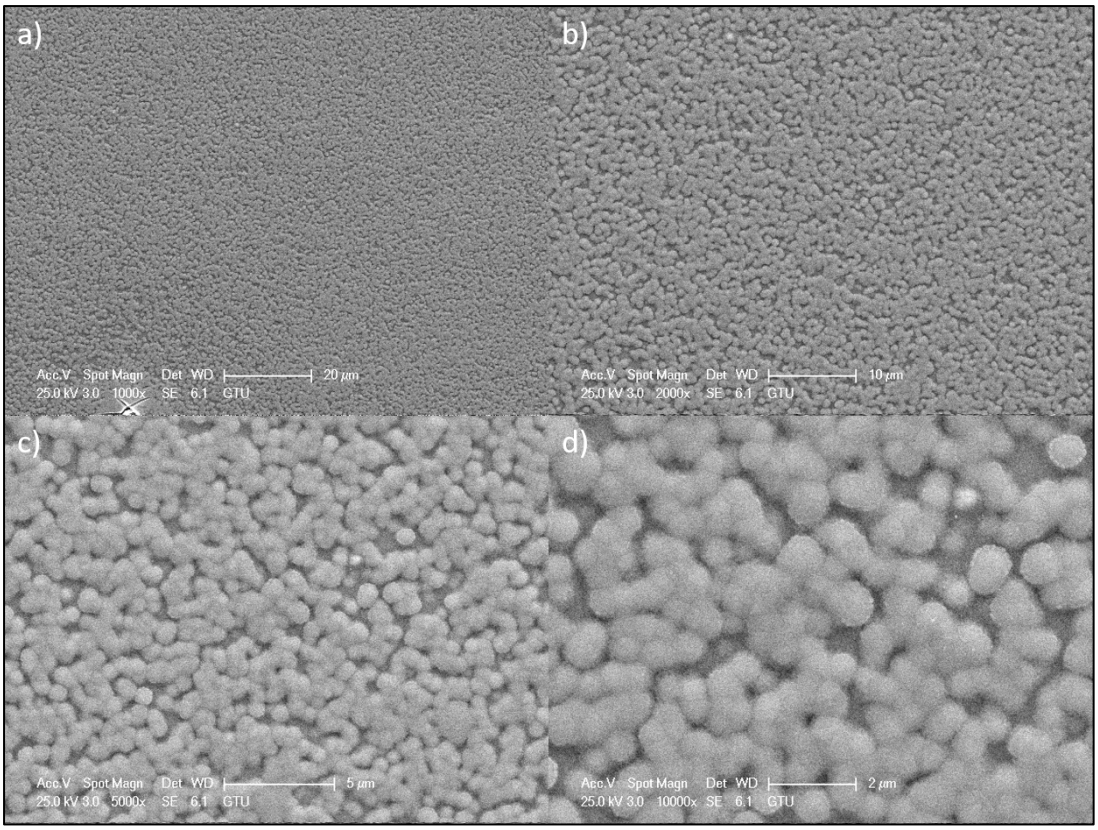


Figure 4.7: SEM micrographs of the PZT thin film (TF14) with 2%-mole Pb excess annealed at 700ºC for 1 hour; a) 1000x, b) 2000x, c)5000x and d) 10000x.

Beside this improvement of the microstructure there are still matrix regions between the rosettes. The main aim for this microstructure study was the eliminate the rosette phase. Increasing annealing temperature gave an approximation to achieve this aim. Moreover, some changes in the pyrolysis stage was also affected the crystallization kinetics of the films.

From the Figure 4.8, it was observed that the film and substrate interface has a good adhesion. Also, the surface of the film is uniform. The thickness of the film was measured as ~530 nm from the micrographs. Also, the thickness of the platinum layer was also measured as ~155 nm. All films were prepared as five layers. From these micrographs, it can be also observed that the size of rosettes have increased at the upper parts of the film. It can be related to the pyrolysis step because of using a hot plate.

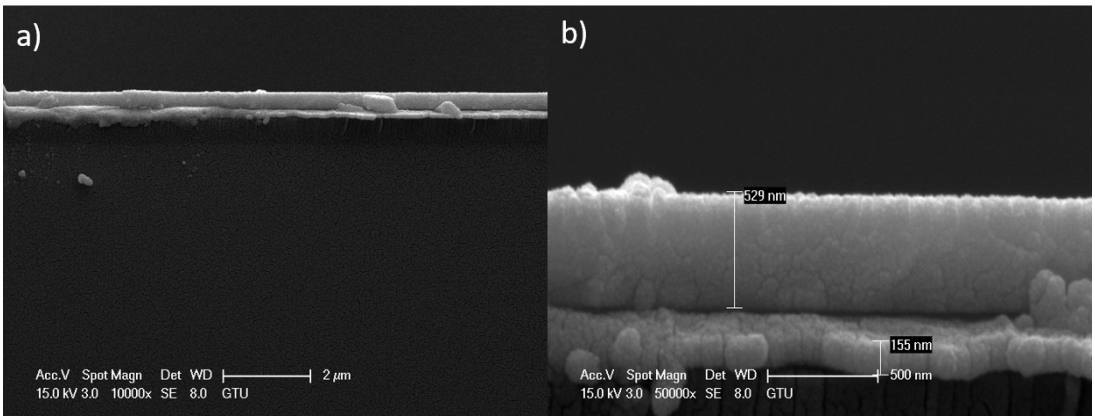


Figure 4.8: SEM micrographs of cross-section of the PZT thin film (TF13) with 2%-mole Pb excess annealed at 700ºC for 1 hour; a) 10000x, b) 50000x

SEM analyses were done for the PLZT films too. PLZT thin films were prepared with the 5%-mole and 20%-mole Pb excess compositions as told before. Figure 4.9 shows the microstructure of the PLZT thin films with the 5%-mole Pb excess composition and annealed at 650ºC for 1 hour. The films were not fully crystallized, obviously. Some big grain clusters with approximately 8μm and small ones with 1μm size were obtained.

When the temperature increased to 725ºC with the purpose of achieving more frequent and merged rosettes, 1-hour annealing resulted with the aimed microstructure. It can be seen that the structure is almost completely crystallized, and rosettes covered the whole structure with only small pyrochlore regions in some areas. This film has pyrolysis stage with 200ºC for 2 minutes and 430ºC for 5 minutes which is same with

the TF24 and TF25 films, they can be seen in Figure 4.10. Growth directions of the rosettes can be seen in Figure 4.10 and some of the rosettes clearly have large size while some of them very small.

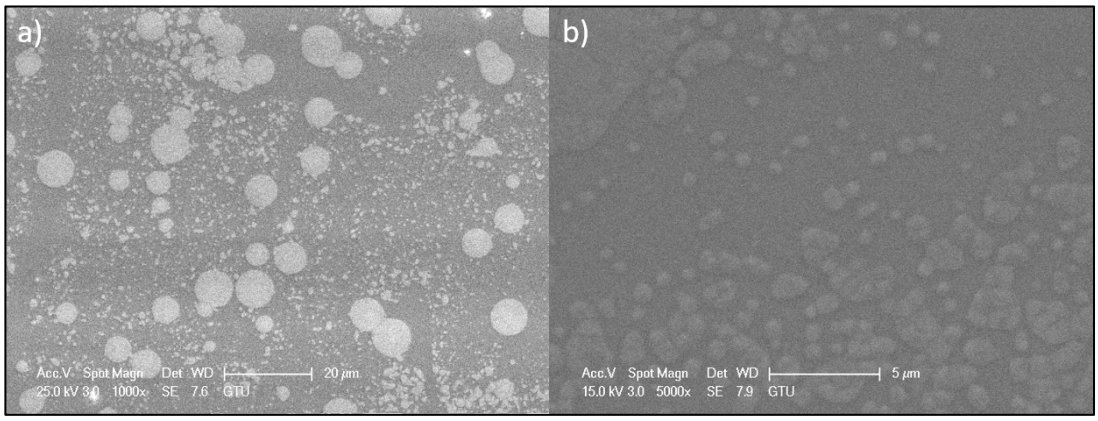


Figure 4.9: SEM micrographs of the PLZT thin films with the 5%-mole Pb excess annealed at 650ºC for 1 hour; a) 2000x (TF25) and b) 5000x (TF24).

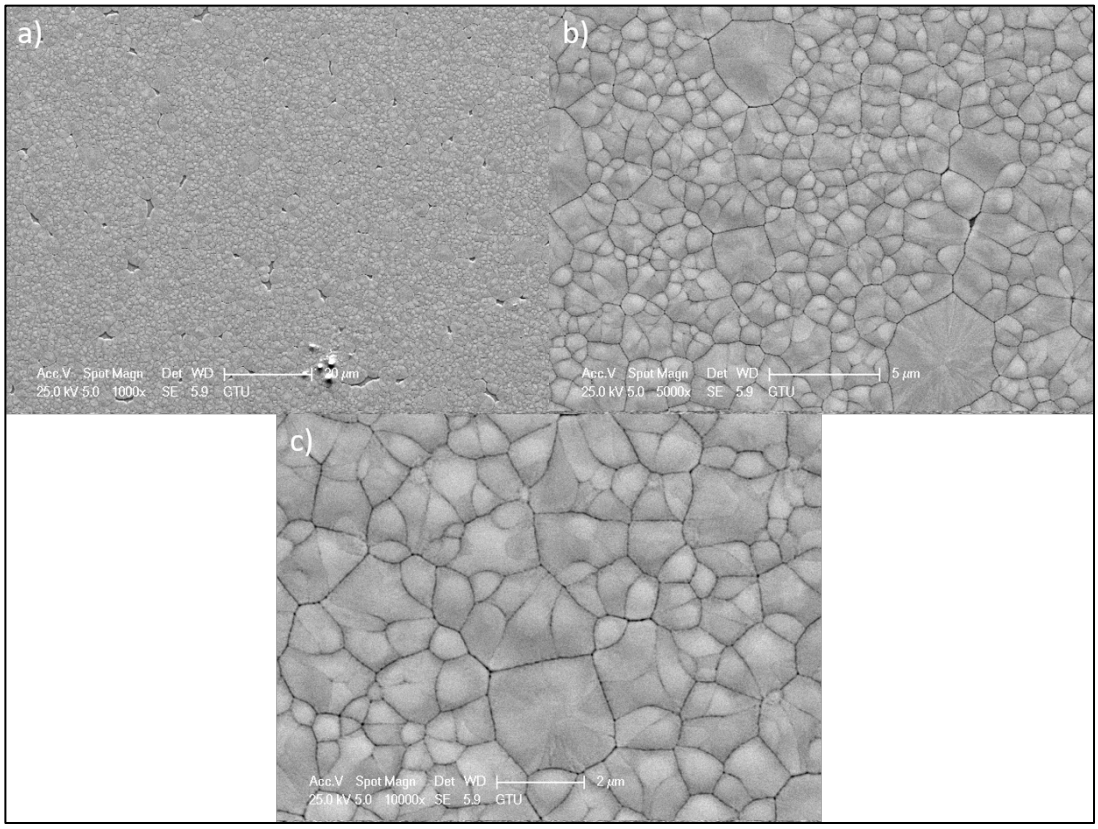


Figure 4.10: SEM micrographs of the PLZT thin film (TF26) with the 5%-mole Pb excess annealed at 725ºC for 1 hour; a) 1000x, b) 5000x and c) 10000x.

Due to achieve aim microstructure for the film, same coating, pyrolysis and annealing conditions repeated to see the reproducibility. Figure 4.11 and Figure 4.12 shows the results of the repeating the production of the film was given in Figure 4.10.

Reproduced films shown almost same microstructure between themselves but small changes with TF26 film which was given in Figure 4.10. SEM micrographs of the reproduced films can be seen in Figure 4.11 and Figure 4.12. The films have frequent rosettes and they are partly merged in some regions. Rosette sizes are more homogenous with compared to TF26, which is a good development for the films. But, TF30 still have some large rosettes in contrary to TF29. The differences between the film may cause from the small-time differences on the pyrolysis stage, heating efficiency of the furnace, self-cooling rate.

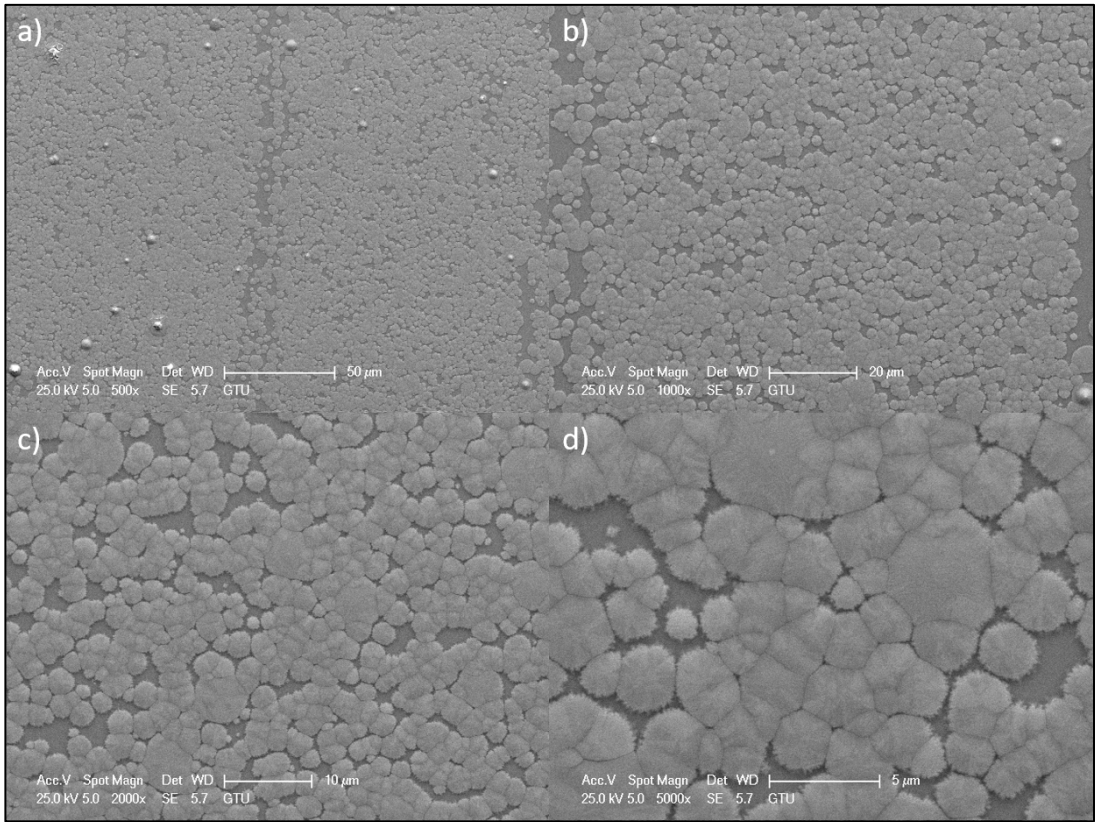


Figure 4.11: SEM micrographs of the PLZT thin film (TF29) with the 5%-mole Pb excess annealed at 725ºC for 1 hour; a) 500x, b) 1000x, c) 2000x and d) 5000x.

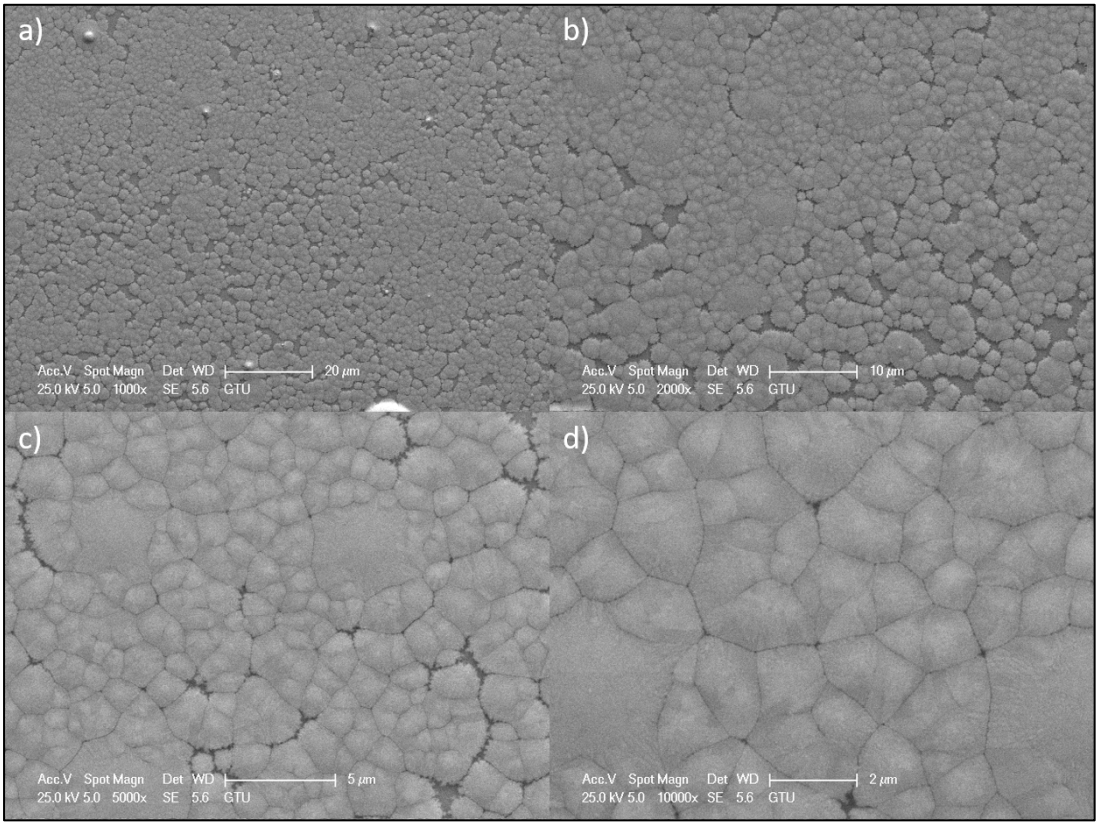


Figure 4.12: SEM micrographs of the PLZT thin film (TF30) with the 5%-mole Pb excess annealed at 725ºC for 1 hour; a) 1000x, b) 2000x, c) 5000x and d) 10000x.

For another film, the excess lead amount increased to the 20%-mole Pb and pyrolysis stage were edited as 200ºC for 5 minutes and 430ºC for 10 minutes. These parameters selected from the between 3 different pyrolysis stages tried on the films coated on GZO coated glass substrates which will be given in next. Selection of the parameters was done by reviewing the SEM images. In contrary to expectation not much change observed in these films. Frequent rosettes can be seen in Figure 4.13 but, they are not frequent as much as in the TF30 which is given in Figure 4.12. Rosette sizes are approximately 3μm. Also, there is some contamination on the surface of the film can be seen in Figure 4.13 (a). SEM micrographs with the increased magnification of the film are given in Figure 4.13. In Figure 4.13, growth direction and protruding boundaries of the rosettes can be seen which can indicate the growth is continuing.

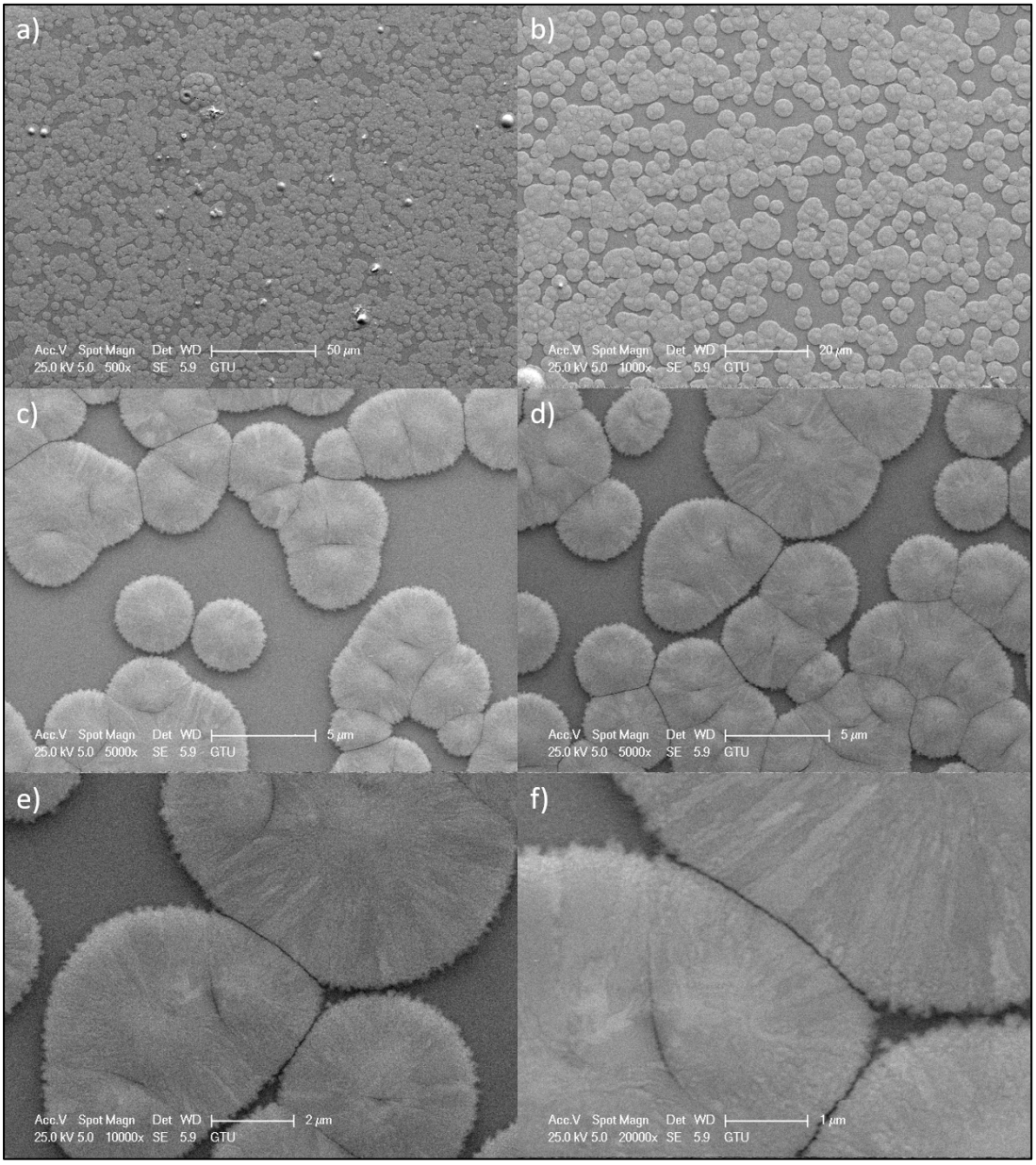


Figure 4.13: SEM micrographs of the PLZT thin film (TF27) with the 20%-mole Pb excess annealed at 725ºC for 1 hour; a) 500x,
b) 1000x, c) 5000x, d) 5000x, e) 10000x and f) 20000x.

4.1.3. Electrical Characterization of the PZT and PLZT Thin Films

Dielectric measurements of the films were carried out using a homemade temperature-dependent thin film probe station and LCR meter. It was observed from the measurements there is a wide distribution with frequency and the measured dielectric constants were so high especially for 1 kHz and 10 kHz frequencies. Measurements were taken from different electrodes of each films.

Homemade thin film probe station measurement system contains two probe tips and a hot plate as seen in Figure 4.14. Measurements were taken at different frequencies such as 1 kHz, 10 kHz, 100 kHz and 1 MHz. As mentioned before, for 1 kHz and 10 kHz, dielectric constant values are not reasonable. So, 100 kHz were used as measurements frequency for all films. Another problem was the set temperature of the system. This probe station also contains thermocouple. In this homemade system, the temperature was tried to control but this is not done accurately. So, many trials were done, and the temperature difference behavior was observed and in the light of this tendency measurement data was corrected.

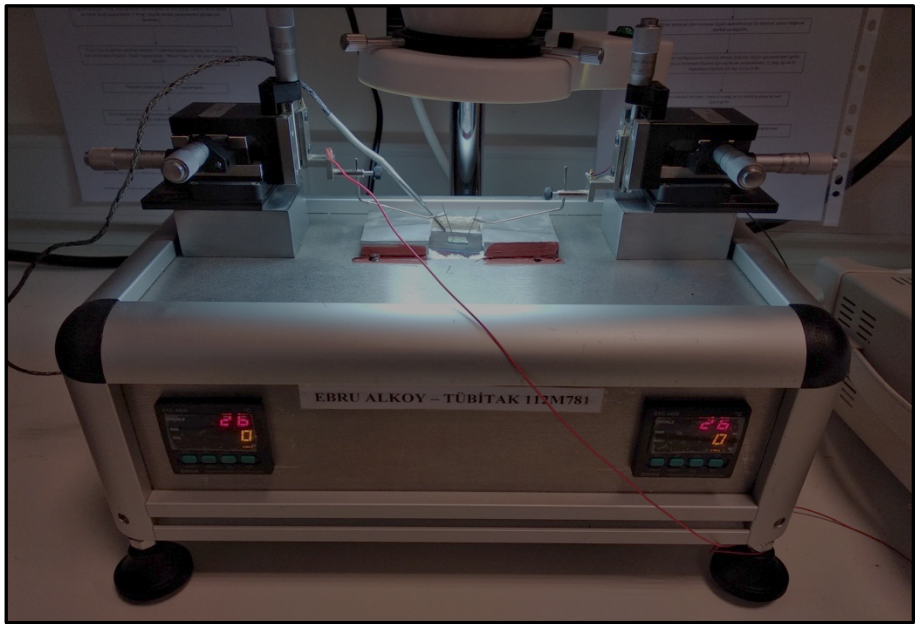


Figure 4.14: Thin film probe station.

The dielectric measurement of the PZT thin film with 2%-mole Pb excess annealed at 600ºC was given in Figure 4.15 and dielectric loss can be seen from the figure. Dielectric constant (ε_r) of this film was measured as 45 at 100 kHz frequency at room temperature. Curie temperature was also found to be a 370ºC at 100 kHz frequency. Dielectric loss (tan loss) versus temperature measurements were also done. At 100 kHz, tan loss was measurement as 0.05 for the film obtained at 600ºC. When annealing temperature was increased to 700ºC, according to Figure 4.16, ε_r and tan loss values were found as 234 and 0.09, respectively.

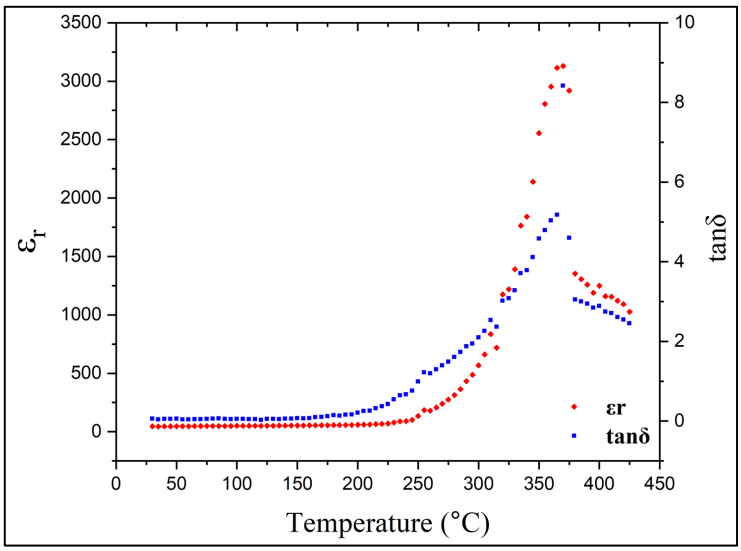


Figure 4.15: Dielectric constant versus temperature of the PZT thin film (TF7) with 2%-mole Pb excess composition, annealed at 600ºC.

Dielectric measurement of the PZT film with 2%-mole Pb excess annealed at 700ºC was given in Figure 4.16 and dielectric loss can be seen from the figure. Dielectric constant of this film was measured as 234 at 100 kHz frequency at room temperature. Curie temperature was also found to be as 330ºC at 100 kHz frequency.

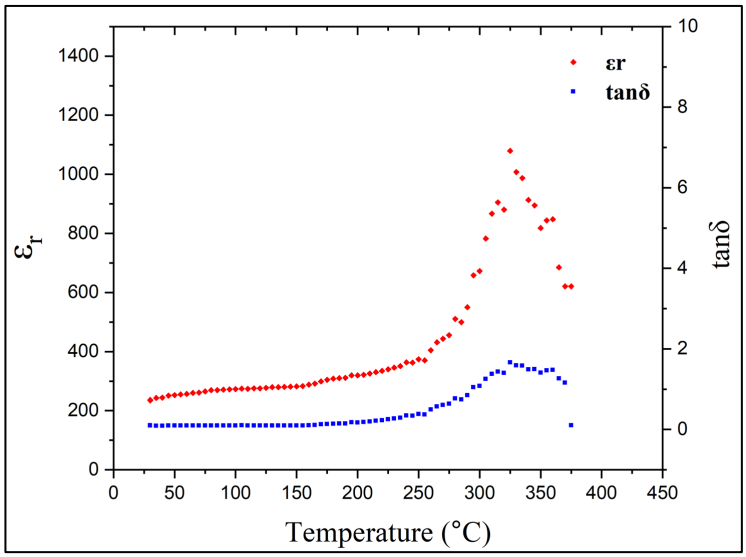


Figure 4.16: Dielectric constant versus temperature of the PZT thin film (TF16) with 2%-mole Pb excess composition, annealed at 700ºC.

The dielectric measurement of the PLZT film with 5%-mole Pb excess annealed at 650ºC was given in Figure 4.17 and dielectric loss can be seen from figure. The dielectric constant of this film was measured as 130 at 100 kHz frequency at room temperature. Curie temperature was also found to be as 370ºC at 100 kHz frequency.

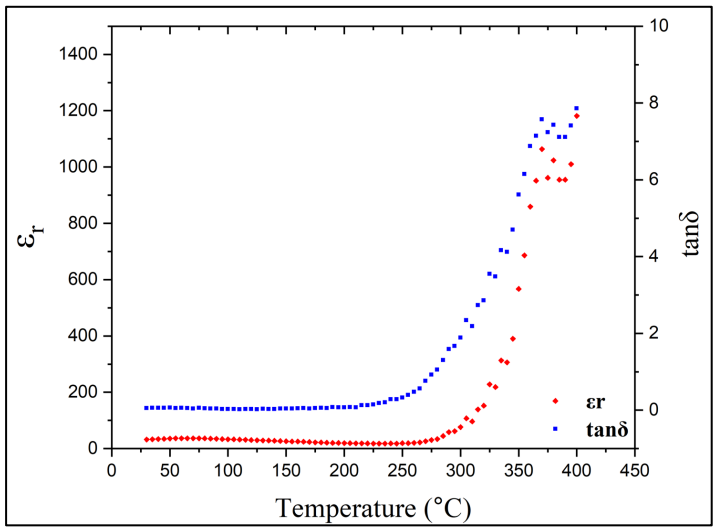


Figure 4.17: Dielectric constant versus temperature of the PLZT thin film (TF20) with 5%-mole Pb excess composition, annealed at 650ºC.

The dielectric measurement of the PLZT film with 5%-mole Pb excess annealed at 725ºC was given in Figure 4.18 and dielectric loss can be seen from figure. Dielectric constant of this film was measured as 1246 at 100 kHz frequency at room temperature. Curie temperature was also found to be as 65ºC at 100 kHz frequency.

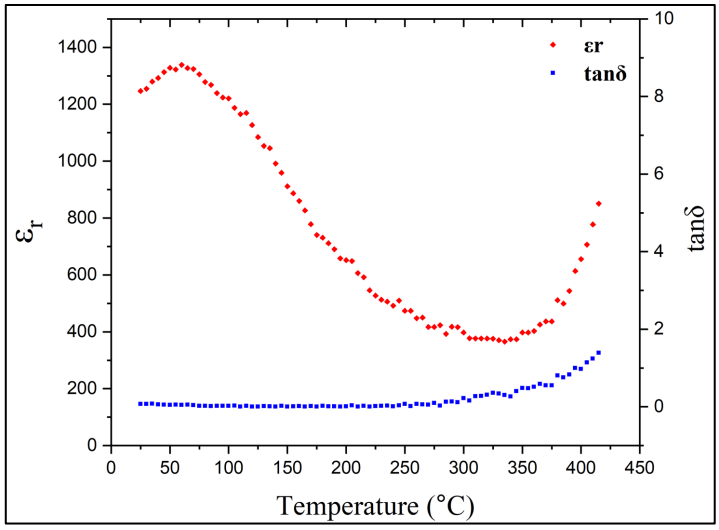


Figure 4.18: Dielectric constant versus temperature of the PLZT thin film (TF27) with 5%-mole Pb excess composition, annealed at 725ºC.

It can be seen from the Figure 4.18, there were not a sharp peak observed. It was thought reason of this broad peak is fine crystal size of the thin film. This approach was explained with the strain received by the film from substrate [67].

Table 4.1: Dielectric values of the measured films.

Composition	Annealing Temperature (ºC)	Curie Temperature(ºC)	Dielectric Constant (ε_r)	Dielectric Loss (tanδ)
PZT with 2%-mole Pb excess	600	370	45	0.05
	700	330	234	0.09
PLZT with 5%-mole Pb excess	650	370	130	0.05
	725	65	1246	0.07

Current density (J) versus electric field (E), J-E measurements were also done for the PZT with 2%-mole Pb excess films, annealed at 600ºC and 700º temperatures. As shown in the SEM micrographs Figure 4.6 and Figure 4.7 in the previous section, increasing annealing temperature has a strong effect on the rosette phases and their sizes. Furthermore, densification of the microstructure was also increased with increasing annealing temperature. But according to J-E measurements, the level of current densities was measured as ~10^{-10} A/cm^2. As seen from the Figure 4.19 and Figure 4.20, there was no drastic change for the current density of these two films.

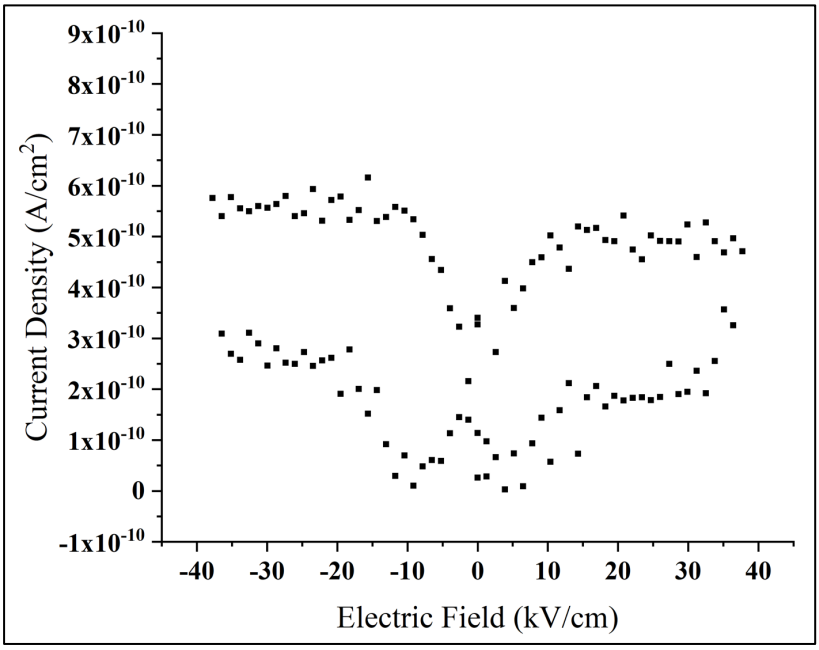


Figure 4.19: J-E characteristics of the PZT thin film with the 2%-mole Pb excess composition annealed at 600ºC for 1 hour (TF9).

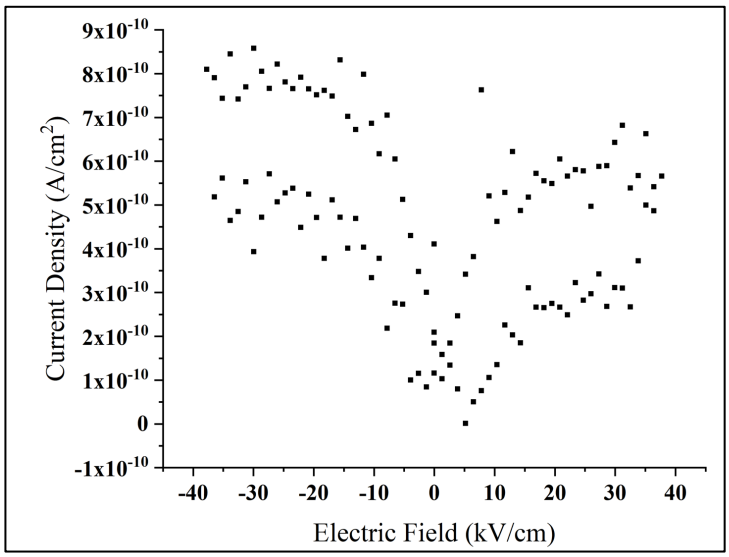


Figure 4.20: J-E characteristics of the PZT thin film with 2%-mole Pb excess composition annealed at 700ºC for 1 hour (TF16).

4.2. PZT and PLZT Films Obtained on the Gallium doped Zinc Oxide (GZO) Coated Glass Substrates

The results of phase analyses, microstructural analyses and, electrical properties of the PZT and PLZT films fabricated on gallium doped zinc oxide (GZO) coated glass substrates will be discussed in this section.

4.2.1. Phase Analyses of the Thin Films

First of all, XRD pattern of the GZO coated glass substrate was given in Figure 4.21. XRD pattern of the PZT with 2%-mole Pb excess composition is given in Figure 4.22 for different annealing temperatures. Results of the XRD analyses show that annealing temperature is very important on crystallization of the film.

In this part of the study, annealing process was tried to apply at different temperatures; 600ºC, 700ºC and 725ºC. RTA process was used, and annealing time was kept as 1 hour. Also, GZO layer had been coated on glass substrates and these substrates were commercial as mentioned in experimental part in Section 3.

From the Figure 4.22, it can be seen that with the increasing annealing temperature crystallization level of the films increasing too. The peak at the 2θ=34º indicates the main peak of GZO coated glass substrate. XRD pattern of the film annealed at 600ºC for 1 hour there was a peak at the 2θ=29º and 30º and it indicates the pyrochlore phase for the films fabricated at this temperature. When annealing

temperature was increased to 700ºC, a full perovskite phase with preferred (110) orientation was obtained. But there was no big difference for the intensity of the peak of (110) plane for the film obtained at 700ºC and 725ºC.

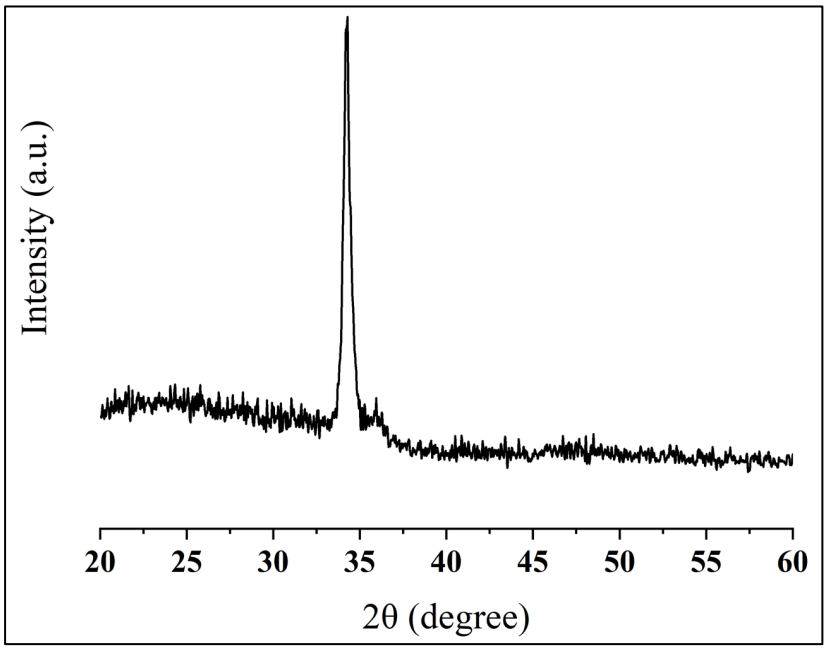


Figure 4.21: XRD patterns of the GZO coated glass substrate.

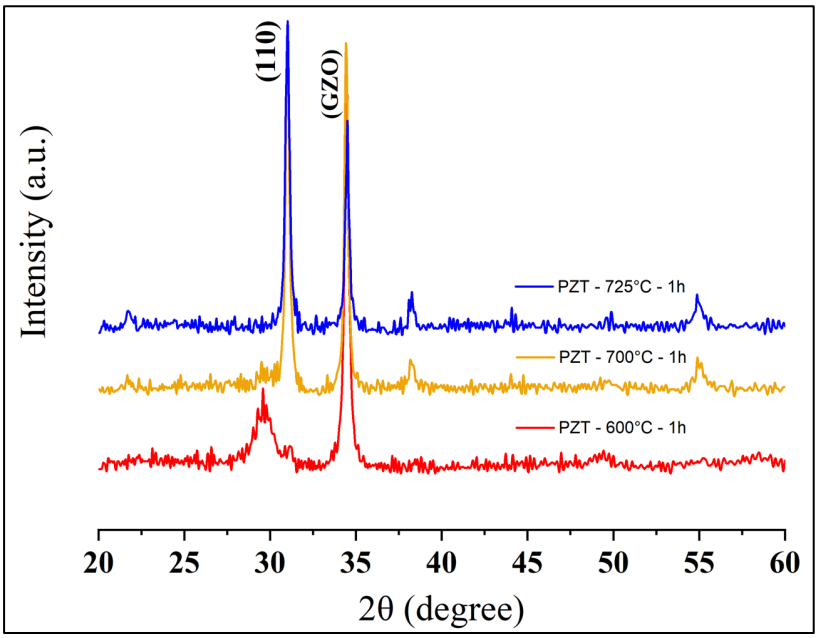


Figure 4.22: XRD patterns of the PZT thin films with 2%-mole Pb excess coated on GZO coated glass substrates.

XRD patterns of the PLZT thin films were given in Figure 4.23. These films were annealed at different temperatures; 650ºC and 725ºC. These annealing temperatures was selected due to the DTA-TG results for this composition. First annealing temperature selected as 650ºC and it wasn't sufficient to promote the crystallization in preferred orientation and there were peaks at the 2θ=29º and 30º and they indicate the pyrochlore phase. Then annealing temperature increased to 725ºC and resulted with (110) preferred orientation, full perovskite phase.

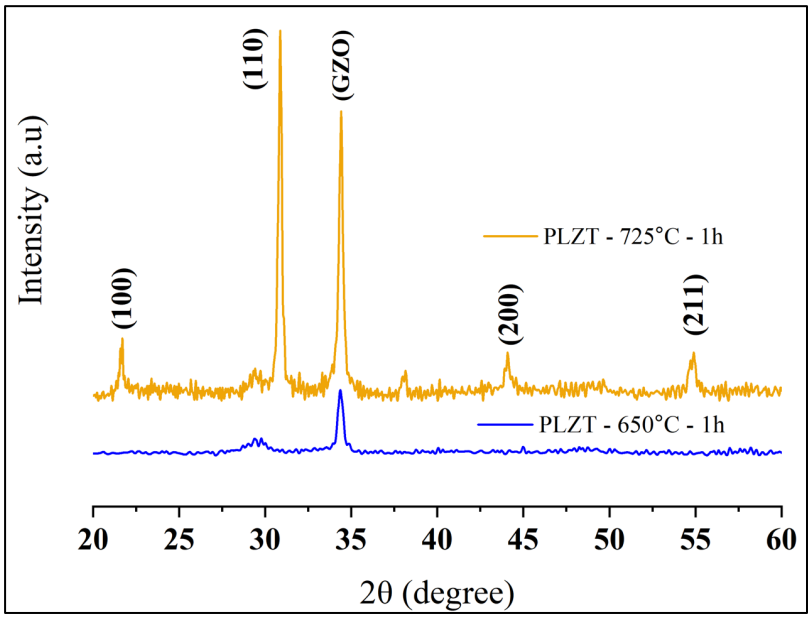


Figure 4.23: XRD patterns of the PLZT thin films with 5%-mole Pb excess coated on GZO coated glass substrates.

4.2.2. SEM Analyses of the PZT and PLZT Thin Films

SEM analyses were done to characterize the microstructure of the films and defining the optimum processing parameters for the films obtained on GZO coated glass substrate.

In Figure 4.24, SEM micrographs of the PZT films obtained at 600ºC were given. It can be mentioned that, the structure is dense and instead of grain, rosette formation is observed again. Rosette size of the film is approximately 5μm and there is no merged rosettes in the structure. Figure 4.25 shows the SEM micrographs of the PZT thin film with 2%-mole Pb excess annealed at 700ºC for 1 hour. According to these micrographs, it can be said that the rosettes are merging at this annealing

temperature and at the merging points there are some small rosettes. Some porosities can be seen in between the rosettes. Rosettes sizes are approximately 7μm.

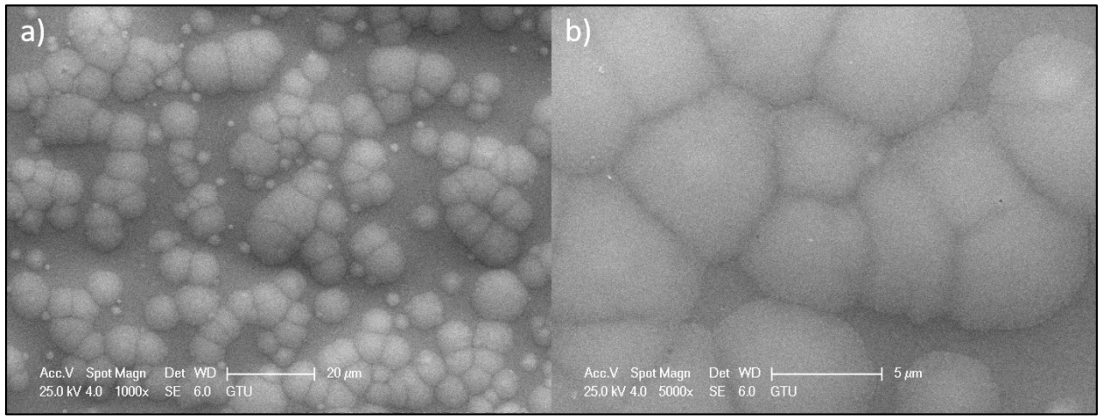


Figure 4.24: SEM micrographs of the PZT thin film (TCO3) with the 2%-mole Pb excess annealed at 600ºC for 1 hour; a) 1000x,
b) 5000x

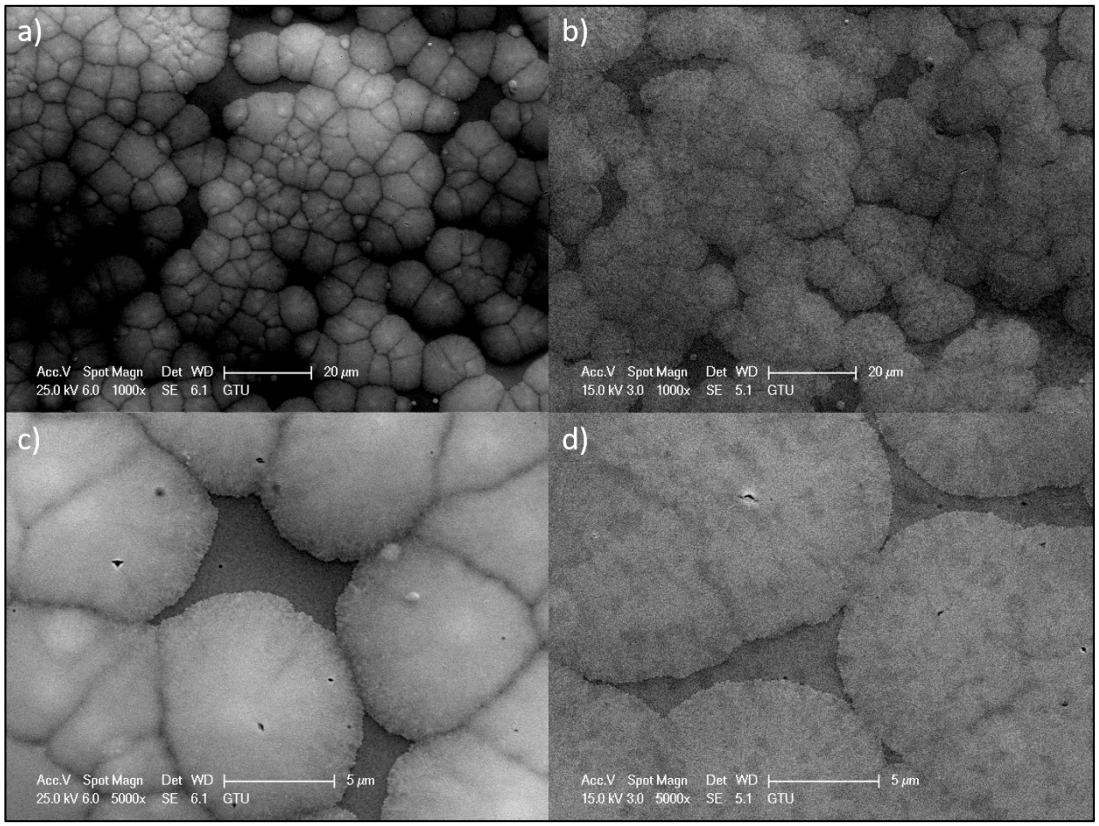


Figure 4.25: SEM micrographs of the PZT thin film (TCO7) with the 2%-mole Pb excess annealed at 700ºC for 1 hour; a) 1000x,
b) 1000x, c) 5000x and d) 5000x.

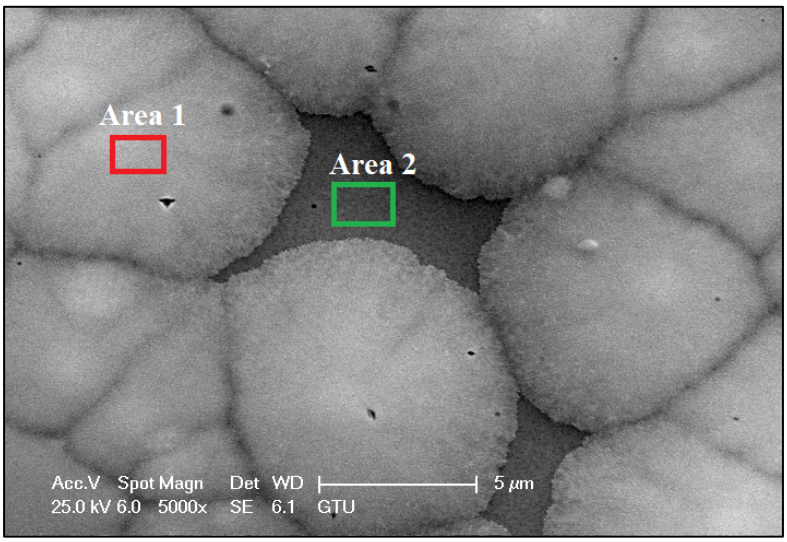


Figure 4.26: Selected spots of the TCO7 thin film for EDX analyses.

Results of the EDX analyses taken from the areas as given in Figure 4.26 are also given in Figure 4.27 and Figure 4.28, respectively. Atomic weight percent are also reported in Table 4.2 and Table 4.3 for both phases. As expected, analyses showed that the lead content is low at the outside of the rosette, in another words matrix phase, with compare to the rosette.

Table 4.2: EDX analyses of the inside of the rosette (Area 1) for TCO7.

Element	**Weight (%)**	**Atomic (%)**	**Net Int.**
O	26.43	75.09	315.42
Zr	13.31	6.63	752.99
Ti	6.92	6.57	474.39
Pb	53.34	11.7	477.14

Table 4.3: EDX analyses of the matrix phase (Area 2) for TCO7.

Element	**Weight (%)**	**Atomic (%)**	**Net Int.**
O	34.74	80.28	364.42
Zr	15.64	6.34	752.15
Ti	7.62	5.88	454.02
Pb	42.01	7.5	310.03

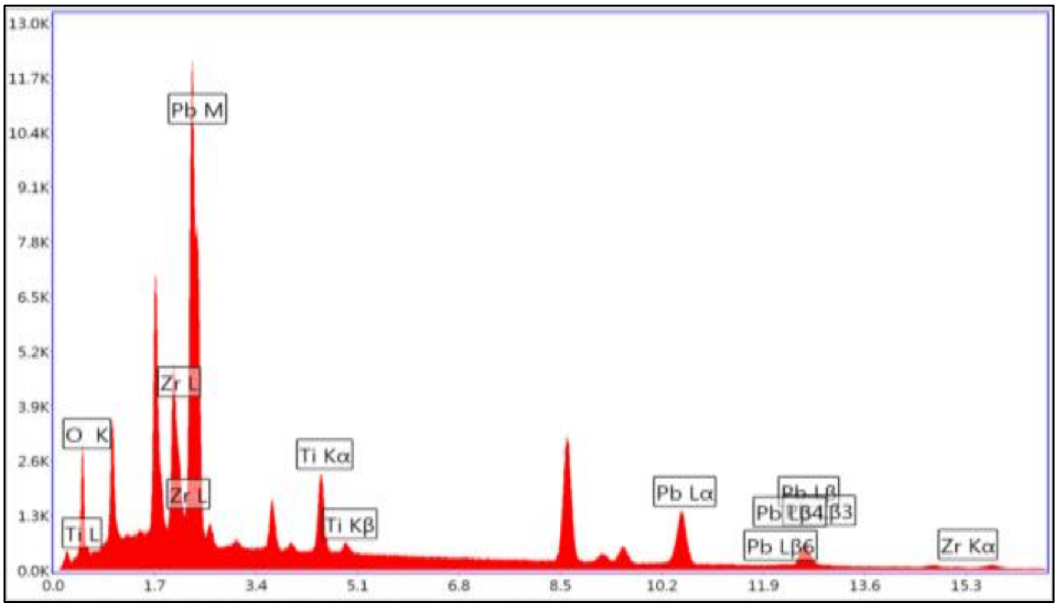


Figure 4.27: EDX analyses of the inside of the rosette (Area 1) for TCO7.

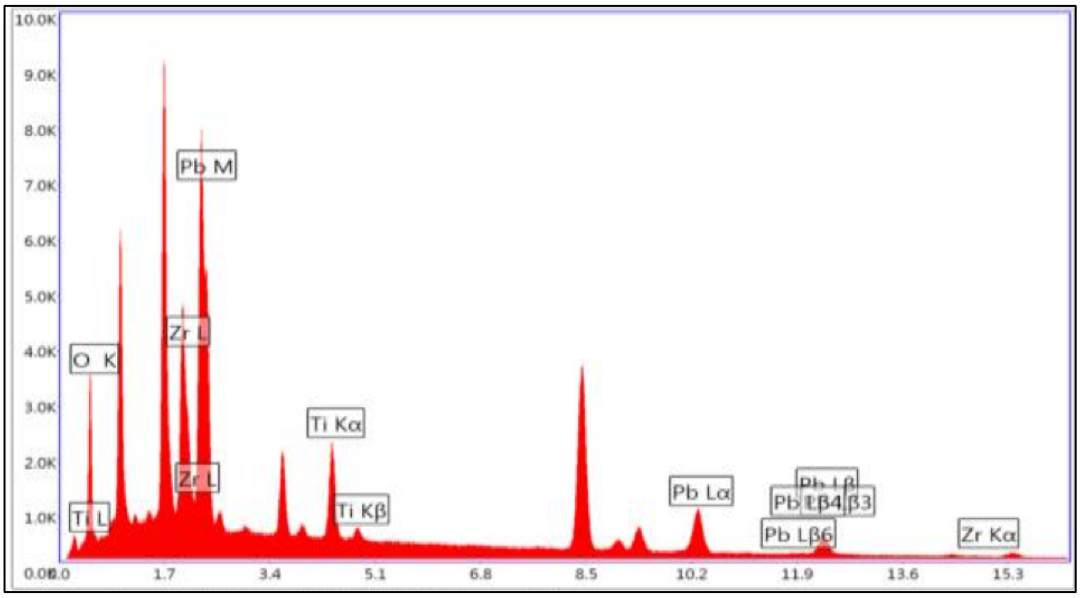


Figure 4.28: EDX analyses of the matrix phase (Area 2) for TCO7.

As a conclusion of EDX analyses, matrix is a lead deficient phase. Decreasing the amount of matrix phase in whole the whole film will improve the electrical and optical properties. So, these analyses are very crucial for this study.

Annealing the PZT film with 2%-mole Pb excess at 725ºC resulted with intense rosettes and less matrix phase. In Figure 4.29, it can be seen that the growth directions of the rosettes are very clear. All this temperature, the rosette frequency is very high and microstructure is very dense comparing to the films annealed at 700ºC ones.

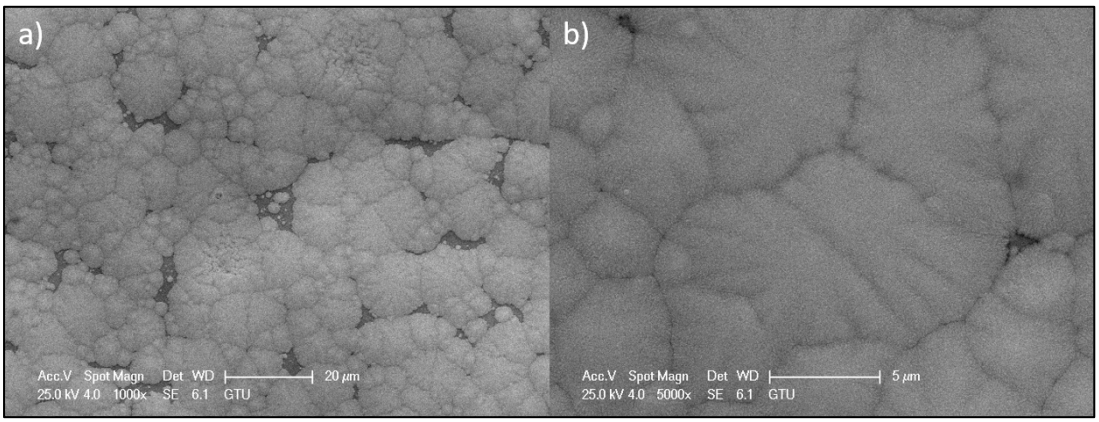


Figure 4.29: SEM micrographs of the PZT thin film (TCO27) annealed at 725ºC; a) 1000x, b) 5000x magnifications.

In Figure 4.30, SEM micrographs of the cross-section of the PLZT thin film was given. The thickness of the GZO coated glass substrate and PLZT film were measured as ~320 nm and ~600 nm, respectively. The surface of the film was quite homogeneous; no islands or peelings were observed. There is another was layer was observed with ~380 nm thickness, under the both of GZO and PLZT layers. Total film thickness was measured and used as ~600nm for the optical calculations

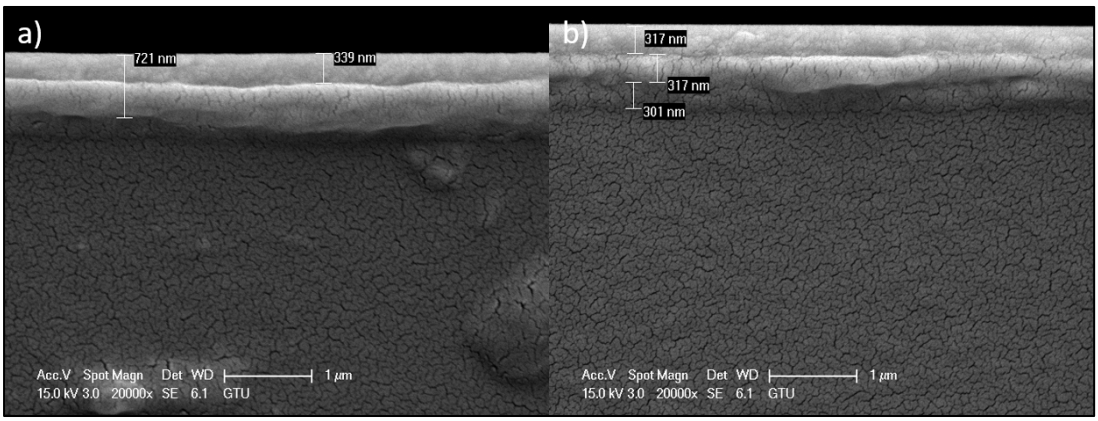


Figure 4.30: SEM micrographs of cross-section of the PLZT thin film (TCO16) annealed at 650ºC; a) 20000x, b) 20000x magnifications.

SEM micrographs of the PLZT film annealed at 700ºC was given in the Figure 4.31. According these micrographs, it can be said that the rosettes were merged partially, and the mean size of the rosettes are found to be as ~5 μm. The ratio of the rosette/matrix phase is not high at this composition. So, it was believed that the annealing temperature or pyrolysis conditions were not sufficient at this time.

In the light of these results, pyrolysis conditions of the films were changed, and the annealing temperature of the films increased to 725ºC. Annealing time kept constant as 1 hour. All pyrolysis conditions were given in Table 3.3.

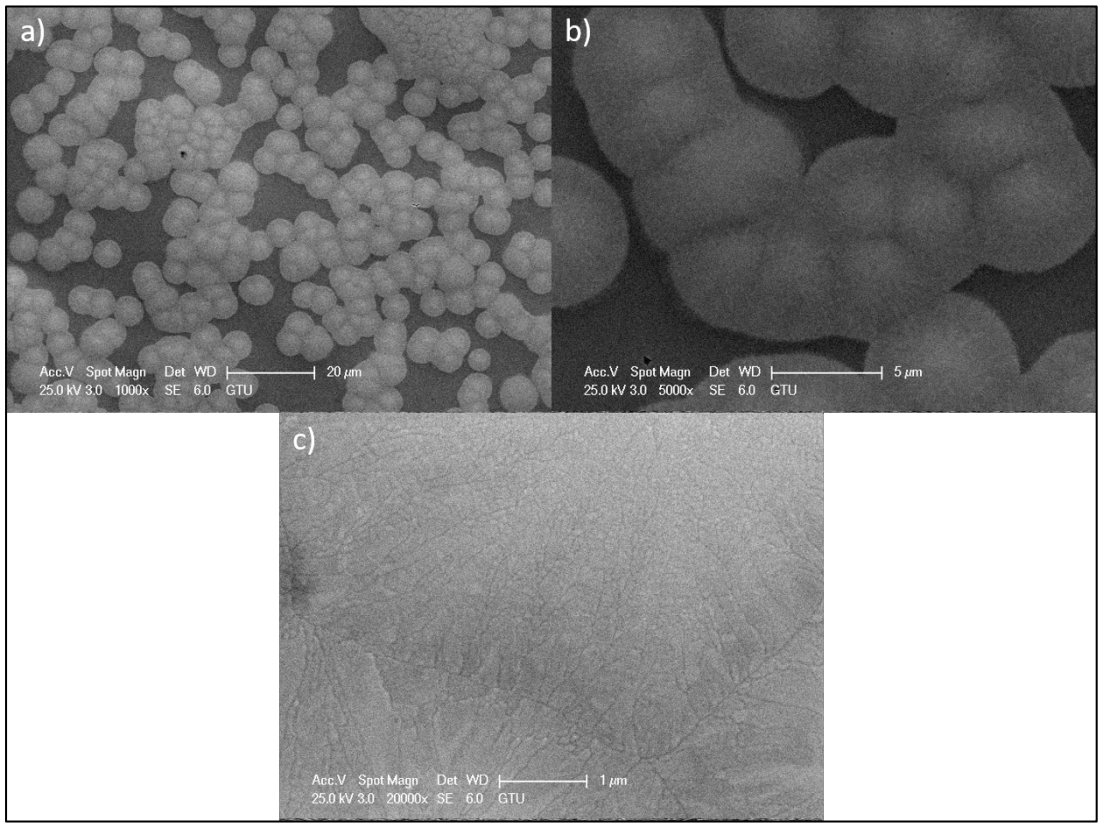


Figure 4.31: SEM micrographs of the PLZT thin film (TCO23) with the 5%-mole Pb excess annealed at 700ºC for 1 hour; a) 1000x,
b) 5000x, c) 20000x.

Annealing temperature was increased to 725ºC and as a remarkable change, pyrolysis conditions were changed at this annealing temperature. SEM micrographs of the PLZT thin film named as TCO 29 were given in Figure 4.32. This film was fabricated with pyrolysis condition as 200ºC for 5 minutes and 430ºC for 5 minutes. The rosettes were quite frequently in this condition with compare to the film given in Figure 4.31 and rosettes has merged completely in some regions.

SEM micrographs of the PLZT thin film with pyrolysis condition as 200ºC for 5 minutes and 430ºC for 10 minutes were given in Figure 4.33. This processing condition resulted in a quite dense microstructure. Merged rosettes were observed on the whole surface. There were some secondary matrix phases also was observed but not much as the previous films.

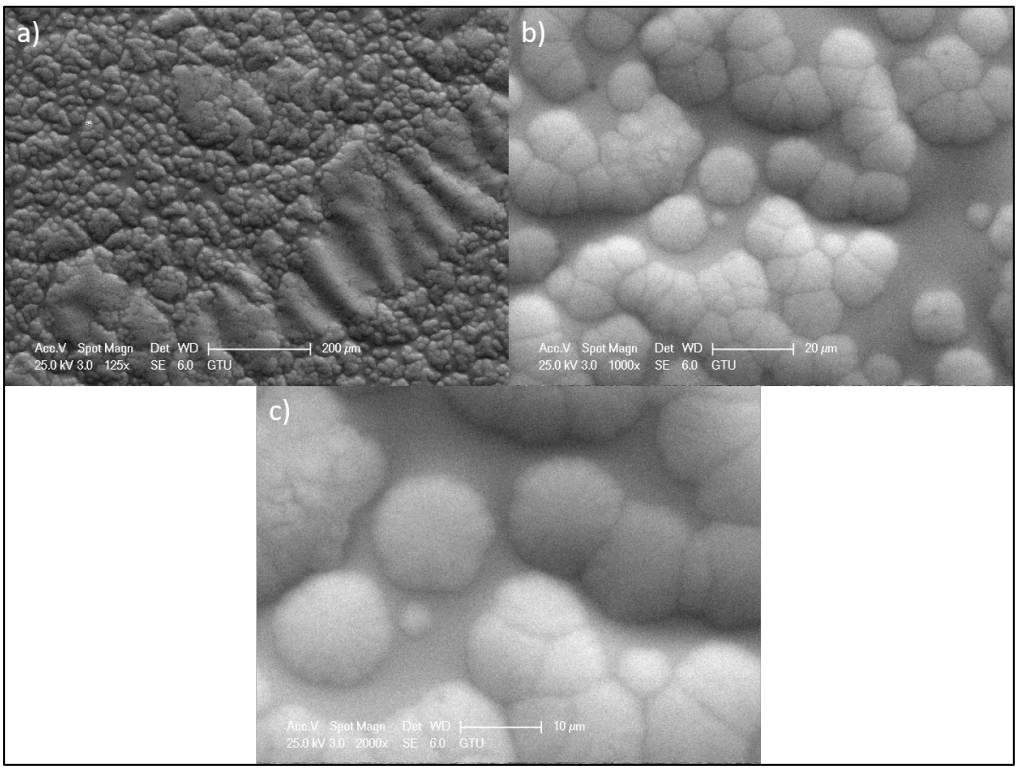


Figure 4.32: SEM micrographs of the PLZT thin film (TCO29) with the 5%-mole Pb excess annealed at 725ºC for 1 hour; a) 125x,
b) 1000x, c) 2000x.

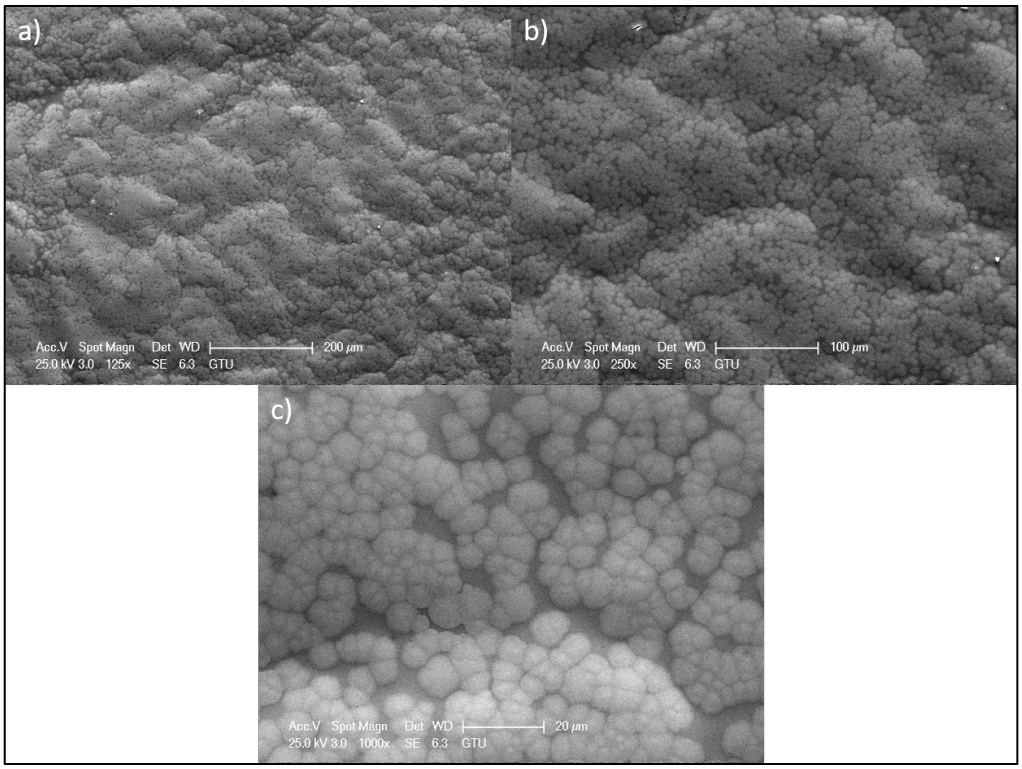


Figure 4.33: SEM micrographs of the PLZT thin film (TCO30) with the 5%-mole Pb excess annealed at 725ºC for 1 hour; a) 125x,
b) 250x, c) 1000x.

The last pyrolysis condition was selected as 200ºC for 2 minutes and 430ºC for 10 minutes. Result of this condition is given in Figure 4.34. Merged rosettes were also seen in some regions but these regions were not much wide. Compared to previous films, the microstructure is not dense for this pyrolysis condition.

As a result, generally, with compare to films coated on $Pt_{(111)}/Ti/SiO_2/Si_{(100)}$ substrates, rosette size was more homogenous and the pyrolysis condition as 200ºC for 5 minutes and 430ºC for 10 minutes is effective for the PLZT film obtained at 725ºC. But in every condition, the rosette phase was still observed in different ratios.

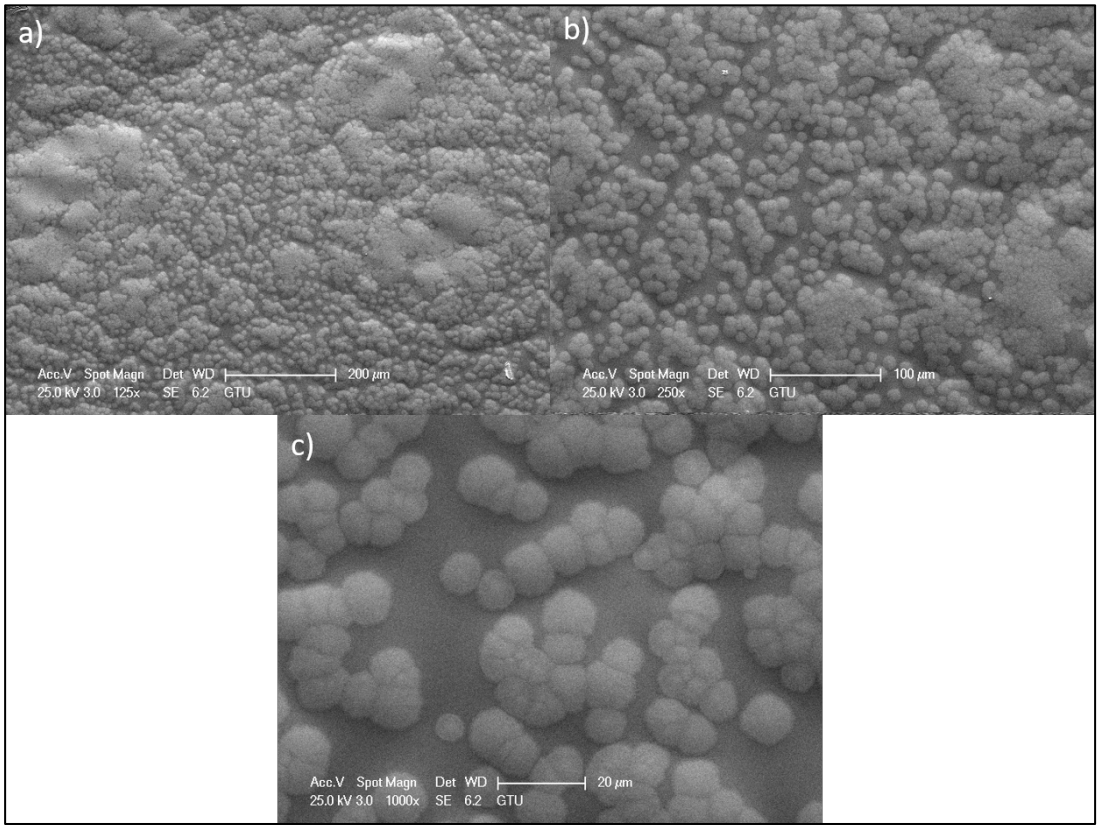


Figure 4.34: SEM micrographs of the PLZT thin film (TCO31) with the 5%-mole Pb excess annealed at 725ºC for 1 hour; a) 125x, b) 250x, c) 1000x.

4.2.3. Optical Measurements of the PZT and PLZT Thin Films

To characterize the optical behavior of the films, UV-Vis measurements were carried out using UV-Vis spectrometer. Measurements were done in the 200-1000 nm wavelength range. Also, the optical band gap (E_g) values of the films were calculated. The calculation made by using equation given at below.

$$\alpha h\nu = A(h\nu - E_g)^{n/2} \quad (4.1)$$

In Equation 4.1, "A" is a constant, "n" representing the transition type as direct or indirect allowed the transition. Plotting the $(\alpha h\nu)^2$ versus $h\nu$ and linear fitting the data gives the optical absorption edge (E_g) of the material. These techniques were also used by a researcher form our group [68-71].

In Figure 4.35, transmittance values of the PZT thin films annealed at different temperatures were given. The film annealed at the 600ºC has ~60% transmittance level for the 500nm wavelenght. When the temperature was increased to 725ºC, transmittance level dropped to ~50% levels. This descending trend can be reasoned by the further crystallization and formation of grains with sizes, probability on the order of 400-900 nm. As a result of this, scattering regions such as grain boundaries, grains of the microstructure increases. Also, from the Figure 4.35, the sharp drop at around 400 nm wavelength corresponds to the band gap (absorption edge, E_g).

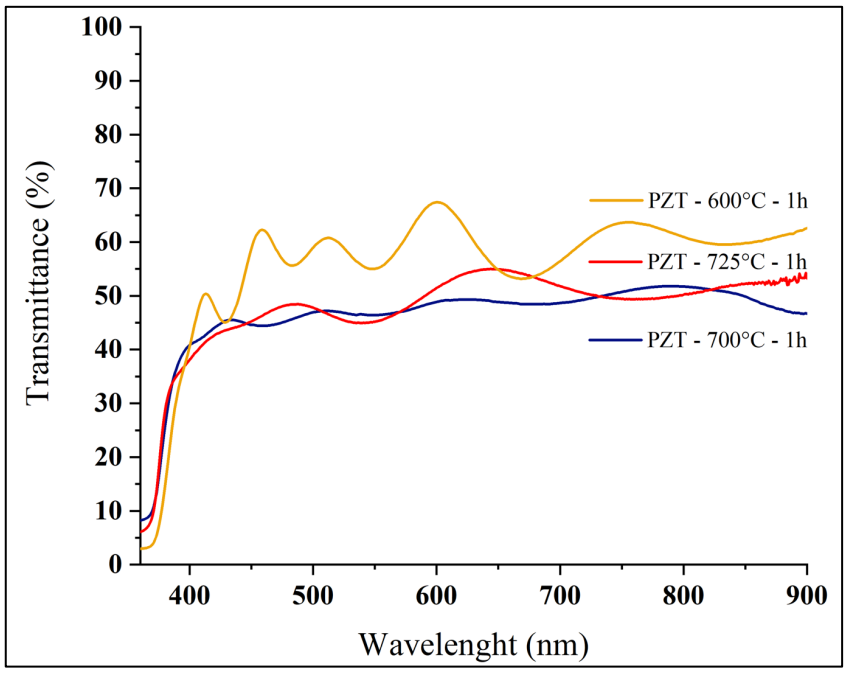


Figure 4.35: Optical transmittance values of the PZT thin films with the 2%-mole Pb excess annealed at 600ºC, 700ºC and 725ºC.

Using Equation 4.1, optical band gap calculations were done. In Figure 4.36, $(\alpha h\nu)^2$ versus $(h\nu)$ graph was given for PZT films. The band gap value for the film annealed at 600ºC was found as 3.23 eV, while it was 3.23 eV for 700ºC and 3.27 eV for the film annealed at 725ºC.

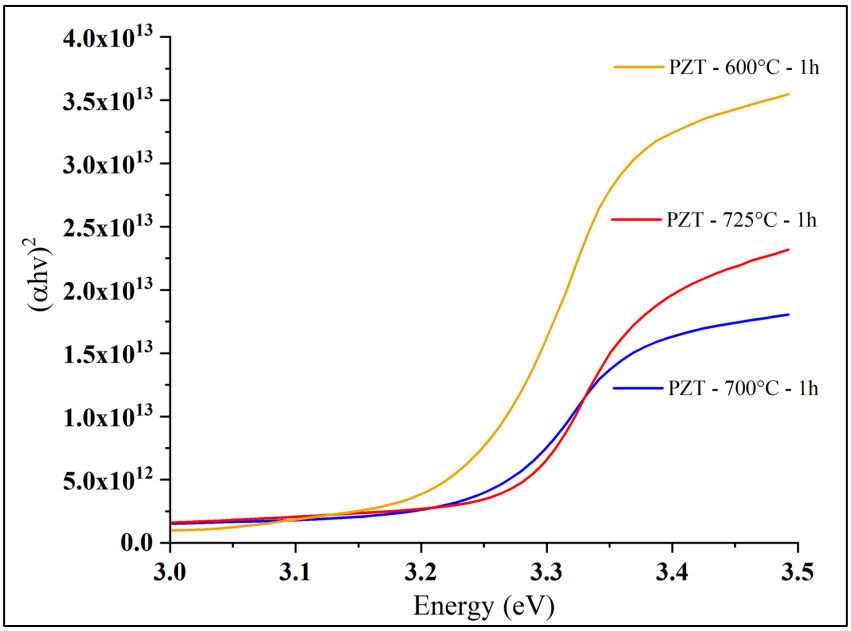


Figure 4.36: Optical band gap values of the PZT thin films with the 2%-mole Pb excess composition and annealed at 600ºC and 725ºC for 1 hour.

As a conclusion, in ultraviolet (UV) region, as seen in Figure 4.35, electromagnetic radiation was almost absorbed by the PZT films. But after UV region, the transmission levels changed from 30% at the 400 nm wavelength to 65% at the 550 nm depending on the film. It can be assumed that the rest of radiation is reflected back from or absorbed by grains.

Optical transmittance values of the PLZT thin films were found to be higher than PZT thin films ones in order to La-addition and transmission values can be seen in Figure 4.37. The transmittance of the PLZT film annealed at 650ºC is found around 90% levels at 650nm wavelenght. The transmittance value of the PLZT thin film annealed at 700ºC was found at 50% levels at the same wavelength region. With increasing the temperature to 725ºC, there was not any big changes in transmittance levels.

It can be speculated that absorption centers do not exist in 400-900 nm region for the PLZT films annealed at 650ºC, and this resulted with 100% transmittance. Generally, the transmittance of the films was decreased with increasing temperature.

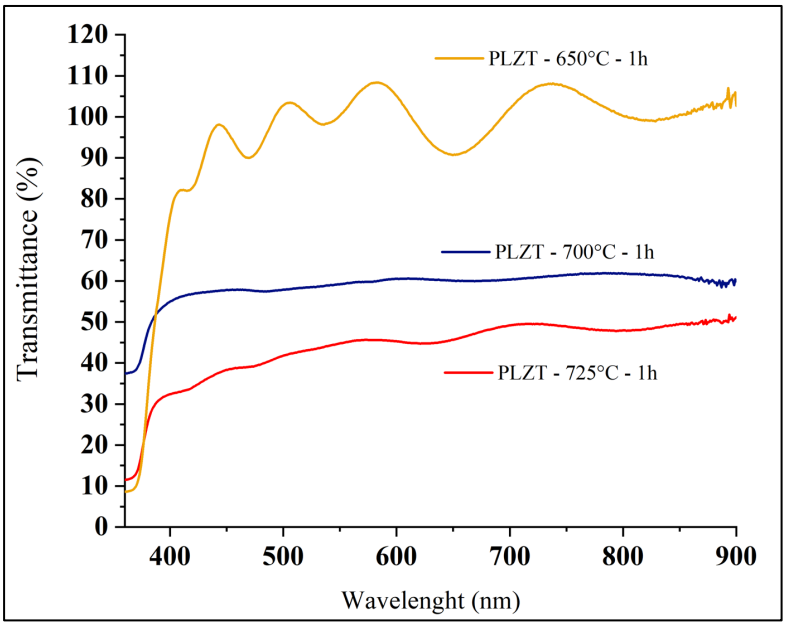


Figure 4.37: Optical transmittance values of the PLZT thin films with the 5%-mole Pb excess annealed at 700ºC and 725ºC.

Optical band gap values of the films were calculated using Figure 4.38 and band gap values showed a difference. The band gap value of the film annealed at 600ºC was found from the slope of the figure as 3.23 eV. For the film annealed at 700ºC it was 3.22 eV. When the sintering temperature was increased up to 725ºC, the band gap value was calculated as 3.27 eV.

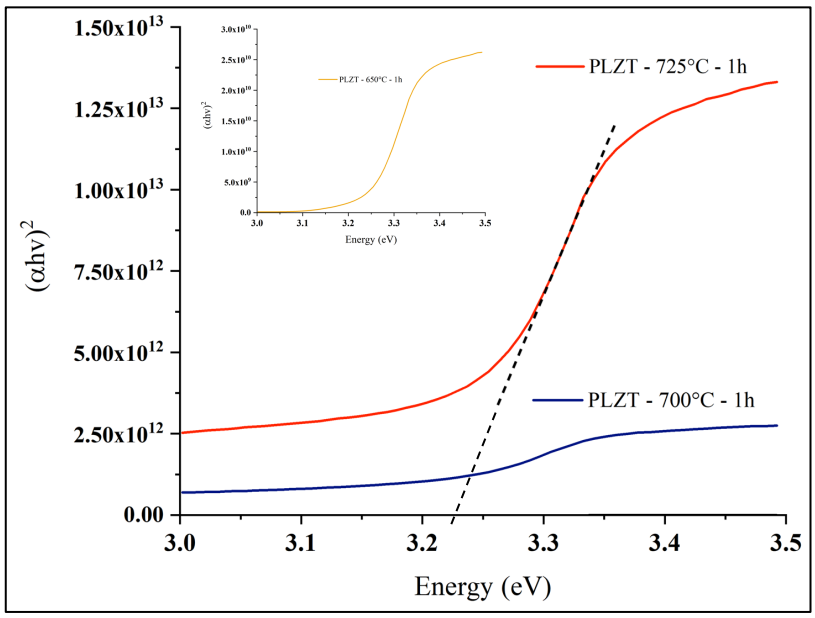


Figure 4.38: Optical band gap values of the PLZT thin films with the 5%-mole Pb excess annealed at 650ºC, 700ºC and 725ºC.

Table 4.4: Band gap values of the films.

Composition	Annealing Temperature (ºC)	Band Gap (eV)
PZT with 2%-mole Pb excess	600	3.23
	700	3.23
	725	3.26
PLZT with 5%-mole Pb excess	650	3.23
	700	3.22
	725	3.27

4.2.4. Piezo Response Force Microscope and Atomic Force Microscope Analyses of the Films

Piezo response force microscope (PRFM) analyses were done with AC amplitude 18V and ~41kHz AC frequency by Nanomagnetic, Ankara. These analyses for PZT film named as TCO6 were given in Figure 4.39. According to figure, rosette phase has domain structure. Because the lighten area indicates ferroelectric domains in the films.

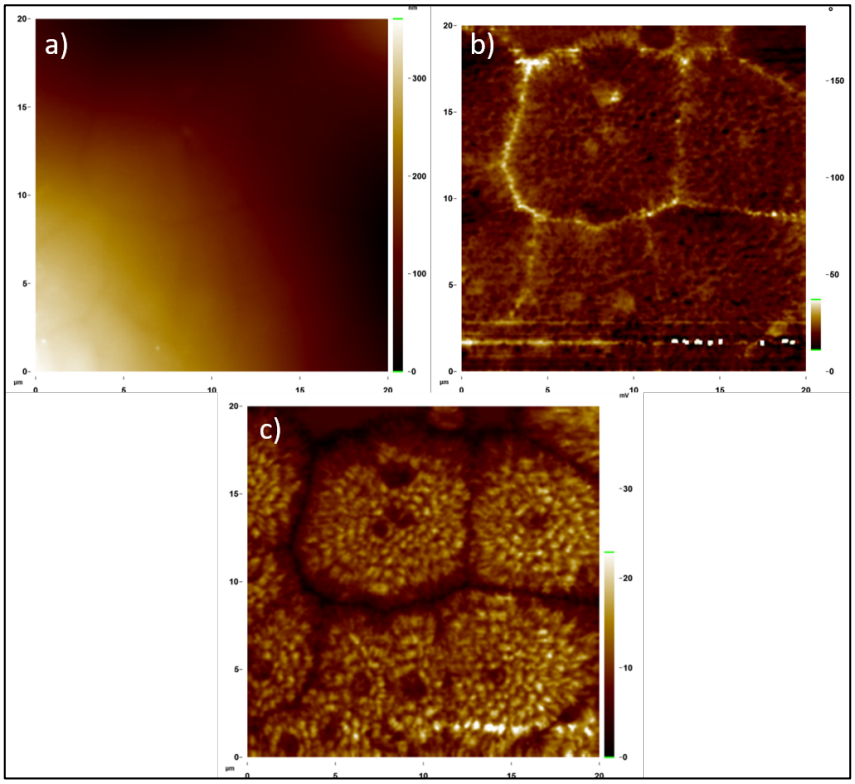


Figure 4.39: PRFM analyses of PZT thin film (TCO6) annealed at 700ºC for 1 hour; a) Topography, b) PRFM Phase and c) PRFM Amplitude.

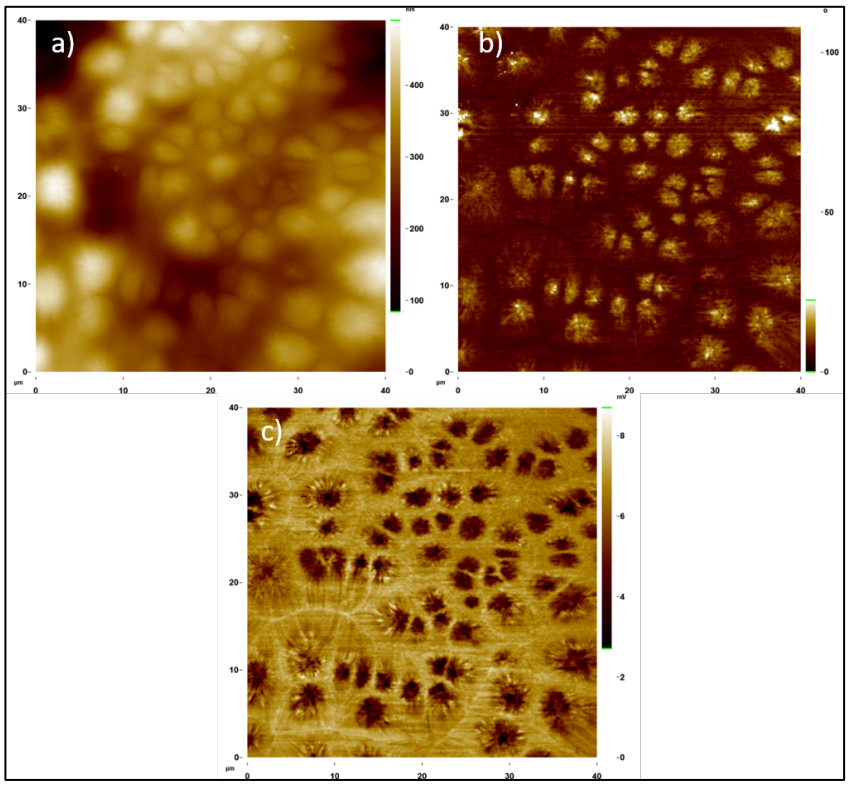


Figure 4.40: PRFM analyses of PLZT thin film (TCO32) annealed at 700ºC for 1 hour; a) Topography, b) PRFM Phase and c) PRFM Amplitude.

Atomic force microscope (AFM) analyses were also done to investigate the surface characterizations of the films. Characterizations were revealed the rosette and matrix phase has topographic structure. Rosette phase has higher altitude with compare to matrix phase. Despite the pyrochlore phase were not detected by XRD, SEM results showed that there is secondary matrix phase in the structure of PLZT films. It was concluded that pyrolysis steps could control the ratio and frequency of rosette phase. Figure 4.41 shows that matrix and rosette phases of PLZT annealed at 725ºC and pyrolysis steps as 200ºC 2 min + 430ºC for 5 min. The film has different texture and roughness. It is clearly seen from that rosette phases starts from a nuclei and growing direction can be followed in this figure. Figure 4.42 shows AFM graph of another PLZT film annealed at 725ºC and pyrolysis steps as 200ºC 5 min + 430ºC for 10 min. The film was also given for another reason which is observed merged rosettes and the boundaries are very clear.

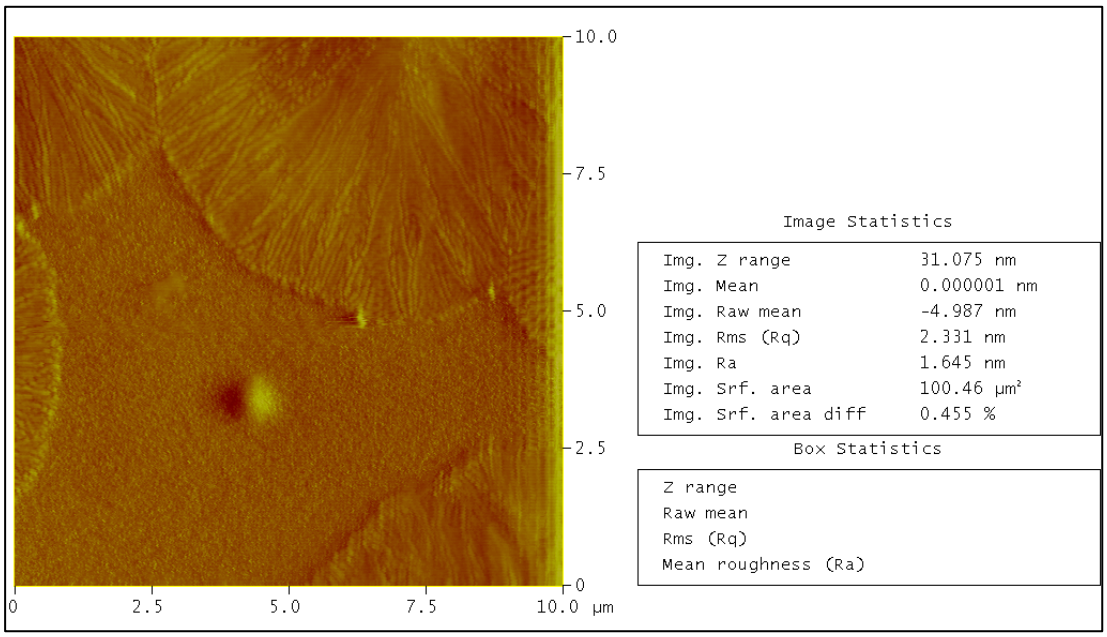


Figure 4.41: AFM surface image of PLZT film annealed at 725ºC and pyrolysis steps as 200ºC 2 min + 430ºC for 5 min.

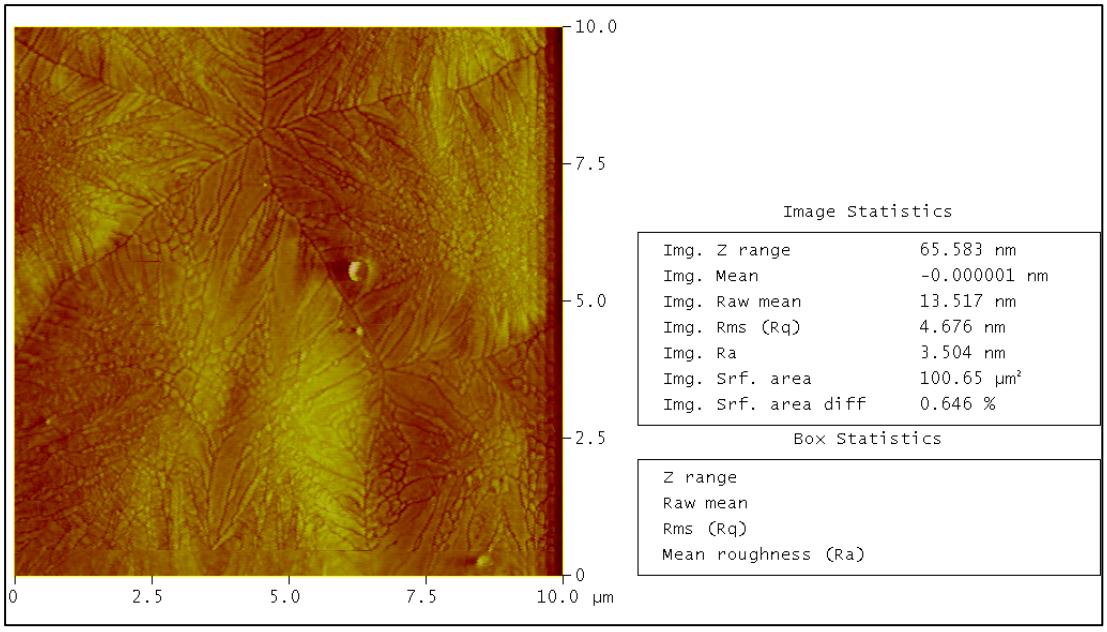


Figure 4.42: AFM surface image of PLZT film annealed at 725ºC and pyrolysis steps as 200ºC 5 min + 430ºC for 10 min.

AFM analyses of PZT films also showed that the increasing of annealing temperature resulted with the merged rosettes. AFM surface images of PZT films annealed at 600ºC and 725ºC were given in Figure 4.43 and 4.44, respectively.

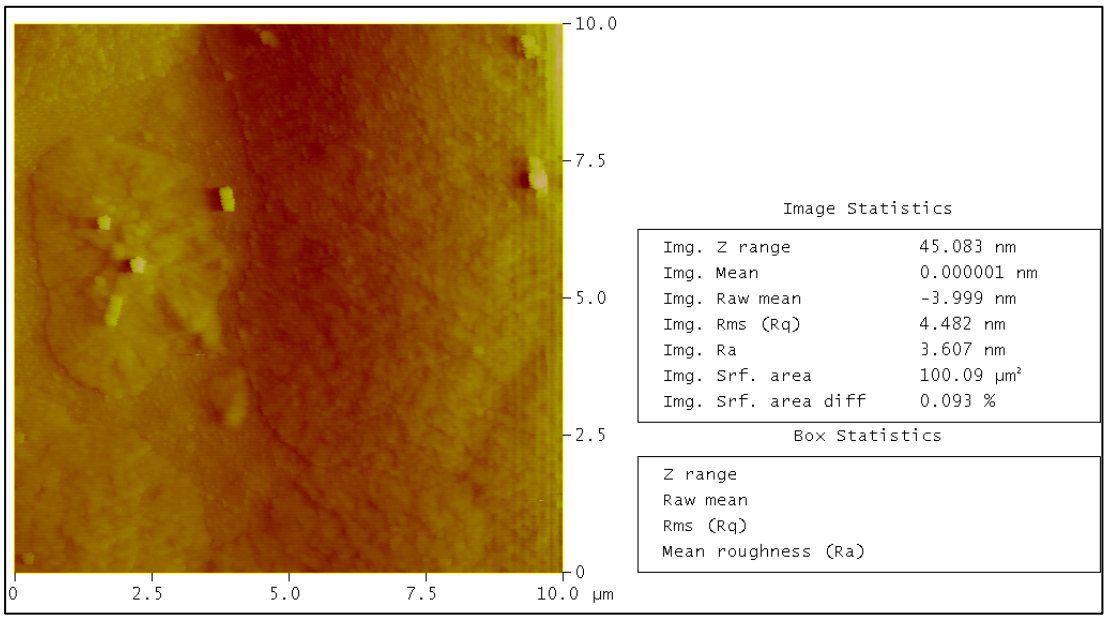


Figure 4.43: AFM surface image of PZT film annealed at 600ºC and pyrolysis steps as 250ºC 5 min + 400ºC for 5 min.

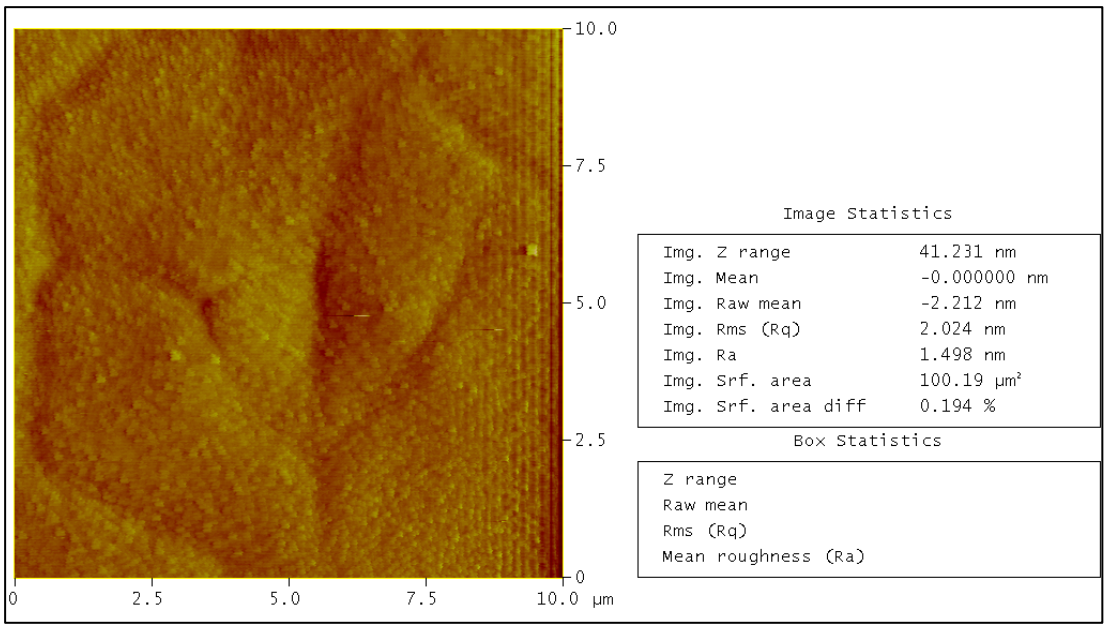


Figure 4.44: AFM surface image of PZT film annealed at 700ºC and pyrolysis steps as 250ºC 5 min + 400ºC for 5 min.

4.3. Bulk PZT and Cobalt doped PZT Studies

In this section of thesis, the experimental results of the studies were made with the powders synthesized by sol-gel method will be discussed. Phase analyses of the powders in calcination and sintering, ferroelectric characterizations will be given.

4.3.1. Phase Analyses of the Calcined PZT and Cobalt doped PZT Powders

PZT powders with 2%-mole Pb excess composition were calcinated at 800ºC for 2 hours. XRD pattern of this composition is given in Figure 4.45. In Figure 4.45, it was also observed a small peak for pyrochlore which was indicated as (Py) in figures.

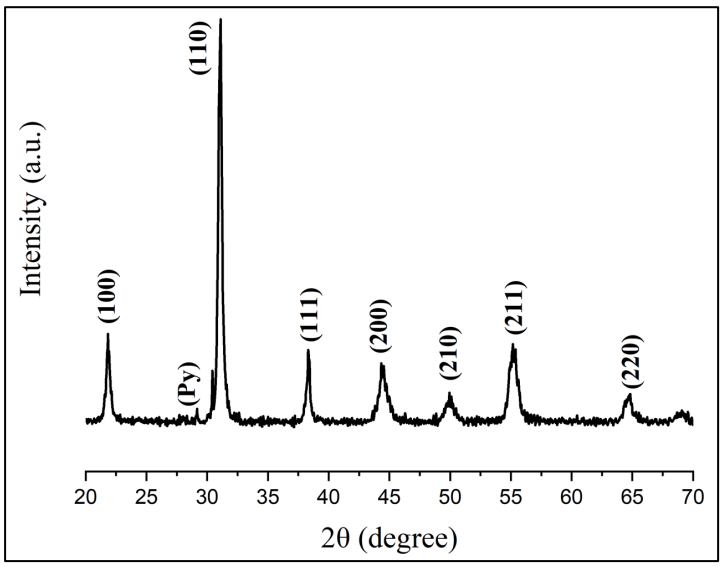


Figure 4.45: XRD pattern of PZT powders with 2%-mole Pb excess calcinated at 800ºC for 2 hours.

$PbTi_{0.50}Zr_{0.45}Co_{0.05}O_3$ (0.05-Co PZT) powders were calcinated at 800ºC for 2 hours and at 850ºC for 4 hours. The XRD patterns of the 0.05-Co PZT powders is given in Figure 4.46. $PbTi_{0.50}Zr_{0.30}Co_{0.20}O_3$ (0.20-Co PZT) powders were calcinated at 800ºC for 2 hours and at 850ºC for 4 hours. The XRD patterns of 0.20-Co PZT powders is given in Figure 4.47. From the figure, it can be said that increasing the calcination temperature from 800ºC to 850ºC and extending time from 2 hours to 4 hours was resulted with further crystallization of the powders and only a small amount of pyrochlore peak was observed.

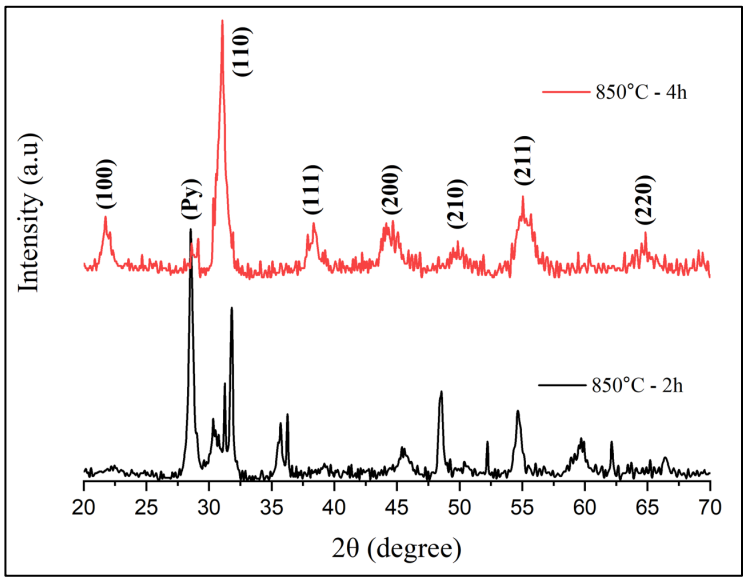


Figure 4.46: XRD pattern of 0.05-Co PZT powders calcinated under different conditions.

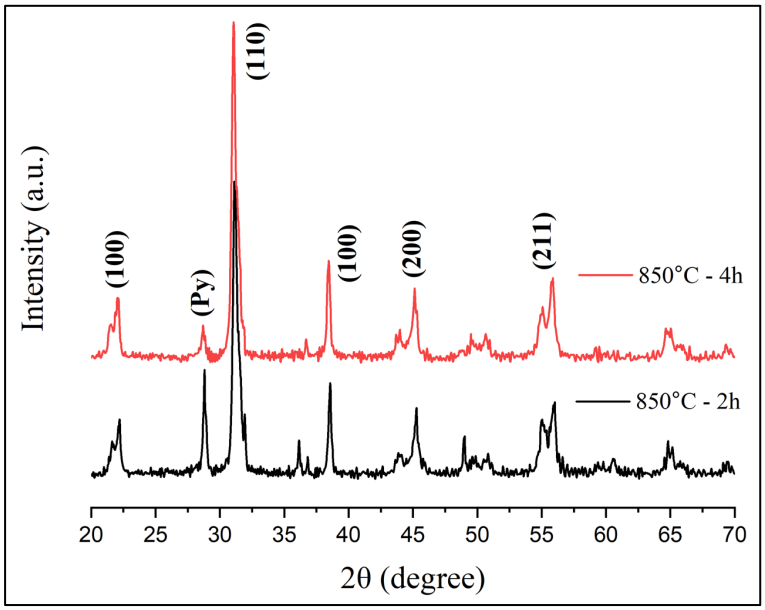


Figure 4.47: XRD pattern of 0.20-Co PZT powders calcinated under different conditions.

This composition was prepared with another solvent too. The results of the XRD analyses of the powders prepared with isopropanol instead of 2-methoxyethanol is given in Figure 4.48. It was not observed any big difference due to this solvent change but the intensity of the pyrochlore phase was higher than the composition prepared with 2-methoxyethanol.

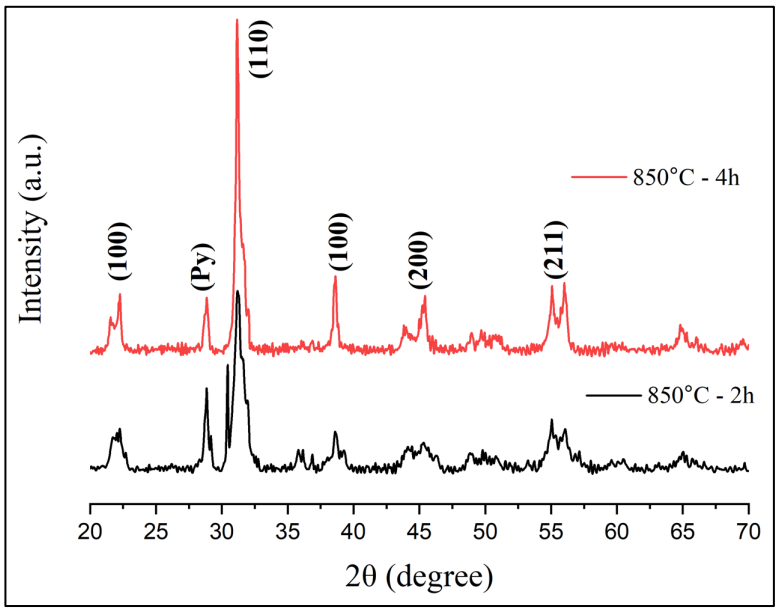


Figure 4.48: XRD pattern of 0.20-Co PZT powders prepared with isopropanol and calcinated under different conditions.

4.3.2. Phase Analyses of the Sintered PZT and Cobalt doped PZT Samples

PZT with 1%-mole and 2%-mole Pb excess pellets were sintered at 1260ºC for 4 hours. In the Figure 4.49, XRD patterns of these pellets are given. XRD patterns of the pellets showed not much differences to each other. Even the XRD patterns of these compositions after calcination were so different.

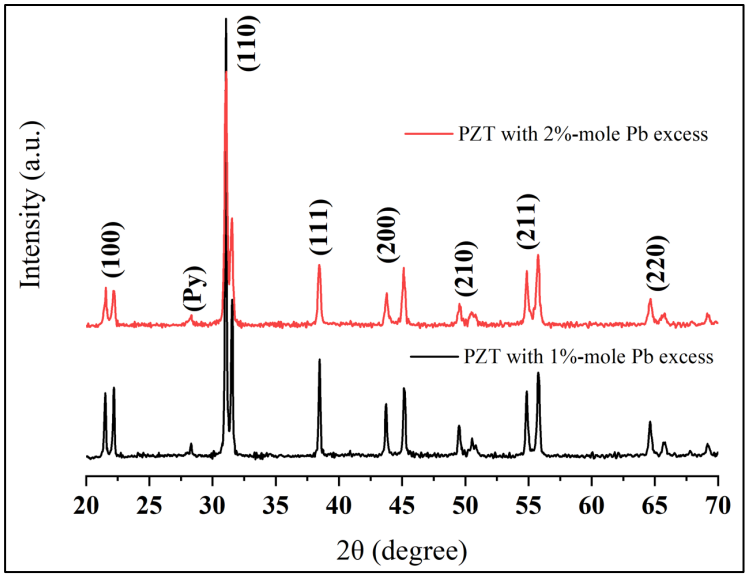


Figure 4.49: XRD patterns of PZT pellets with 1%-mole and 2%-mole Pb excess sintered at 1260ºC for 4 hours.

Sintering of the pellets with 0.05-Co PZT composition is given in Figure 4.50. XRD analyses were resulted with perovskite structure but small pyrochlore peak was also observed. The pellets with 0.2-Co PZT composition were sintered at 1260ºC for 2 hours and 4 hours. XRD patterns of the pellets are given in Figure 4.51. It can be seen from the figure; peak splits were changed with sintering time. The peak at the 2θ=22º was disappeared when the sintering time is extended to 4 hours. Also, the tendency to split at the 2θ=45º was decreased. Besides that, for the pellet sintered for 4 hours, there is an untagged peak was observed at 2θ=60º.

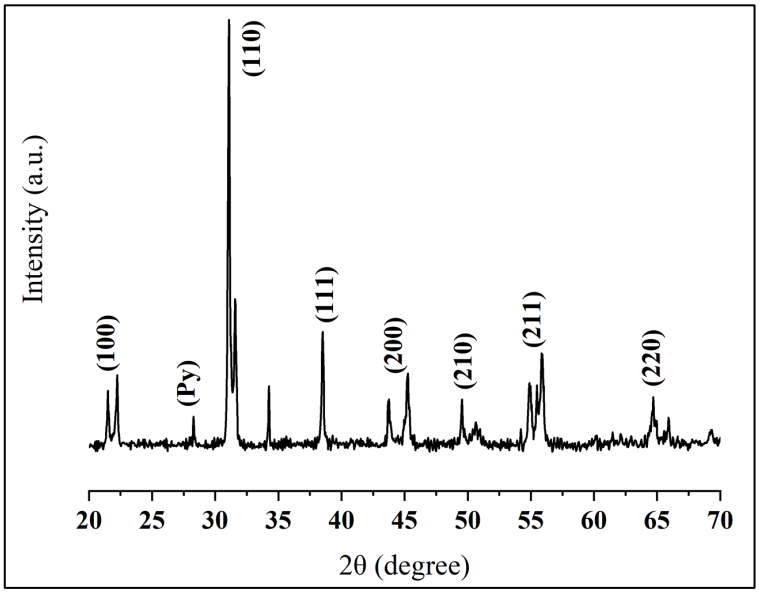


Figure 4.50: XRD patterns of 0.05-Co PZT pellets sintered at 1260ºC for 2 hours.

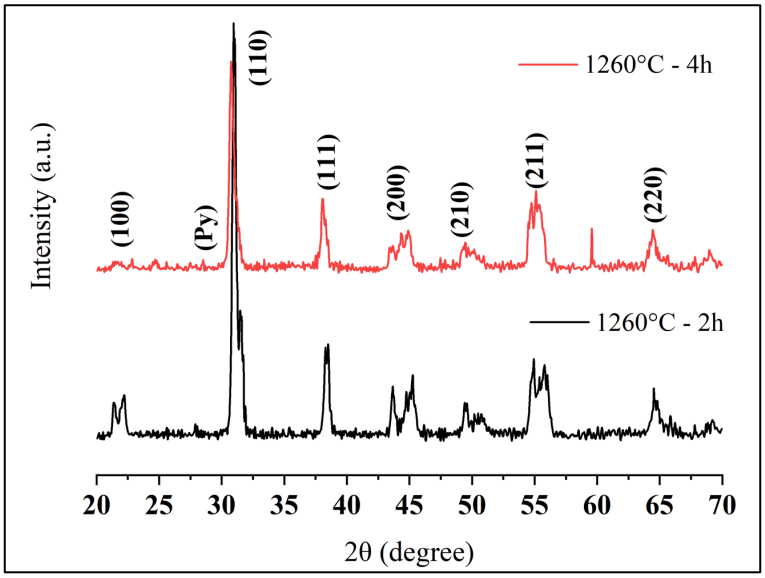


Figure 4.51: XRD patterns of 0.20-Co PZT pellets sintered at 1260ºC for 2 hours and 4 hours.

4.3.3. Polarization and Strain Behavior of PZT and Cobalt doped PZT Samples

In this section, ferroelectric and piezoelectric characterizations of bulk samples will be discussed. These measurements were carried out for the samples with composition as PZT with 1%-mole and 0.05-Co PZT. Maximum 45 kV electric field was applied to the samples.

The hysteresis loop of the sample with composition as PZT with 1%-mole Pb excess is given in Figure 4.52. The sample resulted with values as $2P_r$=8.94 $\mu C/cm^2$ and $2E_c$=32.26 kV/cm for 45 kV electric field.

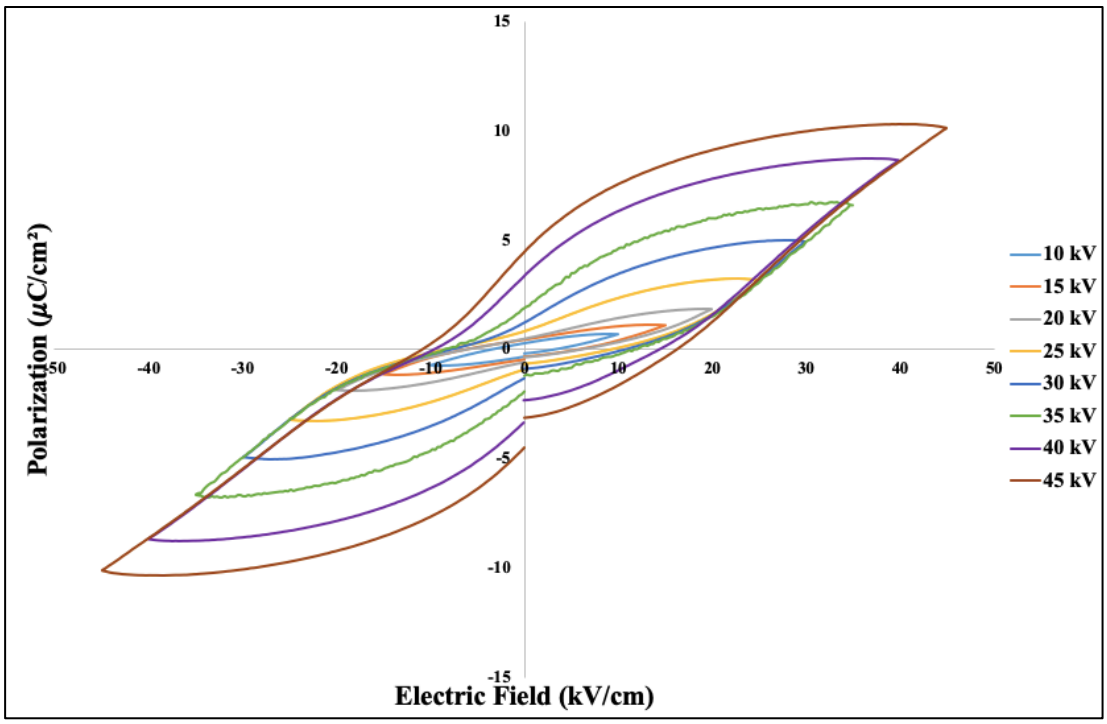


Figure 4.52: Polarization-electric field hysteresis loops of the PZT with 1%-mole Pb excess.

Strain versus electric field values were also measured. This measurement was also carried out with maximum 45 kV electric field. The butterfly shape hysteresis of the PZT with 1%-mole Pb excess sample is given in Figure 4.53. The strain level of the sample was ~0.22% when the applied electric field was 45 kV.

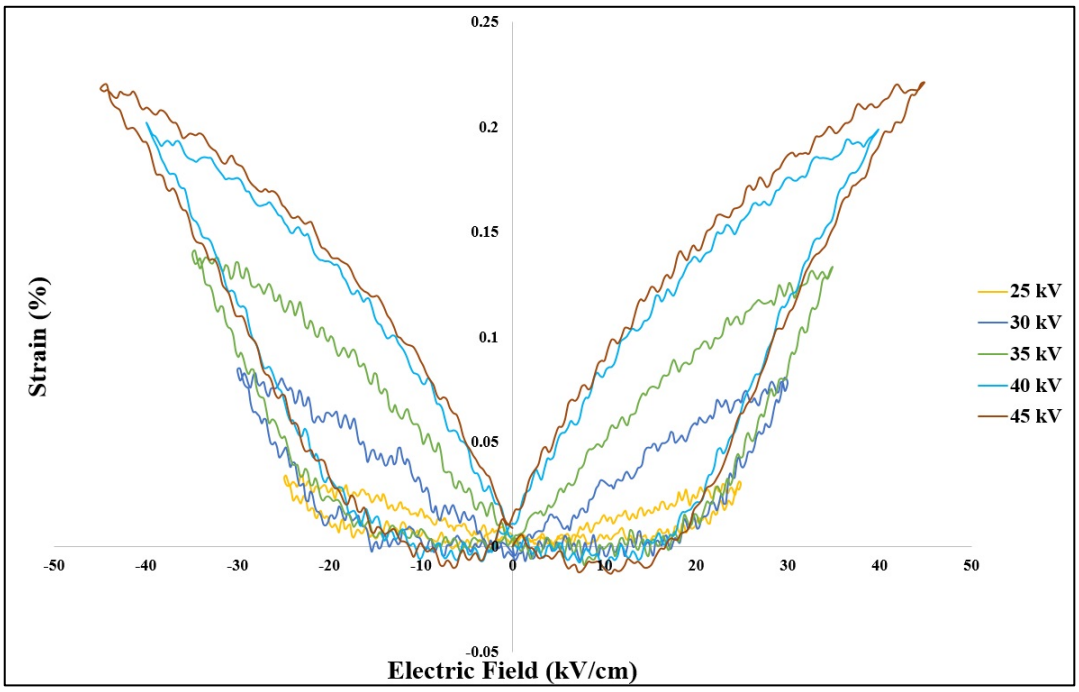


Figure 4.53: Strain-electric field hysteresis loops of the PZT with 1%-mole Pb excess.

The hysteresis loop of the sample with composition as PZT with 2%-mole Pb excess is given in Figure 4.54. The sample resulted with values as $2P_r$=9.02 μC/cm^2 and $2E_c$=26.74 kV/cm for 40 kV electric field.

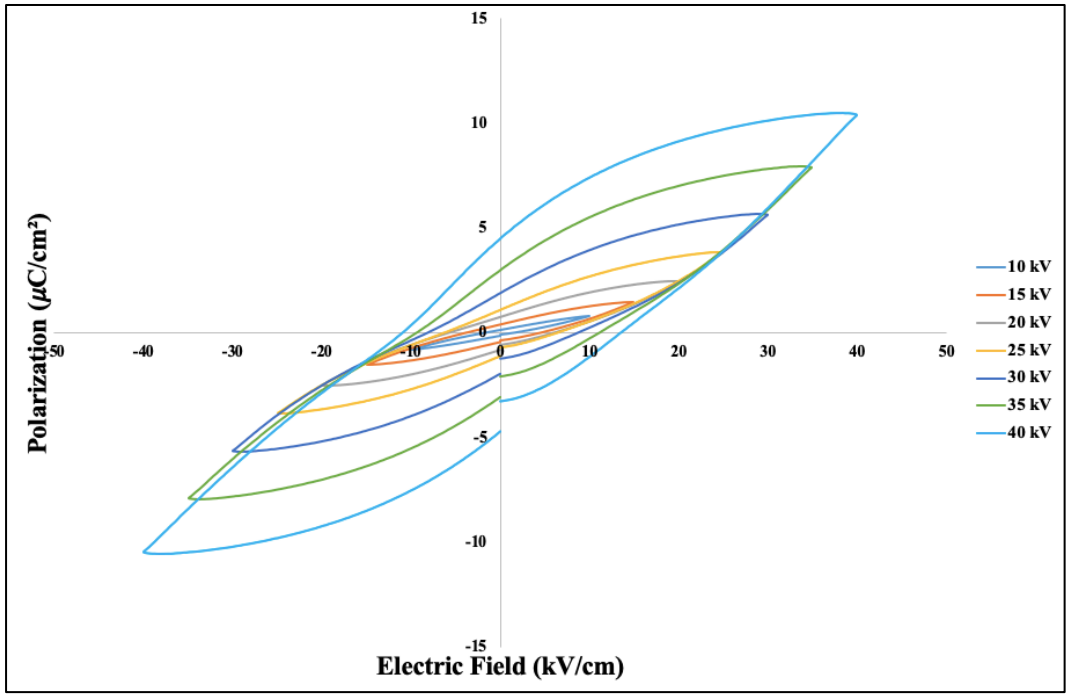


Figure 4.54: Polarization-electric field hysteresis loops of the 0.05-Co PZT.

Strain versus electric field measurement was carried out with maximum 40 kV electric field. The butterfly shape hysteresis of the 0.05-Co PZT sample is given in Figure 4.55. The strain level of the sample was ~0.08% when the applied electric field was 40 kV.

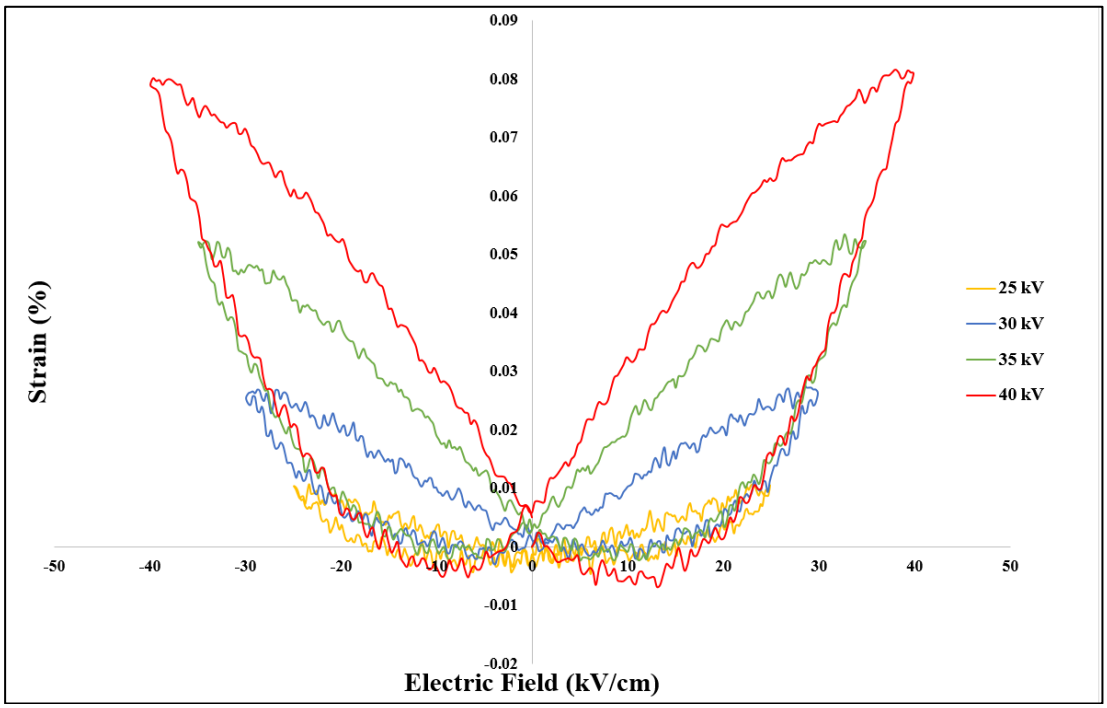


Figure 4.55: Strain-electric field hysteresis loops of the 0.05-Co PZT.

5. CONCLUSION

Microstructurally improvement of the thin films prepared on platinum coated silicon substrates were done. For PZT films, annealing at 700ºC for 1 hour was selected as optimum condition. This parameter was eliminated the most of the pyrochlore phase. These films were had ~530 nm thickness and it was quite homogenous. Electrical measurements of the PZT films annealed at 700ºC for 1 hour had transition point at 456ºC. Leakage current of this films were $8x10^{-10}$ A/cm^2 at 40 kV/cm. PLZT films have shown best microstructure with merged rosettes under annealing condition as 725ºC for 1 hour. Transition temperature of these films were measured as 560ºC.

The films coated on GZO coated glass substrates were also have good microstructure, but they were quite rough. PZT films have shown best microstructure properties after annealing at 725ºC for 1 hour. These films were had ~50% transparency and 3.22 eV band gap value. PLZT films have shown best microstructure properties under the pyrolysis conditions as 200ºC for 5 minutes and 430ºC for 10 minutes and after annealing at 725ºC for 1 hour. These films were had ~60% transparency and 3.27 eV band gap value.

For the future study, it is aimed that setting-up the I-V measurement system in laboratory with existing facilities, investigation of the electrical properties of the films coated on both substrates in detail and achieving reliable data.

REFERENCES

[1] Mahmood A., Naeem A., Kaya M. Y., Yasin M., Mensur-Alkoy E., Alkoy S., (2015), "Effect of Co/Mg ratio on the phase, microstructure, dielectric and impedance properties of lead zirconate titanate", Journal of Materials Science-Materials in Electronics, 26 (12), 10123-10131.

[2] Miglioli L., (2013), "Synthesis and characterization of ferroelectric Lead Zirconate Titanate Pb(Zr,Ti)O3 thin films", Master of Science Thesis, Politecnico di Milano.

[3] Huang C. L., Chen B. H., Wu L., (2004), "Application feasibility of Pb(Zr,Ti)O-3 ceramics fabricated from sol-gel derived powders using titanium and zirconium alkoxides", Materials Research Bulletin, 39 (4-5), 523-532.

[4] Bag S. P., Her J. L., Pan T. M., (2017), "Frequency-independent coercive field in Pb(Zr0.52Ti0.48)O-3 polycrystalline thin film based on sol-gel synthesis", Materials Science in Semiconductor Processing, 64, 24-28.

[5] Rahman M. F., Miglioli L., (2016), "Fabrication and Characterization of Lead Zirconate Titanate (PZT) Thin Films by Sol-Gel Technique", International Journal of Nanoscience, 15 (3).

[6] Batra V., Kotru S., (2017), "Illumination effects on the ferroelectric and photovoltaic properties of Pb0.95La0.05Zr0.54Ti0.46O3 thin film based asymmetric MFM structure", Journal of Applied Physics, 122 (23).

[7] Woo D. C., Koo C. Y., Lee C. H., No K. S., Lee H. Y., (2001), "Ferroelectric PLZT thin films prepared by chemical solution deposition", Ferroelectrics, 260 (1-4), 641-647.

[8] Kim J. M., Yoon D. S., No K., (1994), "Electrical-Properties of Sol-Gel Processed Plzt Thin-Films", Journal of Materials Science, 29 (24), 6599-6603.

[9] Khodorov A., Gomes M. J. M., (2006), "Preparation and optical characterization of lanthanum modified lead zirconate titanate thin films on indium-doped tin oxide-coated glass substrate", Thin Solid Films, 515 (4), 1782-1787.

[10] Govindan A., Sharma A., Pandey A. K., Gaur S. K., (2011), "Piezoelectric and pyroelectric properties of lead lanthanum zirconate titanate (PLZT) ceramics prepared by sol gel derived nano powders", Indian Journal of Physics, 85 (12), 1829-1832.

[11] Ichiki M., Maeda R., Morikawa Y., Mabune Y., Nakada T., Nonaka K., (2004), "Photovoltaic effect of lead lanthanum zirconate titanate in a layered film structure design", Applied Physics Letters, 84 (3), 395-397.

[12] Qiu S. J., Zheng X. D., Gao C., Gan X. X., Chen J., Yang C., Fan H. Q., (2009), "Pb(Zr0.95Ti0.05)O-3 powders and porous ceramics prepared by one-step pyrolysis process using non-aqueous Pechini method", Ceramics International, 35 (2), 733-740.

[13] Newnham R. E., (2004), "Properties of materials anisotropy, symmetry, structure", 1st Edition, Oxford University Press.

[14] Damjanovic D., (1998), "Ferroelectric, dielectric and piezoelectric properties of ferroelectric thin films and ceramics", Reports on Progress in Physics, 61 (9), 1267-1324.

[15] Oliveira C. A., Longo E., Varela J. A., Zaghete M. A., (2014), "Synthesis and characterization of lead zirconate titanate (PZT) obtained by two chemical methods", Ceramics International, 40 (1), 1717-1722.

[16] Lei C., (2008), "Studies of Novel Lead-Free Piezoelectric and Relaxor Ferroelectric Materials", Simon Fraser University.

[17] Eitel R. E., Randall C. A., Shrout T. R., Rehrig P. W., Hackenberger W., Park S. E., (2001), "New high temperature morphotropic phase boundary piezoelectrics based on Bi(Me)O-3-PbTiO3 ceramics", Japanese Journal of Applied Physics Part 1-Regular Papers Short Notes & Review Papers, 40 (10), 5999-6002.

[18] John E. V., (2012), "Spectroscopic Investigation of Lattice Dynamics in Multidomain Ferroelectrics", Charles University.

[19] Kao K.-C., (2004), "Dielectric phenomena in solids : with emphasis on physical concepts of electronic processes", 1st Edition, Academic Press.

[20] Alkoy E. M., Shiosaki T., (2008), "Electrical properties and leakage current behavior of un-doped and Ti-doped lea zirconate thin films synthesized by sol-gel method", Thin Solid Films, 516 (12), 4002-4010.

[21] Setter N., Damjanovic D., Eng L., Fox G., Gevorgian S., Hong S., Kingon A., Kohlstedt H., Park N. Y., Stephenson G. B., Stolitchnov I., Taganstev A. K., Taylor D. V., Yamada T., Streiffer S., (2006), "Ferroelectric thin films: Review of materials, properties, and applications (vol 100, art no 051606, 2006)", Journal of Applied Physics, 100 (10).

[22] Cohen R. E., (2006), "Materials science - Relaxors go critical", Nature, 441 (7096), 941-942.

[23] Meng X. J., Sun J. L., Yu J., Ye H. J., Guo S. L., Chu J. H., (2001), "Preparation of highly (100)-oriented metallic LaNiO3 films on Si substrates by a modified metalorganic decomposition technique", Applied Surface Science, 171 (1-2), 68-70.

[24] Scott J. F., Melnick B. M., McMillan L. D., de Araujo C. A. P., Azuma M., (1993), "Dielectric Breakdown in High-E Films for Ulsi Drams", Ferroelectrics, 150 (1), 209-218.

[25] Narayanan M., Ma B. H., Balachandran U., Li W., (2010), "Dielectric spectroscopy of Pb0.92La0.08Zr0.52Ti0.48O3 films on hastelloy substrates with and without LaNiO3 buffer layers", Journal of Applied Physics, 107 (2).

[26] Haertling G. H., (1999), "Ferroelectric ceramics: History and technology", Journal of the American Ceramic Society, 82 (4), 797-818.

[27] Zhang J., Cole M. W., Alpay S. P., (2010), "Pyroelectric properties of barium strontium titanate films: Effect of thermal stresses", Journal of Applied Physics, 108 (5).

[28] Martin L. W., Rappe A. M., (2017), "Thin-film ferroelectric materials and their applications", Nature Reviews Materials, 2 (2), 16087.

[29] Uchino K., (2009), "Ferroelectric Devices", 2nd Edition, CRC Press Book.

[30] Yang C. T., Liu J. S., Zhang S. R., Chen Z. D., (2003), "Characterization of Pb(Zr,Ti)O-3 thin film prepared by pulsed laser deposition", Materials Science and Engineering B-Solid State Materials for Advanced Technology, 99 (1-3), 356-359.

[31] Sung-Gap L., Young-Jae S., Jin K. C., Jun-Ki C., (2008), "Structural and dielectric properties of Pb(Zr,Ti)O-3 heterolayered thick films", Journal of Alloys and Compounds, 449 (1-2), 73-76.

[32] Laurenti M., Cauda V., (2017), "ZnO Nanostructures for Tissue Engineering Applications", Nanomaterials, 7 (11).

[33] Chen X., Han X., Shen Q. D., (2017), "PVDF-Based Ferroelectric Polymers in Modern Flexible Electronics", Advanced Electronic Materials, 3 (5).

[34] Moulson A. J., (2003), "Electroceramics", 2nd Edition, John Wiley & Sons.

[35] Mishra S. K., Pandey D., Singh A. P., (1996), "Effect of phase coexistence at morphotropic phase boundary on the properties of Pb(ZrxTi1-x)O-3 ceramics", Applied Physics Letters, 69 (12), 1707-1709.

[36] Yamashita K., Okuyama M., (2004), "Characterization of piezoelectric property of sol-gel PZT thin films and its improvement by poling", IEEJ Transactions on Sensors and Micromachines, 124 (4), 124-128.

[37] Abadias G., Chason E., Keckes J., Sebastiani M., Thompson G. B., Barthel E., Doll G. L., Murray C. E., Stoessel C. H., Martinu L., (2018), "Review Article: Stress in thin films and coatings: Current status, challenges, and prospects", Journal of Vacuum Science & Technology A, 36 (2).

[38] Heywang W., Lubitz K., Wersing W., (2008), "Piezoelectricity : Evolution and Future of a Technology", Edition, Springer Berlin.

[39] Haertling G. H., Land C. E., (1971), "Hot-Pressed (Pb,La)(Zr,Ti)O3 Ferroelectric Ceramics for Electrooptic Applications", Journal of the American Ceramic Society, 54 (1), 1-+.

[40] Shukla A. K., Agrawal V. K., Das I. M. L., Singh J., Srivastava S. L., (2010), "Temperature dependence of electromechanical properties of PLZT x/57/43 ceramics", Bulletin of Materials Science, 33 (4), 383-390.

[41] Es-Souni M., Abed M., Piorra A., Malinowski S., Zaporojtchenko V., (2001), "Microstructure and properties of sol-gel processed Pb(1-x)La(x)(Zr(0.52), Ti(0.48))(1-x/4)O(3) thin films. The effects of lanthanum content and bottom electrodes", Thin Solid Films, 389 (1-2), 99-107.

[42] Nampoori H. V., (2012), "Pb0.95La0.05Zr0.54Ti0.46O3 THIN FILMS FOR PHOTOVOLTAIC APPLICATIONS", Doctoral Thesis, The University of Alabama.

[43] Saleh B. E. A., Teich M. C., (2007), "Fundamentals of photonics", 2nd Edition, Wiley.

[44] Wasa K., Hayakawa S., (2012), "Handbook of sputter deposition technology : principles, technology and applications", 2nd Edition, Noyes.

[45] Alkoy E. M., Alkoy S., Shiosaki T., (2007), "The effect of crystallographic orientation and solution aging on the electrical properties of sol-gel derived Pb(Zr0.45Ti0.55)O-3 thin films", Ceramics International, 33 (8), 1455-1462.

[46] Yang F., Fei W., (2008), "Texture Evolution of Sol-Gel-Derived Pb (Zr, Ti) O3 Film on Platinum Bottom Electrode with Different Annealing Process", Rare Metal Materials and Engineering, 37 (10), 1760-1765.

[47] Meng X. J., Cheng J. G., Sun J. L., Tan J., Ye H. J., Chu J. H., (2000), "Dependence of texture development on thickness of single-annealed-layer in sol-gel derived PZT thin films", Thin Solid Films, 368 (1), 22-25.

[48] Park B. E., Sakai I., Tokumitsu E., Ishiwara H., (1997), "Hysteresis characteristics of vacuum-evaporated ferroelectric PbZr0.4Ti0.6O3 films on Si(111) substrates using CeO2 buffer layers", Applied Surface Science, 117, 423-428.

[49] Jambunathan M., Elfrink R., Vullers R., vanSchaijk R., Dekkers M., Broekmaat J., (2012), "Pulsed Laser Deposited-Pzt Based Mems Energy Harvesting Devices", 2012 International Symposium on Applications of Ferroelectrics Held Jointly with 11th Ieee Ecapd and Ieee Pfm (Isaf/Ecapd/Pfm).

[50] Bi Z. X., Zhang Z. S., Fan P. F., (2007), "Characterization of PZT Ferroelectric Thin Films by RF-magnetron Sputtering", Proceedings of the International Conference on Nanoscience and Technology, 61, 120-124.

[51] Schwartz R. W., Schneller T., Waser R., (2004), "Chemical solution deposition of electronic oxide films", Comptes Rendus Chimie, 7 (5), 433-461.

[52] Dawber M., Rabe K. M., Scott J. F., (2005), "Physics of thin-film ferroelectric oxides", Reviews of Modern Physics, 77 (4), 1083-1130.

[53] Brinker C. J., Scherer G. W., (2010), "Sol gel science the physics and chemistry of sol gel processing", 2nd Edition, Academic Press.

[54] Dobrzański L., Szindler M., (2012), "Sol gel TiO2antireflection coatings for Silicon solar cells", Journal of Achievements in Materials and Manufacturing Engineering, 52 (1), 7--14.

[55] Qiu S. J., Gao C., Zheng X. D., Chen J., Yang C., Gan X. X., Fan H. Q., (2008), "Pb(Zr0.95Ti0.05)O-3 powders prepared by aqueous Pechini method using one-step pyrolysis process: characterization and porous ceramics", Journal of Materials Science, 43 (9), 3094-3100.

[56] Hubault C., Davoisne C., Boulle A., Dupont L., Demange V., Perrin A., Gautier B., Holc J., Kosec M., Karkut M. G., Lemee N., (2012), "Strain effect in PbTiO3/PbZr0.2Ti0.8O3 superlattices: From polydomain to monodomain structures", Journal of Applied Physics, 112 (11).

[57] Türküz S., (2010), "İndiyum Kalay Oksit İnce Filmlerin Optoelektronik Özelliklerinin İyileştirilmesi", Doctoral Thesis, Istanbul Technical University.

[58] Minami T., (2005), "Transparent conducting oxide semiconductors for transparent electrodes", Semiconductor Science and Technology, 20 (4), S35-S44.

[59] Mattox D., Mattox V., (2007). "Review of transparent conductive oxides (TCO)", Society of Vacuum Coaters.

[60] Janotti A., Van de Walle C. G., (2009), "Fundamentals of zinc oxide as a semiconductor", Reports on Progress in Physics, 72 (12).

[61] Chen Y. F., Bagnall D. M., Koh H. J., Park K. T., Hiraga K., Zhu Z. Q., Yao T., (1998), "Plasma assisted molecular beam epitaxy of ZnO on c-plane sapphire: Growth and characterization", Journal of Applied Physics, 84 (7), 3912-3918.

[62] Castro M. V., Tavares C. J., (2015), "Dependence of Ga-doped ZnO thin film properties on different sputtering process parameters: Substrate temperature, sputtering pressure and bias voltage", Thin Solid Films, 586, 13-21.

[63] Ko H. J., Chen Y. F., Hong S. K., Wenisch H., Yao T., Look D. C., (2000), "Ga-doped ZnO films grown on GaN templates by plasma-assisted molecular-beam epitaxy", Applied Physics Letters, 77 (23), 3761-3763.

[64] Yang Z., Liu J. L., (2010), "Donor-acceptor-pair photoluminescence in Ga-doped ZnO thin films grown by plasma-assisted molecular beam epitaxy", Journal of Vacuum Science & Technology B, 28 (3).

[65] Alkoy E. M., Alkoy S., Shiosaki T., (2005), "Microstructure and crystallographic orientation dependence of electrical properties in lead zirconate thin films prepared by sol-gel process", Japanese Journal of Applied Physics Part 1-Regular Papers Brief Communications & Review Papers, 44 (12), 8606-8612.

[66] Mensur-Alkoy E., (2006), "Study on Improvement of Fatigue Behaviour of Ferroelectric Pb(Zr,Ti)O3 Thin Films Using PbZrO3 Buffer Layers", Doctoral Thesis, Nara Institute of Science and Technology.

[67] Kawano T., Sei T., Tsuchiya T., (1991), "Preparation of Ferroelectric (Pb, La)(Zr, Ti)O3 Thin Films by Sol-Gel Process and Dielectric Properties", Japanese Journal of Applied Physics, 30 (9B), 2178-2181.

[68] Alkoy E. M., Kelly P. J., (2005), "The structure and properties of copper oxide and copper aluminium oxide coatings prepared by pulsed magnetron sputtering of powder targets", Vacuum, 79 (3-4), 221-230.

[69] Aslan M. H., Mensur E., Basaran E., Oral A. Y., (2004), "The sol-gel-like preparation of Cu0.95Me0.05Ox thin films and the study of their microstructures and optical properties", Key Engineering Materials, 264-268, 573-576.

[70] Aslan M. H., Oral A. Y., Mensur E., Gul A., Basaran E., (2004), "Preparation of c-axis-oriented zinc-oxide thin films and the study of their microstructure and optical properties", Solar Energy Materials and Solar Cells, 82 (4), 543-552.

[71] Oral A. Y., Mensur E., Aslan M. H., Basaran E., (2004), "The preparation of copper(II) oxide thin films and the study of their microstructures and optical properties", Materials Chemistry Physics, 83 (1), 140-144.

BIOGRAPHY

Mustafa Çağrı Bayır was born in İskenderun in 1995. He finished his high school education in 2013. In the same year, he started to Kocaeli University, Metallurgical and Materials Engineering. He finished his bachelor's degree in third place in 2017. Then he started to master of science education in Gebze Technical University, Materials Science and Engineering. In May 2018, he started to work as research assistant in the same department. He is planning to achieve master's degree and continue his education for philosophy of doctorate.